UNIVERSITY OF MINNESOTA
ST. ANTHONY FALLS HYDRAULIC LABORATORY
LORENZ G. STRAUB, Director

Technical Paper No. 9, Series B

Design Studies for a Closed-Jet Water Tunnel

by

John F. Ripken

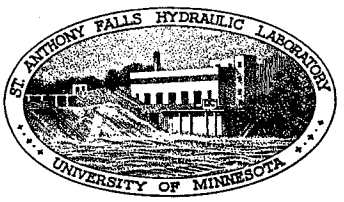

August, 1951

Minneapolis, Minnesota

PREFACE

The design studies presented in this paper relate to the problems and solutions encountered in formulating plans for a large hydrodynamic testing facility proposed for construction by the United States Department of the Navy at the David Taylor Model Basin, Carderock, Maryland. While a water or cavitation tunnel of the type described herein is a rare facility in conventional research or engineering work, many of the problems incident to its design are commonly encountered in general practice. However, it was apparent at an early date that technical information adequate for the quality requirements of this design was not available in the literature and that extensive tests would be necessary for proper planning. Contract arrangements between the St. Anthony Falls Hydraulic Laboratory and the David Taylor Model Basin led to execution of the necessary experimental studies.

Through the very generous cooperation of the David Taylor Model Basin it is the privilege of the St. Anthony Falls Hydraulic Laboratory to make available through this paper the findings of this program. For clarity of purpose this study includes, in addition to the test analyses, prefacing abstracts of the original design papers prepared by the author while a member of the Model Basin staff. The material presented here represents a condensation of numerous interim reports submitted to the Model Basin by the Laboratory and, as such, draws heavily from the discussions and analyses of these reports. Grateful acknowledgement is therefore due Messrs. Alvin G. Anderson, James S. Holdhusen, Owen P. Lamb, and Edward Silberman who contributed to these reports, with special acknowledgement due Mr. Holdhusen for his very extensive contributions.

The investigational program was under the general direction of Dr. Lorenz G. Straub, Director of the St. Anthony Falls Hydraulic Laboratory, and was supervised by the author. The author is indebted to Reuben S. Olson for his technical editorial suggestions and to Loyal A. Johnson for arrangement of the illustrations. Preparation of the manuscript was by Leona S. Wray, Marianne Sturtevant, and E. Roy Tinney.

A B S T R A C T

A variable-pressure water tunnel, which is a testing facility analogous to a wind tunnel, is a useful tool in the study of cavitation or hydrodynamic characteristics of underwater bodies. This paper includes general, selective, hydrodynamic design studies for the construction of a large closed-jet water tunnel, together with experimental model test data and design analysis of a specific selection of flow components. Each flow component is critically examined with regard to its influence on test section flow quality, cavitation susceptibility, and energy head loss. Included are studies of the test section, contraction, diffuser, vaned elbows, and pump. Presentation in chapters devoted to single flow components simplifies the treatment and increases adaptability of the findings to conduit design problems other than water tunnels.

CONTENTS

C O N T E N T S (Continued)

LIST OF ILLUSTRATIONS

LIST OF ILLUSTRATIONS (Continued)

LIST OF TABLES

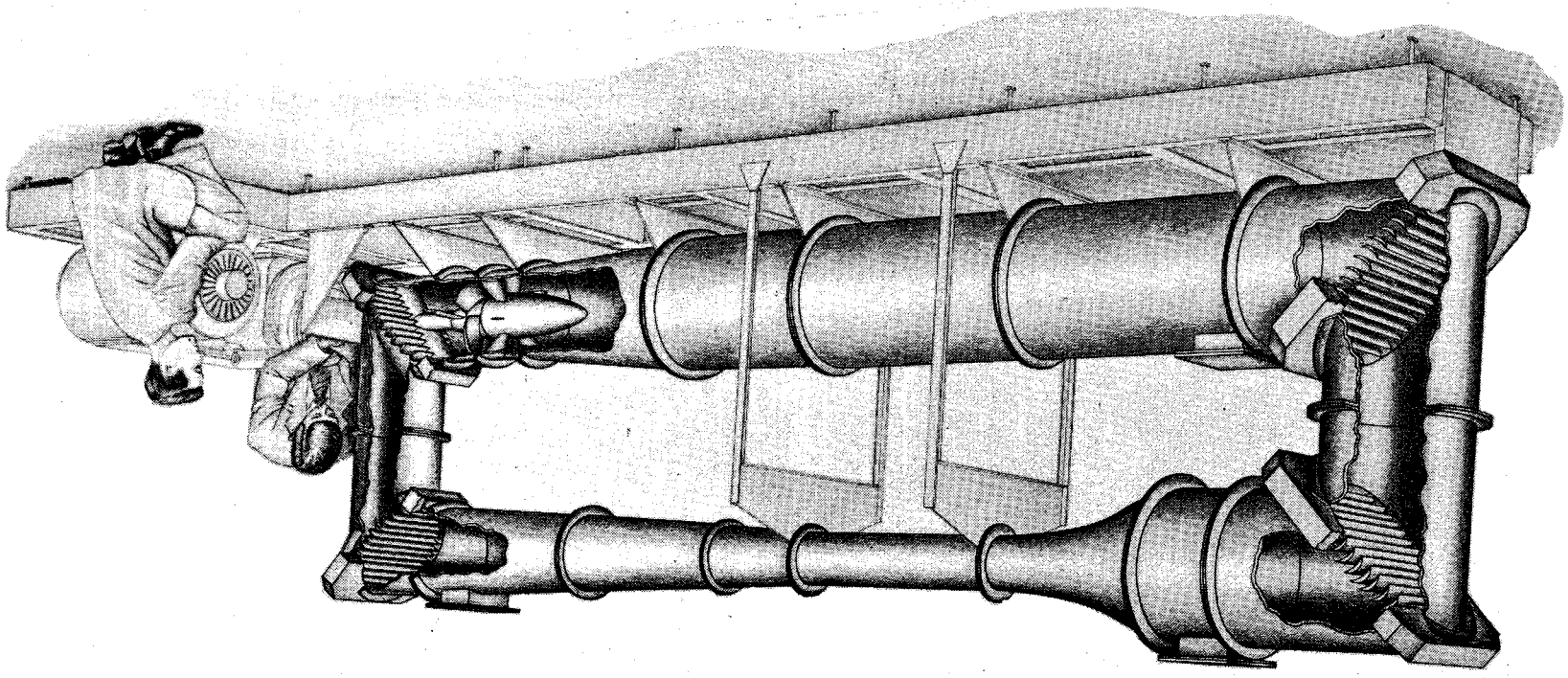

DESIGN STUDIES FOR A CLOSED-JET WATER TUNNEL

CHAPTER I. INTRODUCTION

A. The General Problem

Since the advent of practical high speed prime movers late in the last century, the problems of the designer concerned with the motion of solid bodies through water have been ever increasing whether they be with respect to ship hulls, rotating blades, or the extreme speeds encountered with aircraft-launched or jet-driven ordnance bodies.

These design studies have been of increasing difficulty because of the necessity for finding experimental methods of a suitable and practical nature for determining the characteristics of body forms which cannot be designed by pure analytical methods. For a large range of these problems, a workable solution has been found in form studies employing such test facilities as towing basins, whirling towing booms, circulating and non-recirculating water channels, and open water or prototype test ranges wherein resistance forces and pressure distribution can be measured on a model or prototype body. However, for another important group of body forms, the most important determination has been the presence and effect of local body pressures which are low enough to vaporize or boil the water and thus produce cavitation bubbles. For such cavitation studies, adequate control can be achieved only if the environmental pressure can be varied or reduced to a desired level. This necessitates a closed pressure vessel and for economy usually requires a recirculating system to produce the water motion at the test section.

Because highest body speeds are normally encountered in rotating blade systems, specialized cavitation test facilities for pumps and turbines, which are the commonest of such blade forms, have been highly developed and find extensive use in the laboratories of most large manufacturers of such equipment. These facilities, in general, present no major design difficulties since the testing section of the system is normally built to simulate both the rotating element and the surrounding casing or scroll. In such a relative harness of flow components, satisfactory test results can usually be achieved. However, when analogous methods are employed to test rotating propeller blades

or other body forms which in nature normally move in an infinite flow field, extreme design care is necessary to prevent a material distortion of the flow pattern around the body and a serious lack of similarity due to the presence of the boundary walls of the recirculating pressurizing duct.

It is the purpose of this paper to discuss the problems which arise in attempting to design a large, high speed, general purpose, variable pressure cavitation test facility.

B. Problem at the David Taylor Model Basin

The manifold assignment of research problems to the David Taylor Model Basin during the years of World War II was such that a survey of past and probable future assignments established a need for a large, multiple purpose, cavitation test facility capable of producing conditions simulating a complete range of natural, subsurface conditions.

The survey of need, which was extended to include preliminary directive specifications, was released by the technical director of the Model Basin early in 1945 and was followed by assembly of a complete bibliography relating to similar existing test facilities and findings from visits to and inspections of those units existing in the United States. As an outgrowth of this preparation, a general preliminary design was assembled as a basis for discussion and was followed with detailed hydraulic studies of the principal components. The proposed designs were based on the best available design data of a theoretical and empirical nature, but finally led to the conclusion that proper plans could be achieved only through use of experimental verification of specific design proposals. In accord with these conclusions, experimental studies were initiated at the St. Anthony Falls Hydraulic Laboratory in August, 1946, under the terms of Contract NObs-34208.

C. Studies at the St. Anthony Falls Hydraulic Laboratory

An early analysis of the problems incident to experimental testing of the proposed tunnel design led to the conclusion that the best answer would be found in tests of a complete scale model tunnel in which the mutual effects of the various parts could be carefully studied. In a balance between the economics of testing and the limitations of similitude, it was determined that a one-tenth scale model would be adequate for the needs and, accordingly, a complete unit of this size was fabricated.

While the general properties of this facility and its auxiliaries are rather fully described in the appendix to this paper and specific properties of the components are described in the individual chapters, it is perhaps proper to orient the reader at this time to the salient features of the study. This is deemed necessary because the detailed analysis seems most effectively presented by individual studies which may at times obscure the integrated relation of these parts.

To assist in this integration, it is well for the reader to retain in mind that the experimental studies were conducted on a one-tenth scale model tunnel having a test section diameter of 6 in., a recirculating duct loop oriented in the vertical plane, and a suitable pumping unit. The general arrangement of flow components in the proposed prototype design is shown in Fig. 1, while that of the model is shown in the frontispiece. The ensuing chapters are summary treatments of the experimental studies of the various major tunnel flow components and are accompanied by discussions of the design principles involved.

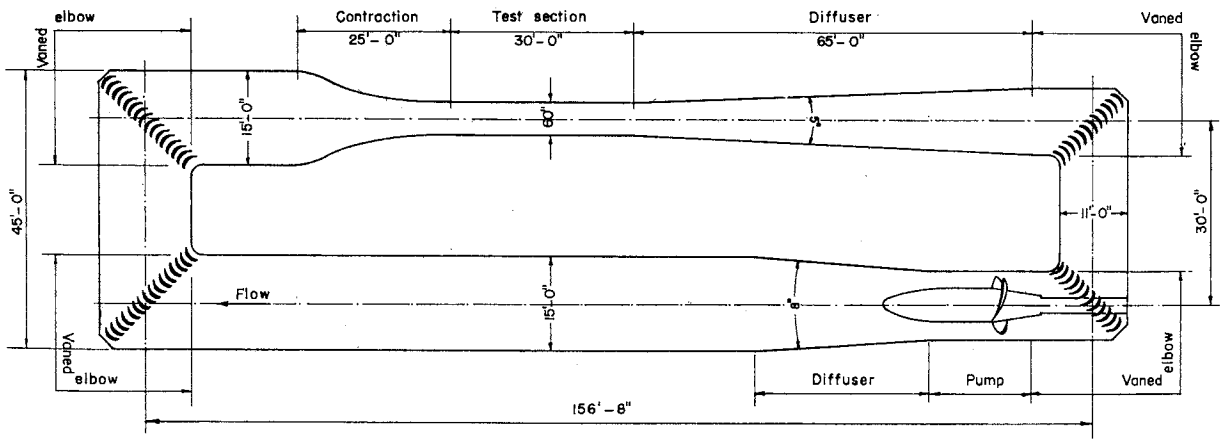

Fig. 1- Proposed 60-in. Water Tunnel

CHAPTER II. TEST SECTION STUDIES

A. General Considerations

The primary objective of a water or cavitation tunnel is the production of a controllable flowing stream of such quality that the mechanics of flow between the stream and the test body, mounted in the test section, most efficiently simulate the actual movement of the prototype body under natural, still water conditions. Special emphasis is placed on the ability of the stream to produce conditions of cavitation on the body.

While later chapters of this paper will serve to show that the various components of the recirculating system are capable of supplying to the test section a flow stream possessing most of the desired properties, it is the objective of this chapter to clarify the manner in which the test section of the tunnel can best perform its function when using the stream supplied by the remainder of the system. In the following pages the reasoning leading to the selection of the geometry and operating limits for the test section of the proposed tunnel will be described.

B. Design Studies

1. Size

a. Area

The size of jet cross section was determined by the nature of the anticipated test studies. A separate study of this problem led to the original directive specification of a cross-sectional area of 16 to 20 sq ft. This study was based on a summary of the anticipated types of tests followed by an analysis of the minimum model size of each type which could produce usable test results. A minimum size of model was desirable for a maximum economy in construction and ease of handling and because it would lead to greater tunnel work output. This minimum-size model was dictated by scale effects involving viscosity or the Reynolds number, pressure or the cavitation parameter, and other minor criteria between the model and prototype, as well as by the minimum size in which suitable instrumentation could be practically installed. Wall interference corrections dictated the size of jet required to accommodate the model.

In this case the jet diameter was arbitrarily made approximately six times the diameter of the critical test body. This ratio was employed

because data from aeronautical literature indicated that a cylindrical body in a cylindrical stream of these proportions would give results in which the wall interference effects were at a limit of acceptability.

In view of the fact that the proposed tunnel was to be an "all purpose" type with an undetermined future use, the area was selected generously in conjunction with the shape determination, as treated below.

b. Shape

The external boundary form of the test section is largely determined by the pressure conditions which are desired to prevail in the test stream. As will be separately described later under the pressure discussion, a boundary form consisting of solid parallel walls or a "closed jet" was elected for the prototype needs.

A circular cross-sectional boundary shape was finally selected for the following reasons:

(1) For general model testing, a circular boundary would probably afford as little wall interference effect as any other shape.

(2) In passing from the contraction to the test section as well as from the test section to the diffuser, area transitions could be accomplished with perfect lateral symmetry without shape transition, if circular transitions were adhered to throughout. Tests indicate a smoother and less turbulent flow could be expected in such a transition. Observations on rectangular transitions have shown vortex filaments in the corner regions.

(3) A circular section is inherently more efficient in the use of structural materials for resistance to the differential pressures to be expected.

(4) Control of dimensional accuracy and surface finish could be achieved most economically when machining circular sections.

The overall shape and size requirements are satisfied by selection of a cylindrical boundary of 60-in. inside diam.

c. Length

One of the longest models proposed for test in the tunnel is a torpedo shaped form and its wake. The total study length of the body and wake may be as much as 30 body diam. If the maximum body diameter is taken as one-sixth that of the test section, as previously selected, the total test section length should be at least 5 section diam.

It is recognized that the downstream portion of the test section jet deteriorates in flow quality as the length increases, but the fact that this is accomplished without significant effect on the quality of the upstream portion of the jet permits arbitrary selection of a generous length. From the economic standpoint a moderate increase of test section length could have but little effect on the total construction cost, as it represents only a small percentage of the total tunnel length; however, it could have an appreciable effect on operating cost, as the input power is largely consumed in the high velocity regions in and adjoining the test section. A consideration of the above factors led to an arbitrary selection of a test section length of 30 ft.

2. Speed

The speed range anticipated as necessary in the proposed tunnel varied from a low value of about 3 fps for certain towed body studies to the maximum which might be practically attained. This maximum was considered desirable for simulation of speeds and cavitation conditions encountered with modern subsurface ordnance.

European practice, for purposes of operating economy, generally leans toward cavitation simulation through operation with low pressures and moderate speeds; however, certain deficiencies inherent to low pressures, such as release of dissolved air, produce difficulties which can be partially eliminated by changing to higher pressures and higher speeds. To permit maximum testing flexibility, it was considered desirable to provide the maximum practical operating speed for the proposed facility. In determining what constitutes the maximum practical speed, two important trends must be recognized. These are the costs attending the rapidly rising power requirements, which vary approximately as the cube of the speed, and the inherent cavitation tendencies of the jet boundaries and model support system. Since economic criteria are always somewhat indeterminate, the speed limit imposed by cavitation conditions will be considered approximately to frame the upper critical speed limit.

In view of the fact that the test model may in itself be designed with optimum streamlining, it becomes apparent that a facility for testing such a model cannot operate appreciably faster than the limits of the test body without incurring serious cavitation on the tunnel boundaries or the model supports. While relatively little data are available as to the limiting

values in such a case, studies conducted in the water tunnel of the California Institute of Technology indicate that a speed of about 70 fps is a practical maximum when used in combination with reasonable pressure values. Since the above value is in fair agreement with the normal limits for the anticipated tests, a speed range from 3 to 85 fps (50 knots) will be assumed as generous coverage for subsequent design studies.

In examining the basic property of speed, it was apparent that a facility attempting to provide a flow stream simulating a body of water at rest must give consideration to the steadiness and uniformity of the velocity front. While it is true that the natural, still water condition is not ordinarily a state of complete rest, it is the objective of the design to produce a stream of maximum practical steadiness and uniformity.

The degree of perfection practically obtainable is the next consideration. The original directive specification states, "The variation in velocity across any transverse plane of the test section, up to within 5 per cent of the diameter from either boundary, shall not exceed 2 per cent." Calibrations of existing tunnels indicated that for most modern designs, a uniformity of about 1.0 per cent was commonly obtainable, and in a few cases values were about 0.5 per cent. In view of this, the proposed design attempted to obtain 1.0 per cent or better. As will be seen in a later chapter, it is the inherent function of the contraction cone preceding the test section to provide the necessary unification of the velocity distribution.

It must be recognized, however, that the mechanics of flow within the test section tend to reshape the uniform entrance velocity to the hyperbolic velocity profile common to stable turbulent flow in pipe lines. The reshaping of the flow takes place gradually with thickening of the retarded wall boundary layer and acceleration of the core flow until the boundary layer expands to a thickness equal to the duct radius. This growth results in an increase in the mean kinetic energy of the flow, with a consequent axial reduction in the pressure on a gradient greater than is usually evidenced by stable wall friction alone. While development of a stable turbulent front usually requires a flow distance of 20 to 40 diam from the point of inception and may normally be computed with fair accuracy, an estimate of growth in the 6 diam of proposed test section length will have no validity since the point of inception is unknown because of the partially developed boundary layer being delivered by the contraction.

Despite the inability of the analysis to yield valid values of the growth, it does show qualitatively the axial deterioration of jet quality and warns that the quality at exit will probably be less than called for in the directive specification. This is an unavoidable consequence of long test sections and must be accepted with their adoption.

In addition to uniform differences in the velocity distribution, due to the internal flow mechanics, unsteady velocity variations with time are also evident in most tunnels. These may be short pulses, long surges, or a continuous drift and may be due to such factors as deficiencies of the pump-motor unit, hunting after starting, temperature variations, power variations, etc. In addition to these bulk flow changes with time, local periodic flow eddies may be shed from certain parts of the contraction walls or other boundary components. While instrumentation obstacles have prevented evaluating these variables in existing water tunnels, evaluations have been made in wind tunnels with variations running as large as 10 per cent of the mean value.

In view of the possibility of using test bodies which may be sensitive to eddy impact or time transients, it will be necessary to design all components with a view to minimizing separation or high turbulence.

In addition to axial flow variations in velocity, it is necessary to make provision for suppressing rotation or angularity of the flow. However, since such variations originate almost wholly in the pumping unit, methods of control will be discussed separately in the chapter concerning the pump unit. In addition to the types of velocity variation just described, another form may occur when very large models are placed in the test section. Tests [1]* with a large model in the 5-ft Royal Aircraft Establishment wind tunnel indicated an image or shadow of the model was impressed on the exit flow to the extent that the shadow was still apparent on the velocity profile entering the test section from the contraction. This is, of course, undesirable and must be eliminated by redistribution of the flow in the return circuit. It is anticipated that the four vaned elbows and the propeller pump of the proposed circuit will give sufficient mixing; if not, a grid or honeycomb may eventually be found necessary in the prototype.

---

*Numbers in brackets refer to the corresponding numbers in the reference list at the end of the chapter.

Bradfield [1] provides an interesting aspect of the shadow problem in saying, "This forms a limit to the efficiency which it is desirable to achieve in tunnel design, because a tunnel requiring very little power to run it can have but little mixing and damping effect."

3. Pressure

Since a water tunnel differs from other types of flow-stream test facilities principally in the controllability of pressure in the test stream, this discussion will open with a review of the three basic ways in which test sections have been built to effect desired control of the pressure variable.

a. Open-Jet Tunnels (Recirculating Type)

In this type of tunnel the fluid jet issues from the contraction cone, flows unconfined through a testing chamber containing the same fluid at rest, exits from this chamber through a pickup cone, and then returns through a recirculating duct. This type of jet was originally evolved for wind tunnel work wherein the testing chamber was simply the open atmosphere. It had the advantage of providing complete vision and ready access to the model, and, because the pressure surrounding the jet boundary was uniform, the internal jet pressure along the axis could be assumed quite uniform. While small non-recirculating tunnels of this type have been built to waste the jet energy, for reasons of power economy, most designs find it necessary to regain this energy by returning the jet in a solid boundary after it leaves the test section. This pickup is usually accomplished by a flared cone followed by a diffuser and a return duct.

Friction between the fast moving test jet and the static fluid surrounding it induces strong eddies at the jet periphery in the form of a rapidly growing mixing zone and a rapidly shrinking jet core. As the distance between the entering contraction and the discharging pickup cones increases, the difficulty of smoothly squeezing the fast jet into the pickup cone rapidly mounts and violent cavitating impact of the eddies on the cone may occur. The net result of this is reduced speeds and short jet lengths if vibrations or pulses are to be avoided and a uniform core is to be attained. Such pulses not only physically hammer the structure but introduce pressure-velocity pulses in the flow which enters the circuit and is returned to the test section. Although numerous studies have been made of this problem, involving altering the cone shape and other artifices, no universally successful method permitting high speeds and long jets is yet known. As a consequence, most wind tunnels

of this type have a jet length less than twice the diameter. Water tunnels, because of the cavitation accompanying the eddies, are usually restricted to jets of a diameter's length and are apparently restricted to speeds of about 50 fps when operating under reduced or cavitating pressures.

In addition to its other deficiencies, the eddy system accompanying open jets consumes considerable amounts of energy. Early wind tunnel measurements indicated that such types of tunnels required twice as much driving power as a comparable closed-jet tunnel. Measurements in more recent tunnels indicate this ratio may now be reduced to 1.5 times or less.

In review of the foregoing, it is apparent that the limiting length and speed of an open jet are such as to eliminate this type of test section from consideration for the proposed tunnel, even though the internal pressure conditions are superior to other types.

b. Closed-Jet Tunnels

In this type of tunnel, the fluid jet issues from the contraction cone and flows through a test section having a solid and continuous peripheral boundary and thence into an expanding recirculating duct. This type of tunnel is seldom employed if an open jet can be applied because the solid boundary complicates mounting and access problems for the model and is the source of the boundary-layer flow which destroys the desired jet uniformity. The boundary layer is serious in that it produces an axially falling pressure gradient as the turbulent layer thickens and the core flow accelerates. However, despite the fact that these influences are detrimental, the presence of the fixed boundary suppresses the boundary layer to small scale eddying; and in consequence, a much more stable and efficient flow results than in the case of the unharnessed open jet. Accordingly, the closed jet is used where stability and speed are necessary, and various types of corrections have been evolved to compensate for its inherent deficiencies.

Among these corrections to the pressure forces acting on a test model is the compensation for the falling pressure gradient occurring axially in the direction of flow. Because this gradient is virtually linear, a simplified treatment of the force system considers this as a "horizontal buoyancy," and a number of papers have developed theoretical procedures for correction. In a parallel with this analytical method of adjustment, considerable work has been done on physical modifications of the test section

to produce a natural compensation. This can be accomplished by providing a slight downstream divergence to the test section boundaries.

The divergence modification has been occasionally used in wind tunnels since the very early days but is no panacea for the pressure problem, because the optimum correction is matched to only one speed of tunnel operation. The Voith (Germany) propeller channel, which is a special purpose tunnel, was tapered to suit the speed of most frequent testing, as were certain of the early Hamburg (Germany) tunnel designs. Divergence has not been employed with tunnels of more recent design; and it is not considered essential for a general purpose tunnel of the proposed type, although this may be considered debatable.

In addition to the above-described pressure problems incidental to the solid-jet boundary, other problems arise because of the interference of this boundary with normal flow lines about a mounted test model. While this interference effect is sometimes appreciable, adequate theoretical corrections for measured values are now known if the model size is not too large in relation to the jet size.

Variations of pressure in a plane transverse to the axis of a horizontal jet are of two types, namely, the pressure due to deficiencies of the contraction cone in effecting full pressure-velocity conversion and the pressure due to the normal gravitational gradient. Proper design of the nozzle can eliminate the former, and in most cases the latter gradient is quite consistent with the similitude of the test and should be present; therefore, no special compensation need be made for transverse pressure variations. The hydrostatic pressure induced by the vertical head of the chambered water does, however, determine the lower limit of pressures which may be achieved in the jet.

c. Free-Jet Tunnels

In this type of tunnel, the liquid jet issues from the contraction cone and flows through a test section where it is surrounded by a gaseous medium. This gas is chambered to permit reduction of pressure to very low values and accordingly, the pressure within the jet is everywhere reduced to this same value, both laterally and axially, without the vertical variation and superimposed hydrostatic heads found in the open or closed jets.

Because the jet is not buoyed up by the surrounding fluid, it is subject to the gravity force, and in a horizontal jet assumes a curved

trajectory. With moderate speeds this curvature limits the size of test models to small lengths. Positioning the jet vertically eliminates this difficulty but presents others. No wholly successful tunnel of this type has as yet been built.

The principal field for a free-jet tunnel is in the simulation of high speed underwater ordnance conditions where a very low cavitation pressure is essential for testing. The free jet is unique not only in the uniform, extremely low, static pressures attainable but in the fact that these pressures, being gaseous, are measurable with a high order of accuracy; for these reasons, it is superior to other types of jets for extreme cavitation. The jet is not, however, considered suitable to general purpose work because of the difficulties of operating at low speed and the high energy losses occasioned by trying to pick up the jet and recirculate it.

d. Comparison

In summary analysis of the foregoing tunnel types, it is apparent that the closed-jet form will best answer the need for a facility of high speed and general purpose use. In considering the value of pressure coverage to be desired, it is apparent that the lower limit must approximate the vapor pressure of water while the upper value should be as high as practical. Since the upper limit is largely a matter of balancing the structural costs against the value of the anticipated work program, a fixed selection is beyond the scope of this paper. Position or time variations of pressure are to be avoided and since they are generally intimately related to speed variations, their control will be affected in the manner previously described for the velocity variations.

4. Turbulence

The size and strength of eddy turbulence present in the flow jet of a model testing facility has long been recognized as an important factor in the applicability of the model data to the prototype. To insure that proper correlating indices be recognized, considerable work has been done using drag and pressure studies on spheres, foils, and other devices as a standard basis of comparison of testing facilities.

While the establishment of specifications for desired levels of turbulence is possible from these studies, it is impossible to predict the levels which will be achieved from a given design. Because turbulence is more readily

added to than eliminated from an existing flow structure, it has been considered advisable to design the basic tunnel components with a minimum practical turbulence output as the objective; this concept has been pursued in the designs treated in the later chapters.

It is intended that final turbulence control be effected through suitable honeycombs and grids placed just upstream of the contraction cone, where adequate space should be provided. These devices are capable of reformation and limited addition of turbulence above the minimum basic value provided by the tunnel itself.

5. Air Content

The amount of dissolved gas present in natural waters apparently has some influence on the inception of cavitation on bodies moving through such water, and accordingly, a water tunnel attempting to simulate such cavitation should properly operate with a gas content approximating that in nature. While this is a desirable objective, it is difficult to achieve in a practical water tunnel operating under subatmospheric pressure as this causes gas bubbles to grow and circulate in the flow.

To eliminate the bubble trouble, most tunnels follow a practice of depleting and removing the gas by application of high vacuum prior to the test run. While this procedure prevents true cavitation simulation, it was, at the time of this original design study, the only expedient known to cope with the problem and apparently produced no major discrepancies. Accordingly, no special provision for air content control was made in the basic flow circuit of the proposed design except for three air collection domes to assist in pretest bubble removal.

More recent efforts to improve this condition, in an existing tunnel at the California Institute of Technology, have established that a physical change in circuit form may be made so that the gases released in the low pressure test section may be reabsorbed in the return circuit. This is accomplished by physically extending a leg of the return circuit vertically downward to increase the static pressure and by increasing its diameter and length to such an extent that the return flow is subjected to the increased pressure for sufficient time to permit substantial reabsorption. Since the California Institute of Technology resorber had not been proved at the time these tests were initiated it was not a part of this test program.

6. Temperature

Temperature variations in the testing water of a variable-pressure water tunnel are a natural result of the energy input by the pump in maintaining recirculating flow against internal frictional resistance. It is essential consideration be given to the probable magnitude of such variations and the controls that may be necessary. This is essential because temperature is a fundamental variable in most flow problems and can produce changes of up to 2.5 times in the Reynolds numbers for temperatures varying from 60° to 150° F. While this factor may mean an important extension to the testing range in some problems, it is an annoying variable in many cases.

A review of the problems of heating, cooling, insulating, etc., indicates that a rigidly controlled external thermal unit would probably cost in excess of its worth unless the uncontrolled fluctuations appeared to be excessive. Preliminary estimates of tunnel mass and energy added by the pump indicate the temperature rise will be about 1° F for every 25 min of operation at maximum speed. This takes no account of heat lost through radiation, and for an appreciable span of operation at maximum speed, the rise would probably be less than 2° per hr or 16° in a normal 8-hr day. In view of the apparently nominal temperature rise, the geometry of the proposed design has no provision for temperature controls. If subsequent tests should establish the need, external facilities could be provided to effect the necessary control.

7. Diffuser Transition

The purpose of the diffuser or expanding cone of the water tunnel is to reduce the large discharge velocity of the test section efficiently. A later chapter will discuss the selection and tests on the diffuser proper; but, inasmuch as the boundary-transition curve between the test section and the diffuser is critical to the flow performance of the test section itself, a consideration of the transition characteristics should be included here.

The transition region is of special importance since it is the tunnel wall area on which cavitation first occurs. This is true because the static pressure is inherently lowest there, and in combination with high velocity and the initiation of curvilinear flow, cavitation is promoted. Such tunnel cavitation must be minimized since in body cavitation studies it is desirable to impose as severe conditions as possible on the test body without

cavitating the water tunnel; that is, the static pressure in the test stream should be as small as possible and the velocity on the test body as high as possible without occurrence of cavitation in the tunnel circuit. This is desirable for maintenance of high tunnel efficiency and elimination of boundary pitting and because the increasing use of sonic methods of observing cavitation on the test body makes it desirable to maintain a low ambient noise level.

An analysis of the limited amount of literature on this subject indicates that a number of theories have been advanced for the mathematics of the boundary transition curve to answer best the needs. These theories have been based on such factors as providing uniform rates of retardation (dv/dt = const), uniform velocity changes (dv/dx = const), and uniform head loss (dh_f/dx = const) for the bulk flow. While approaches of this kind are seemingly reasonable for the core flow of the stream, their application to the complex conditions existing at the boundary wall is highly questionable since the mechanics of combining an existing boundary layer with the unstable force influences attending expansion of flow is analytically indeterminate. In view of these inadequacies of the theory, there appears little justification for trying to approximate any transition curve on the basis of rates of change; rather, the total length of transition should be made long enough to avoid excessive rates of curvature and short enough to avoid the friction losses accompanying extended flow at high velocity.

On a purely arbitrary basis the transition was, therefore, made parabolic in form between points of tangency with the cylindrical test section wall and the 5° conical diffuser (Chapter IV) and of a total axial length between tangents equal to 1/2 test section diam or 30 inches. For this arrangement, in which $r_1 = 30$ and $dr/dx = 0$ when $x = 0$ and $dr/dx = \tan 5/2$ when $x = 30$, the equation of the curve is

$$r = 0.000728\, x^2 + 30$$

It is to be noted that the x-value refers to an origin shown in Fig. 27 rather than the more commonly used origin shown in Fig. 2.

C. Experimental Studies

1. Apparatus and Procedures

The test section for the model studies consisted of an aluminum alloy casting, machined to cylindrical form to make a smooth juncture at its

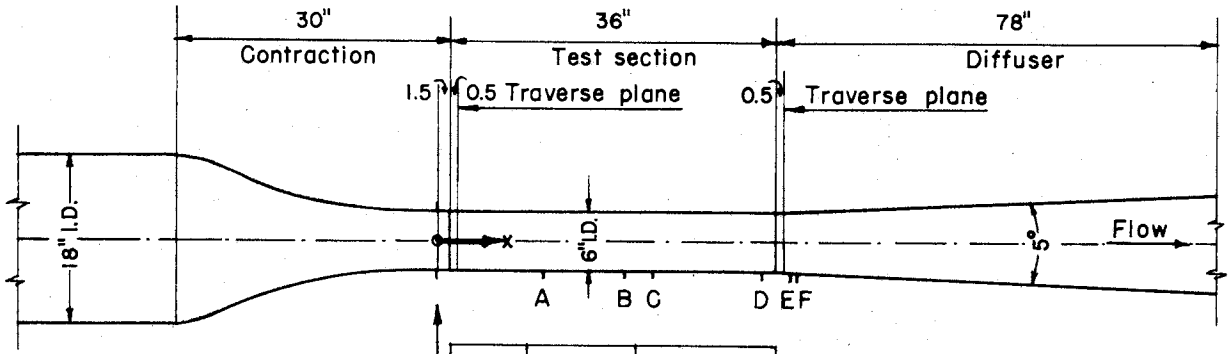

Tap	X(in)	Diam(in)
R	0.0	6.004
A	12.0	6.006
B	21.0	6.015
C	24.0	6.018
D	36.0	5.999
E	39.0	6.015
F	39.8	6.062

Fig. 2 - Sectional Elevation of Flow Circuit at Test Section

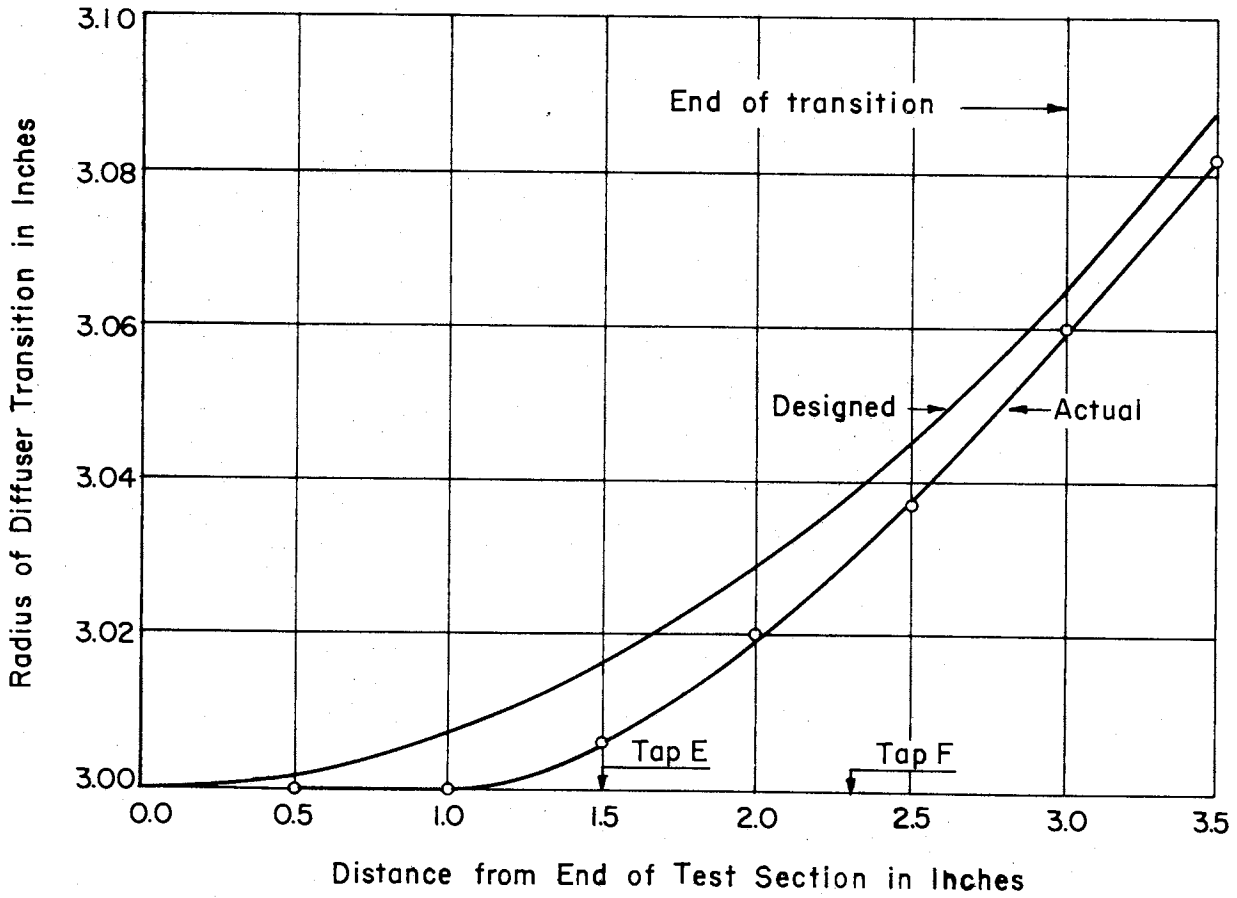

Fig. 3 - Actual and Designed Model Diffuser Transition Boundaries

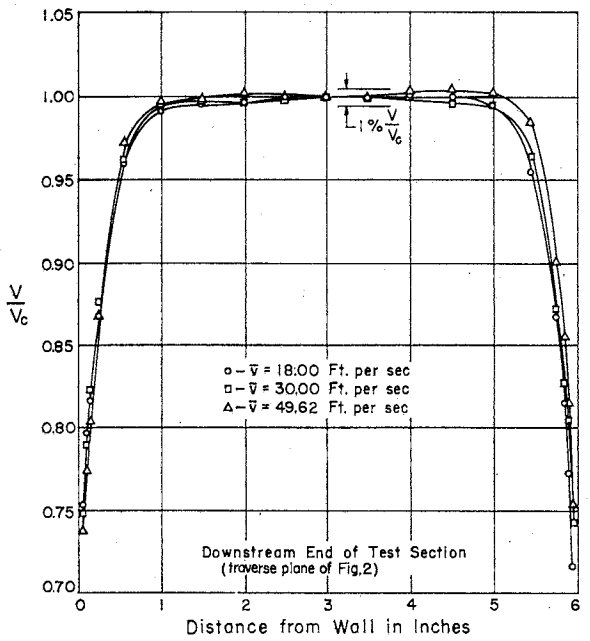

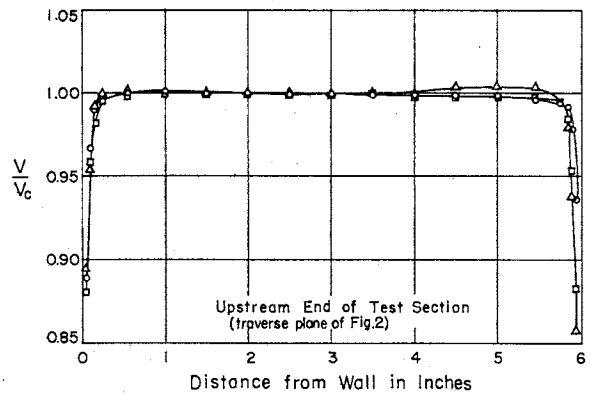

Fig. 4 – Velocity Profiles on Horizontal Diameter

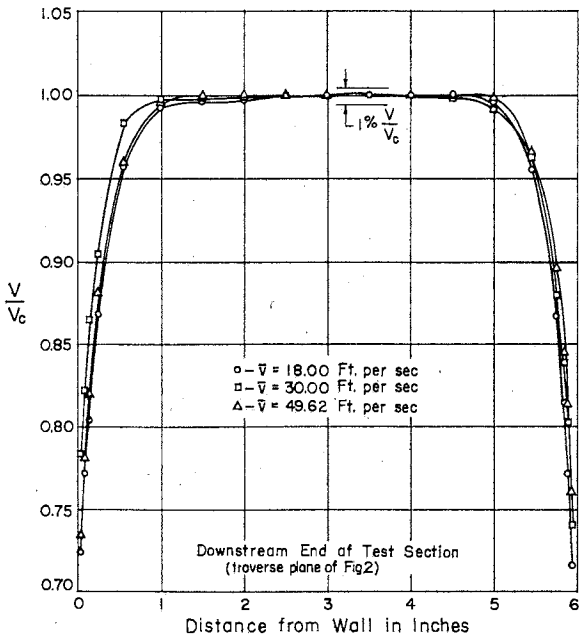

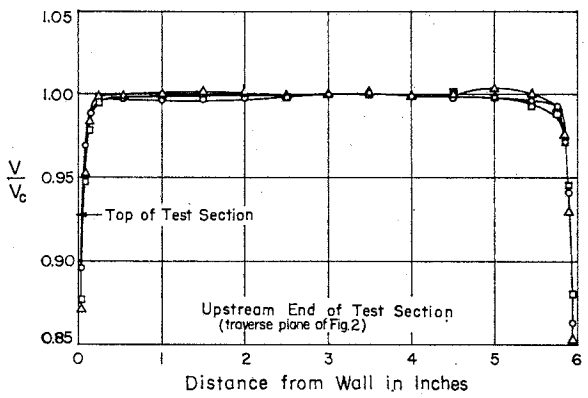

Fig. 5 – Velocity Profiles on Vertical Diameter

is well within the maximum prescribed variation of 1 per cent. Only in the boundary layer does the velocity fall below 99 per cent of the velocity at the axis of the test section and at the downstream end this has a measured thickness value of about 0.90 in. (0.15 diam).

An analysis of the thickness of the boundary layer in the test section of the prototype tunnel is made difficult because the Reynolds numbers of proposed operations are considerably higher than those for which the best ties between theory and data have presently been established. The problem is further complicated by ignorance of the exact state of flow in the boundary layer which the contraction would supply to the test section.

In accord with the following equation of Prandtl [2], the prototype boundary layer thickness at any point will be estimated from:

$$\frac{\delta}{x} = \frac{0.377}{Re_x^{1/5}}$$

where δ = thickness of boundary layer, x = distance between check point and point where boundary layer begins to form and $Re_x = Vx/\nu$. Although this formula is supposedly valid only for Re_x up to 2×10^7, it will be presumed reasonably valid for the prototype test section wherein Re_x will probably attain values to 2.3×10^8.

If ℓ_r is the scale ratio between prototype and model (in this case $\ell_r = 10$) for equal mean velocities of flow and equal kinematic viscosities,

$$\frac{\delta_p}{\delta_m} = \ell_r^{4/5} = 10^{4/5} = 6.31$$

In this relation, δ_p equals boundary layer thickness in the prototype, and δ_m equals the corresponding boundary layer thickness in the model. If this ratio were applied to the average thickness of 0.90 in., as measured at the downstream end of the test section, the corresponding prototype thickness would be of the order of $0.90 \times 6.31 = 5.68$ inches in from the boundary. Since the above value is based on an average velocity value of about 40 fps, the boundary thickness for the maximum proposed speed of 85 fps may be extrapolated from the above by noting that Prandtl's equation gives decreasing thickness with speed. This refinement will not be employed, however, as neither the average measured thickness nor Prandtl's equation are necessarily any better than approximations in this case. It will, therefore, be concluded that the approximate thickness of boundary layer at the downstream end of the test section will be around 5 to 6 in. for the higher speeds.

It should be noted that growth of a boundary layer in accord with the foregoing represents a deceleration of the boundary layer and a corresponding acceleration of the core flow to satisfy continuity conditions. Some insight into this progressive acceleration of the flow stream was gained by suitable integration of Figs. 4 and 5; and it was disclosed that for the model, the velocity of the central core was 1.010 $\overline{V}$ at the upstream end of the test section and 1.050 $\overline{V}$ at the downstream end where $\overline{V}$ is the mean section velocity. In the prototype, because the boundary layer is relatively thinner than in the model, the 6.31 thickness ratio will yield an upstream core velocity of 1.004 $\overline{V}$ and a downstream value of 1.036 $\overline{V}$.

3. Energy Loss and Pressure Distribution

The prime intent of boundary pressure studies in the test section is the evaluation of the high rate of energy loss occasioned by the local high velocities and a determination of the lack of uniformity of test section flow evidenced by an axial pressure gradient. Since no accepted method is available for computation of the energy loss in the inlet length of smooth cylindrical pipes, recourse is made to the more illuminating laws which have been derived for progressive skin-friction changes for flow along a flat plate held parallel to the stream. While there are some physical discrepancies involved in distorting a flat plate to a cylindrical pipe, it is a rational approximation where the boundary layer is thin relative to the pipe diameter. The validity of the application is verified by the model data.

The flat plate equations which will be used for the data analysis include the Prandtl [2] formula

$$C_f = \frac{0.074}{Re_x^{1/5}} \tag{1}$$

where C_f is the coefficient of drag. This is supposedly valid up to $Re_x = 2 \times 10^7$, or in the region in which the seventh-root law of velocity distribution exists. In addition, for Reynolds numbers higher than 2×10^7, the Kármán-Schoenherr formula [2], which is based on the logarithmic law of velocity distribution, has been found to be in accord with general experimental results:

$$\frac{1}{\sqrt{C_f}} = 4.13 \log_{10} (Re_x C_f) \tag{2}$$

Both Eqs. (1) and (2) are plotted in Fig. 6 for comparison with the test data.

Values of C_f in the model were determined by measuring the pressure drop along the test section using the pressure taps previously described and employing three different mean velocities of flow (18.0, 30.0, and 49.6 fps). The total pressure drop as experimentally determined and divided by the velocity head of the test stream is shown in Fig. 7.

In order to determine the portion of the total head loss properly assignable to frictional effects, the pressure drop as determined experimentally was corrected for the change in kinetic energy of the stream as it passed through the test section. This was based on values of:

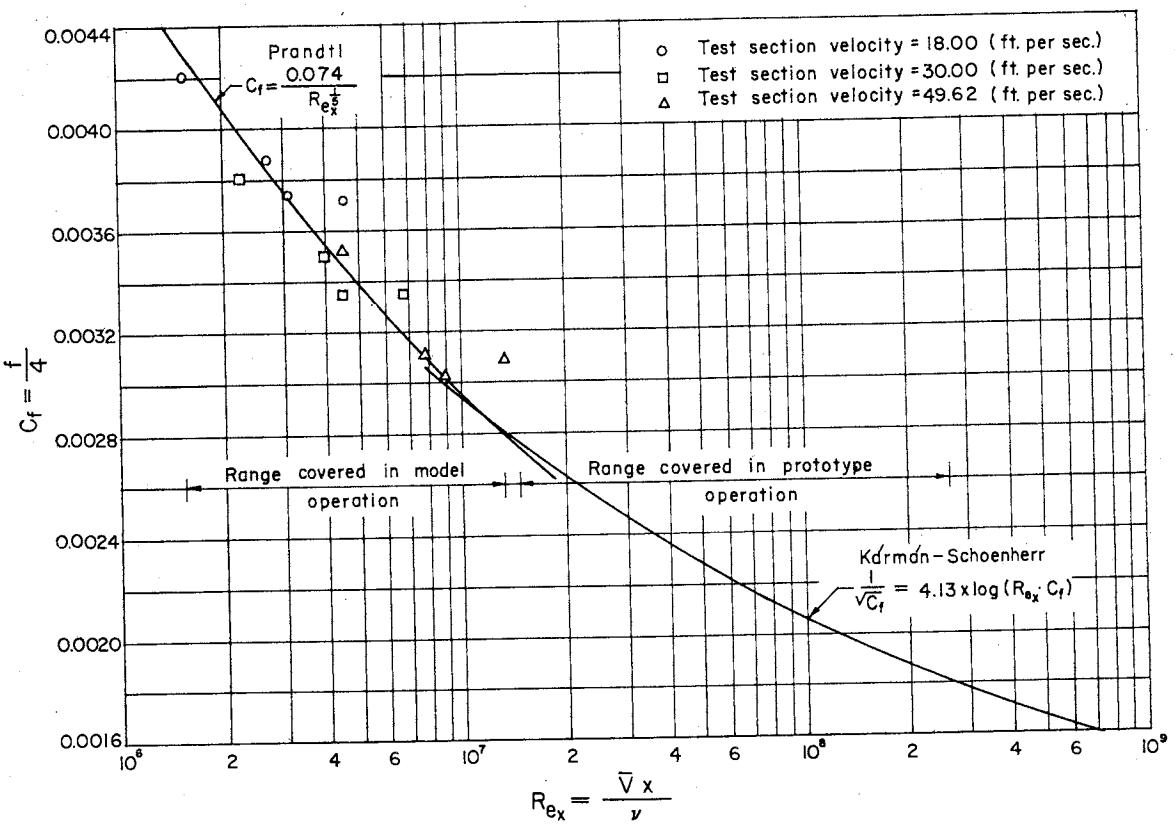

Fig. 6 - Friction Factor Vs Reynolds Number

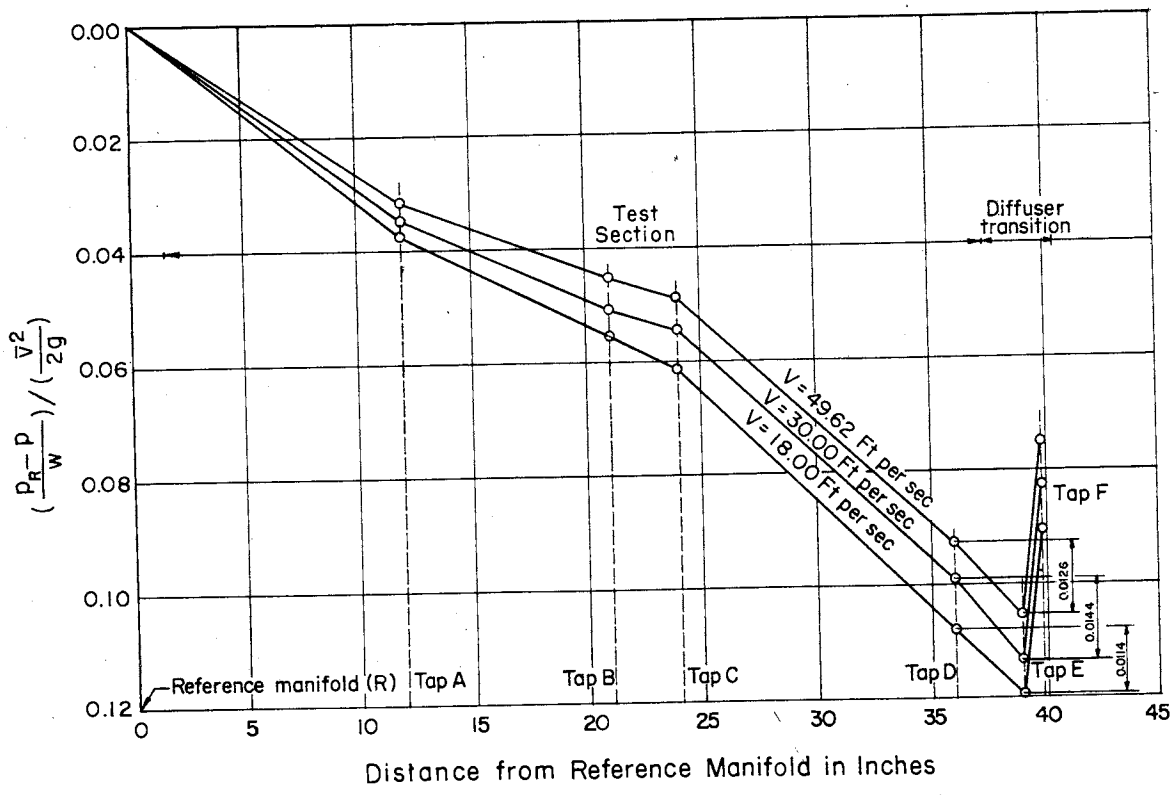

Fig. 7 - Measured Pressure Drop in Model Tunnel Test Section

$$\alpha = \frac{\Sigma \Delta A V^3}{A \overline{V}^3}$$

integrated from the velocity traverses of Figs. 4 and 5 and resulted in $\alpha = 1.0015$ at the upstream end and $\alpha = 1.0160$ at the downstream end. Values of α at the pressure taps and reference manifold were computed by linear interpolation or extrapolation. Since the diameter varied slightly, as shown in Fig. 2, correction was also made for the pressure change caused by the area change.

The total pressure drop was related to the frictional loss by using Bernoulli's equation

$$\frac{p_R}{w} + \alpha_R \frac{\overline{V}_R^2}{2g} = \frac{p}{w} + \alpha \frac{\overline{V}^2}{2g} + f \frac{x}{d} \frac{\overline{V}_R^2}{2g}$$

between the reference manifold and any tap where

p = pressure at a tap (pounds per square foot),
w = specific weight of water (pounds per cubic foot),
$\overline{V}$ = mean velocity of flow at a pressure tap (feet per second),
f = coefficient of friction,
x = distance from reference manifold to a pressure tap,
d = diameter of test section at piezometer tap, and
subscript R refers to the reference manifold.

From this

$$f \frac{x}{d} = \left[\frac{\frac{p_R - p}{w}}{\frac{\overline{V}_R^2}{2g}} + \alpha_R - \alpha \frac{d_R^4}{d^4} \right]$$

Values of f (x/d) based on the experimental data applied to Eq. (3) are shown in Fig. 8.

In order to extend the energy loss data from the model to the prototype through use of the flat plate extrapolation, the functional relation between f and C_f may be arrived at as follows. Since C_f as used in Eqs. (1) and (2) is defined by the drag expression:

$$F = C_f A \frac{\rho V^2}{2} = \overline{\tau}_o A$$

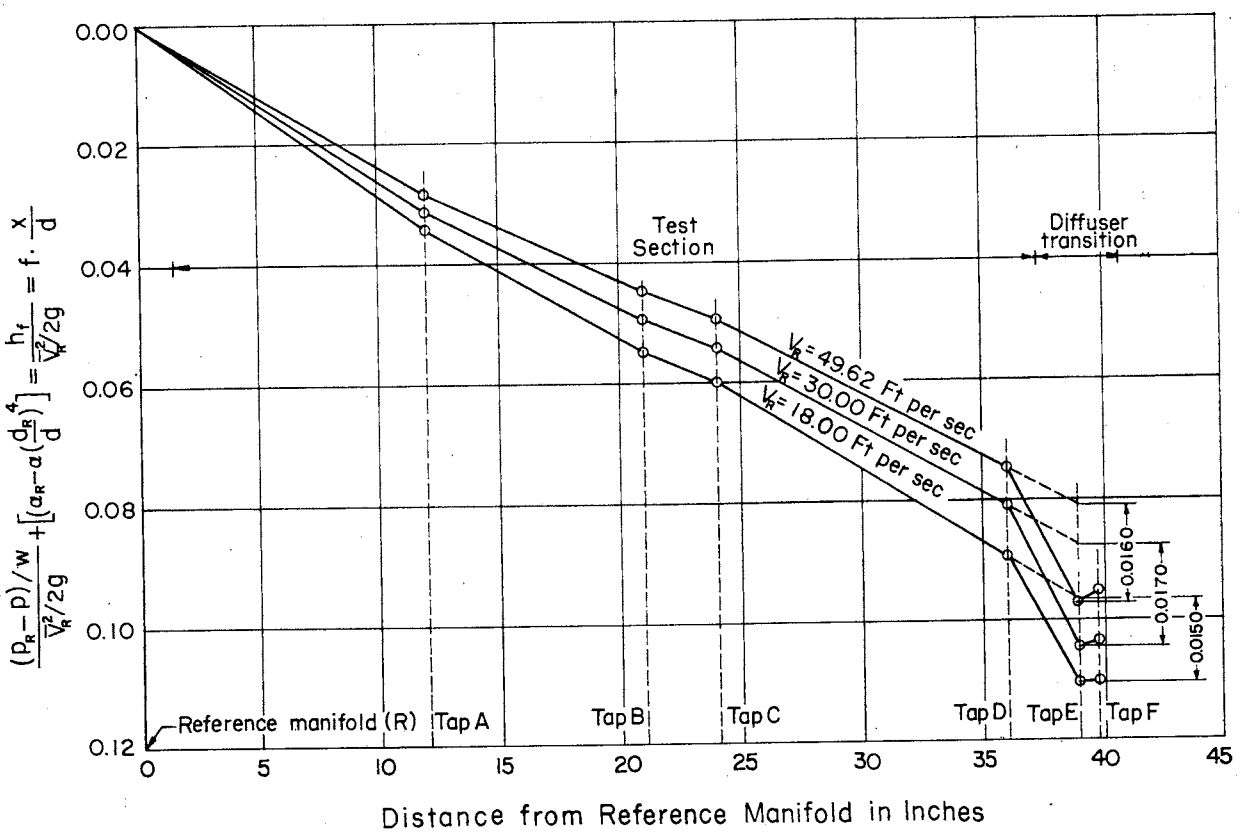

Fig. 8 – Computed Head Loss in Model Tunnel Test Section

where F = frictional drag force on one side of a plate of area A,

ρ = density of fluid,

V = velocity of free stream, and

$\bar{\tau}_o$ = average boundary shear on plate,

the relation between C_f and f can be computed because in a cylindrical pipe,

$$\bar{\tau}_o = \rho \frac{V^2}{2} \left(\frac{f}{4}\right)$$

Then $C_f = f/4$. Values of $C_f = f/4$ versus $Re_x = Vx/\nu$ are plotted in Fig. 6. In this plotting, values of Re_x were computed assuming x to be the distance from the manifold to a test tap. This seemed a logical assumption to make since the extrapolated values of a were nearly unity at the manifold. It is seen from Fig. 6 that the experimental points are in agreement with the semi-empirical curve of Prandtl.

In extrapolating the foregoing model data to the prototype, it will be necessary to use the Kármán-Schoenherr equation, since the values of Re_x

will, in general, be ten times as great as in the model and thus will exceed the range of Re_x for which the Prandtl equation is valid. Values of Re_x were computed assuming a water temperature of 75° F and assuming the boundary layer will originate at a point 1.25 ft upstream of the test section, which is a point corresponding to that assumed in the model (the reference manifold). Values of Re_x, f/4, and f (x/d) for the prototype test section are tabulated in Table I for four test section velocities at 5-ft intervals along the test section. The values of f (x/d) for x = 31.25 are plotted in Fig. 9, as is the value of

$$\left[\left(f\,\frac{x}{d}\right)_{x\,=\,31.25} - \left(f\,\frac{x}{d}\right)_{x\,=\,1.25}\right]$$

The latter is the expression most consistent with the losses originating in the test section proper.

In computing the variation in pressure along the prototype test section, values of α were recomputed, taking into account the relatively thinner boundary layer in the prototype. On this basis, the value of α at the upstream end of the test section will be approximately 1.0003 and at the downstream end 1.0127. It was again assumed that the variation in α between these points was linear and that α was 1.0000 at a point 1.25 ft upstream of the beginning of the test section.

Values for the total prototype pressure gradient including the effects of both the frictional energy loss and the velocity reformation are tabulated in Table I and plotted on modified coordinates in Fig. 10 for four velocities, the ordinate being the pressure difference in feet between the upstream end of the test section and any other point in the test section divided by the velocity head of the stream.

4. Cavitation Indices

As previously indicated under the diffuser transition design considerations, the pressure conditions under which cavitation will prevail in the tunnel are of prime interest for prototype application work. Comparative evaluations of the test pressure conditions will, therefore, be founded on application of the generally accepted index of cavitation,

$$\sigma = \frac{p - \frac{p_{vp}}{w}}{\frac{\bar{V}^2}{2g}} \qquad (4)$$

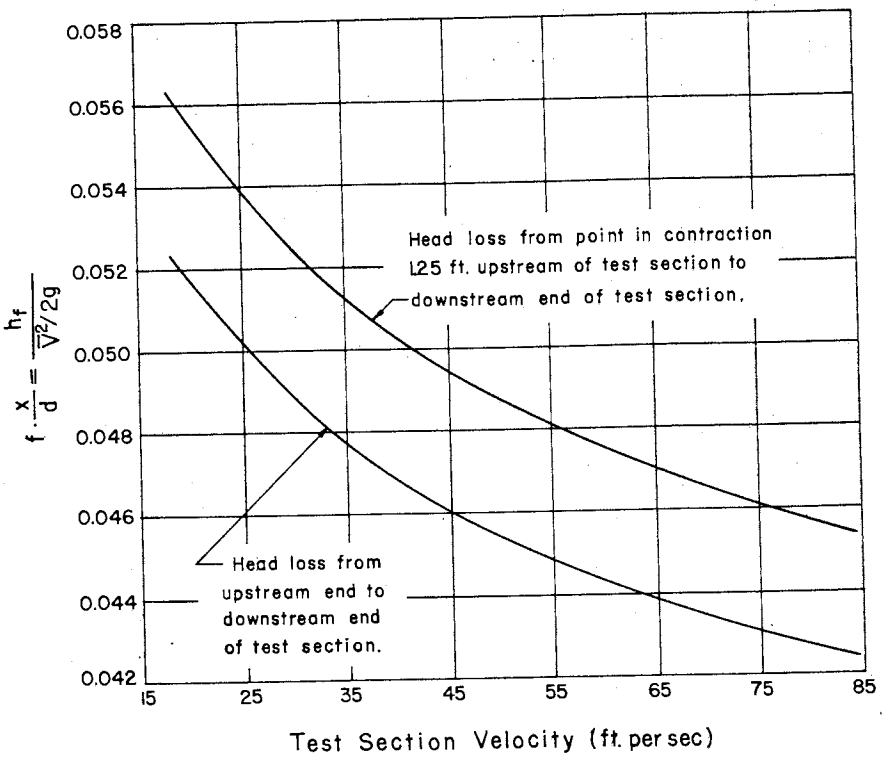

Fig. 9- Head Loss in Prototype Test Section

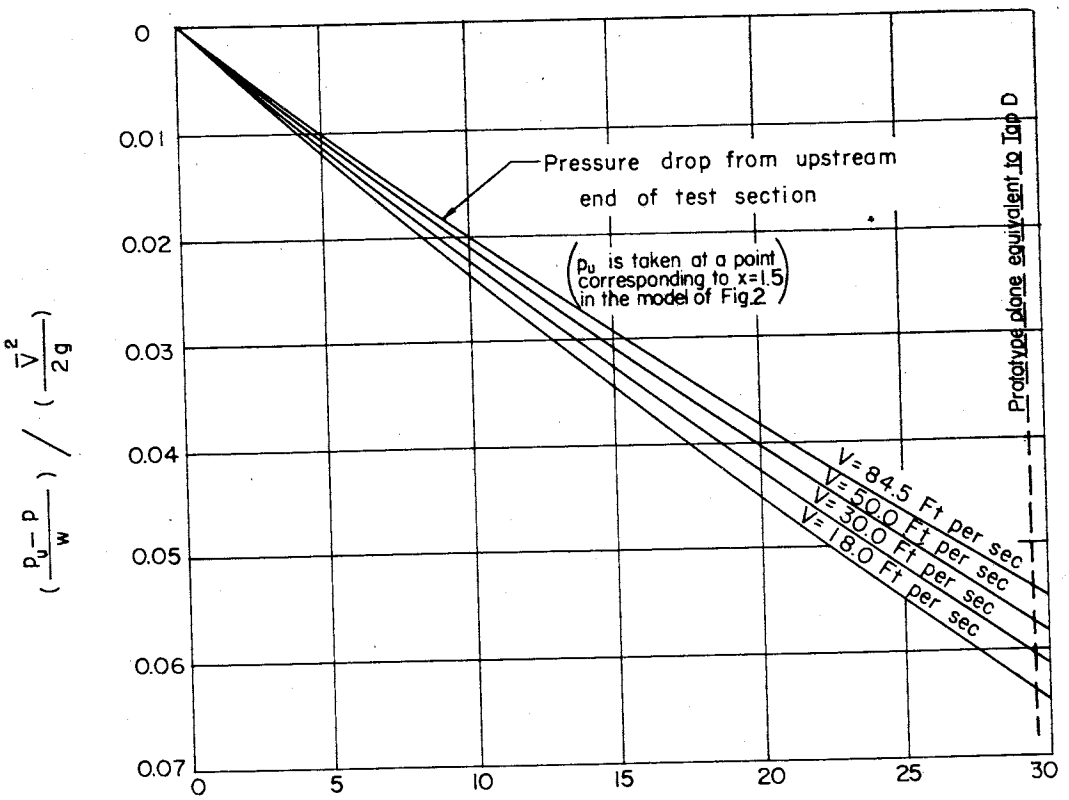

Fig 10- Pressure Drop in Prototype Test Section

TABLE I

TEST SECTION FRICTION AND CAVITATION DATA

x (ft)	$\bar{V}$ = 18.00 fps			$\bar{V}$ = 30.00 fps			$\bar{V}$ = 50.00 fps			$\bar{V}$ = 84.5 fps		
	$Re_x(10^{-7})$	$\frac{f}{4}$	$f\frac{x}{d}$	$Re_x(10^{-7})$	$\frac{f}{4}$	$f\frac{x}{d}$	$Re_x(10^{-7})$	$\frac{f}{4}$	$f\frac{x}{d}$	$Re_x(10^{-7})$	$\frac{f}{4}$	$f\frac{x}{d}$
1.25	0.225	0.00397	0.0040	0.375	0.00357	0.0036	0.625	0.00324	0.0032	1.060	0.00292	0.0029
6.25	1.125	0.00287	0.0143	1.875	0.00265	0.0133	3.125	0.00246	0.0123	5.281	0.00228	0.0114
11.25	2.025	0.00262	0.0236	3.375	0.00243	0.0219	5.625	0.00226	0.0204	9.506	0.00209	0.0188
16.25	2.925	0.00249	0.0323	4.875	0.00230	0.0299	8.125	0.00214	0.0277	13.73	0.00198	0.0258
21.25	3.825	0.00239	0.0406	6.375	0.00222	0.0376	10.625	0.00206	0.0350	17.96	0.00191	0.0322
26.25	4.725	0.00232	0.0486	7.875	0.00215	0.0452	13.125	0.00200	0.0419	22.18	0.00186	0.0391
31.25	5.625	0.00226	0.0563	9.375	0.00210	0.0524	15.625	0.00195	0.0487	26.41	0.00182	0.0454
	$\frac{(p_u - p_x)/w}{\bar{V}^2/2g}$		σ_{min}	$\frac{(p_u - p_x)/w}{\bar{V}^2/2g}$		σ_{min}	$\frac{(p_u - p_x)/w}{\bar{V}^2/2g}$		σ_{min}	$\frac{(p_u - p_x)/w}{\bar{V}^2/2g}$		σ_{min}
1.25	0.000		0.636	0.000		0.314	0.000		0.196	0.000		0.151
6.25	0.0124		0.623	0.0118		0.302	0.0112		0.185	0.0105		0.141
11.25	0.0237		0.612	0.0224		0.292	0.0213		0.175	0.0199		0.132
16.25	0.0345		0.601	0.0325		0.282	0.0307		0.165	0.0290		0.123
21.25	0.0449		0.591	0.0423		0.272	0.0401		0.156	0.0375		0.114
26.25	0.0550		0.581	0.0520		0.262	0.0491		0.147	0.0465		0.105
31.25	0.0647		0.571	0.0612		0.253	0.0579		0.138	0.0548		0.097

Note: The use of values carried to the fifth significant figure is a calculating and reference expedient and is not indicative of the order of accuracy of the experimental work which, in general, can only justify the third significant figure.

This index is a relative and arbitrary evaluation of the tendency of a boundary geometry to produce local regions of low dynamic pressure when subjected to a liquid stream. The local pressures under consideration are those sufficiently low to cause a change of state from liquid to vapor, with the attendant creation of a vapor cavity or bubble.

The three terms constituting the index are:

p = the ambient absolute pressure (pounds per square foot) at a point on a selected axis of the undisturbed flow stream before impinging on or being influenced by the boundary geometry under consideration.

Obviously, this static level of pressure is important to any cavity formation irrespective of the pressure changes created by dynamic actions.

p_{vp} = the vapor pressure (pounds per square foot) of the fluid.

$\overline{V}^2/2g$ = the dynamic head represented by the relative velocity (feet) of the undisturbed approaching flow stream. While this velocity is not the local velocity creating a low local dynamic pressure, it is a convenient and usually available value for the relative measurement of the local velocity and the local dynamic pressure.

The combination of these three terms in the form of Eq. (4) has sometimes been described as a ratio of the net pressure available to collapse the vapor cavity (or the pressure necessary to maintain the stream in contact with the body) to the pressure available to open it. The σ_{cr} value for incipient cavitation is the ratio under the particular conditions when the formation of cavities is initially sensed. Intuitive reasoning points out that this critical value will be relatively high for bodies of poor flow form and relatively low for streamlined or faired flow forms.

It should be noted that this index is not as rigidly descriptive of the prevailing cavitation condition for tunnel studies as it is for the moving body studies to which it is normally applied. This is true because the absolute pressure of the undisturbed flow stream in infinite flow fields can normally be treated as a constant quantity with respect to its position in a spatial plane, whereas the pressure in a water tunnel stream varies in all directions, including the axial direction. The data should therefore be presented to show this axial variation in the tunnel.

Since operation of a prototype tunnel will usually be devoted to cavitation studies of submerged body forms mounted on the test section axis, the limiting or least attainable value of the cavitation index along this axis is of prime interest. While the limiting value is desired along the axis, the basic limitation is determined by the inception of cavitation at the crown of the diffuser and the limiting values must be computed by referring to the observed inception values of the model tunnel studies.

When cavitation occurred at the crown of the diffuser transition, the absolute pressure at the top of the transition at tap E was measured and

distribution and led to the prototype extrapolations shown in Fig. 10. Ordinate differences from this curve may be used to evaluate the second term of Eq. (5).

(3) The last two terms combine to measure the influence of the diffuser transition curve on the pressure p by evaluating the local drop in pressure occurring between the equivalent of tap D and the point of cavitation. This local pressure drop is the result of centrifugal effects incident to curvature of the boundary. The magnitude of the total drop is indicative of the effectiveness of the curvature easement and presumably was to be approximated by suitable measurements at the low pressure tap E. In the inception-cavitation tests which were conducted by noting pressures at tap E, an average evaluation of the fourth term of Eq. (5) for four tests was 0.058. It is apparent, however, that if tap E were really located at the point of lowest pressure, p_E should have been nearly equal to p_{vp} and the value of the fourth term would accordingly be nearly zero. Since it was found equal to 0.058, it must be inferred that tap E was not at the point of lowest pressure but instead recorded some pressure between p_D and p_{vp}. Because the fourth term is an incomplete picture of this local pressure drop between p_D and p_{vp}, the third term is introduced for completion and is evaluated at 0.013 as an average from the model tests of Fig. 7. It is probable that this value is influenced somewhat by boundary-layer effects but for lack of a rational basis of modifying it for scale, the full value (presumed conservative) will be applied in prototype extrapolations.

(4) The analysis serves to evaluate σ_{min} for the bare test section without a mounted test body. It is apparent that the presence of a test body would have substantial secondary influence on this value, but it is beyond the scope of this paper to give such consideration.

In determining the value of σ_{min} the tunnel water was first deaerated to eliminate the variable and obscuring effects of gas release during the tests. Deaeration was accomplished by lowering the tunnel pressure to approximately -30 ft of water relative while the tunnel was operated at a very slow speed for about 1 hr, or until no more dissolved gas was withdrawn from the water. The instrumentation and control for the pressure and velocity were as described in the appendix.

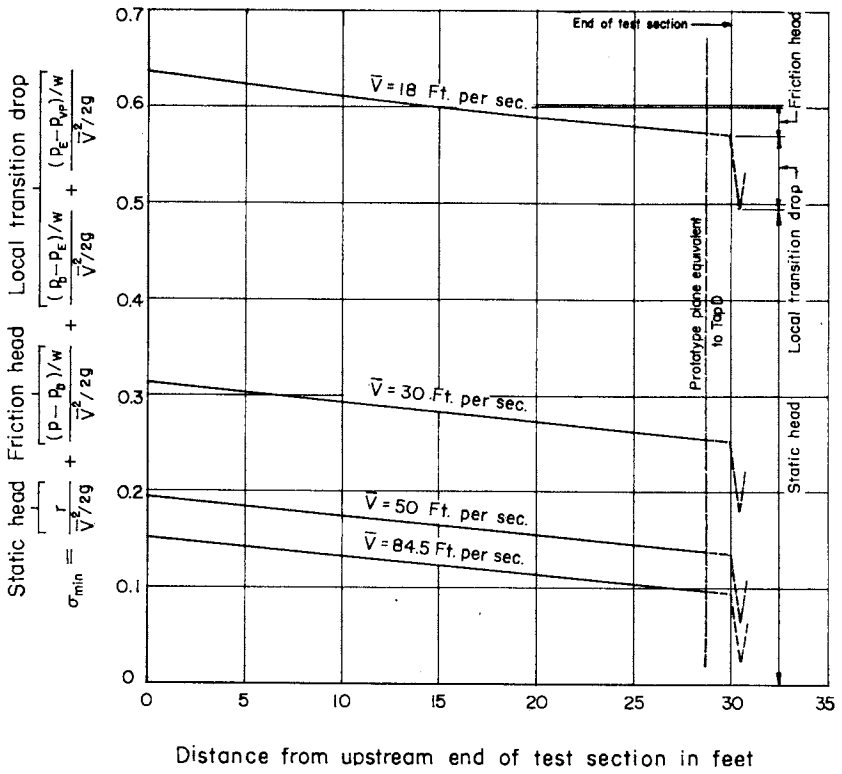

Fig. 11 - Estimated Minimum Cavitation Index Along Axis of Prototype Test Section

After deaeration, the tunnel pressure was raised to above atmospheric pressure and the test section velocity was set at the desired speed. The pressure was again reduced until cavitation occurred quite violently in the diffuser transition, as could be estimated audibly, and then the pressure was allowed to rise slowly. During this rising cycle, pressure was observed at tap E (minimum pressure tap—see Fig. 7) by use of a U-tube mercury manometer and was recorded at the instant audible cavitation ceased. Audible sensory reactions were materially increased by placing one end of a metal rod between the observer's teeth and the other against the wall of the tunnel in the zone of cavitation. The barometric pressure was obtained from an accurate aneroid barometer, while vapor pressures were based on standard tabular values for the measured temperature.

Values of σ_{min} based on the foregoing procedure were computed for 5-ft increments along the test section. The values are listed in Table I and plotted in Fig. 11. It should be noted that values of σ lower than σ_{min} might possibly be attained by increasing the speed or pressure beyond the condition of inception in the diffuser. Such practice will, however, lead to poor flow quality, lowered energy efficiency, and much vibration and noise.

D. Conclusions

On the basis of these design studies and experimental investigations the following general and specific conclusions were drawn with regard to test section design procedures:

(1) The operating requirements of the proposed tunnel apparently will be best served by a test section of the closed-jet type consisting of a circular cylinder of 5-ft diam and 30-ft length. The internal pressure deficiencies of the closed jet are offset by its ability to achieve high speeds with greater stability and efficiency.

(2) The nature of flow in the cylindrical test section of the proposed design was proved by model tests to have less than 1 per cent variation in axial velocities over the core-flow area of any section (central 90 per cent of the diameter).

(3) From tests it is estimated that the boundary layer surrounding the core flow of the prototype will have a thickness of 5 per cent of the test section diameter when measured at the upstream end and 10 per cent when measured at the downstream end.

(4) The presence and growth of the boundary layer is such that the uniform core-flow velocity is somewhat greater than the mean velocity and progressively accelerates in the direction of flow. Estimated values for the prototype indicate that the ratio of core-flow velocity to mean-flow velocity will be 1.004 and 1.036 at the upstream and downstream ends, respectively.

(5) The head loss from a point in the contraction cone 1.25 ft upstream of the beginning of the prototype test section to the downstream end of the test section will vary from $0.056\ \bar{V}^2/2g$ for a test section velocity of 18 fps to $0.045\ \bar{V}^2/2g$ at a test section velocity of 84.5 fps.

(6) The boundary pressure gradient along the designed test section will be nearly linear and the total pressure drop from the upstream end to the downstream end will vary from $0.065\ \bar{V}^2/2g$ for a test section velocity of 18 fps to $0.055\ \bar{V}^2/2g$ for a velocity of 84.5 fps.

(7) A proposed simple parabolic diffuser-transition curve of 1/2 diam length was actually built and tested with a length of 1/3 test section diam. This transition produced a local pressure drop equal to about $0.074\ \bar{V}^2/2g$. It is believed that increasing the length to a full test section diameter should materially reduce the local pressure drop.

(8) Initial cavitation of the tunnel boundary will occur at a point on the crown of the diffuser transition where the influence of curvature produces abnormally low local pressures. The cavitation at this point limits the minimum cavitation index for all other tunnel points by reason of the interconnecting pressure system. The limiting centerline cavitation index is almost linearly variable along the axis because of the existing pressure gradient and has values ranging from 0.636 at the upstream end to 0.571 at the downstream end for a velocity of 18 fps and 0.151 to 0.097 at 84.5 fps. It is important to note that the local pressure deficiency of the diffuser transition is an important factor in establishing a minimum cavitation index for the tunnel, but that its influence may be masked by the static pressures accompanying large test section diameters and by the frictional pressure losses accompanying long test sections. This is especially true in low speed operations, as shown in Fig. 11.

References

[1] Bradfield, F. B. The 5-foot Open Jet Wind Tunnel, Royal Aircraft Establishment. Aeronautical Research Committee Reports and Memoranda No. 1364 (British), 1930.

[2] Rouse, Hunter. Elementary Mechanics of Fluids. New York: John Wiley & Sons, 1946, pp. 187-88.

CHAPTER III. CONTRACTION STUDIES

A. General Considerations

A recirculating type of water tunnel is designed to produce a steady stream of fluid having uniform velocity, pressure, and turbulence characteristics in the test section comparable to those of open water prototype conditions. It is, however, apparent that the test stream as it leaves the test section and enters any conventional type of conduit recirculating system will progressively deteriorate in the uniformity of energy distribution, due to the growth of the boundary layer generated by the interaction of the fluid and the conduit walls. The eventual result of such boundary layer growth will be evidenced by velocity profiles possessing low values near the walls, and high values in the core of the flow, a characteristic which will require major correction before returning the flow to the test section.

In addition to the above deficiency of the recirculating system, it is apparent that the high velocities commonly employed in the test section will lead to excessive frictional energy losses and consequent pumping costs if such velocities are maintained in the recirculating system. It is, therefore, an economic necessity to reduce this velocity as rapidly as possible and to convey the flow at a lower and more practical value through the bulk of the circuit, following in turn with an acceleration to full value just before readmitting the stream to the test section.

Other sections of this treatise serve to show that the action of the diffuser, elbows, pump, and ducts fulfill their purposes in conveying the stream, but none of them operate to delay materially or to correct the establishment of the boundary layer which is so detrimental to the flow as it is discharged into the test section. It will, therefore, be necessary to provide some flow device to accelerate the velocity from the low value employed for economy in recirculation to the high values required in the test section and at the same time to provide a unifying corrective influence on the velocity profile. While a number of devices might conceivably be employed to provide the desired flow, experience dictates that use of a simple boundary contraction produces natural flow phenomena which achieve both desired effects with maximum efficiency. In view of the extreme simplicity of physical form and favorable performance history, it is appropriate that the mechanics of the device be examined to permit maximum utilization of their peculiar properties.

The physical relations producing the desired condition may be determined by applying Bernoulli's equation along a streamline of flow through the contraction, assuming the contraction is preceded and followed by flow conditions possessing static pressure distributions such that the differential pressure drop is practically constant for all flow filaments. Such an assumption is valid for established flow in straight cylindrical approach or exit conduits and should also be valid for a tunnel if the components of the recirculating conduits are properly designed. It should be noted here that all subsequent contraction analysis will be restricted to consideration of physical forms having only circular cross sections. This restriction is in accord with the selection of the test section as it is described elsewhere.

If Bernoulli's equation is written between a point "1" at the contraction entrance and a point "2" at the contraction exit, and energy losses are assumed negligible,

$$\frac{p_1}{w} + \frac{V_1^2}{2g} = \frac{p_2}{w} + \frac{V_2^2}{2g}$$

$$V_2^2 = \left[\frac{p_1}{w} - \frac{p_2}{w}\right] 2g + V_1^2 \tag{6}$$

where p = unit pressure,

V = local velocity of flow on a particular streamline,

w = unit weight, and

g = gravitation acceleration.

In addition to this, the area and velocity may be related by the equation of continuity as follows:

$$\overline{V}_1 A_1 = \overline{V}_2 A_2$$

or

$$\overline{V}_2 = \frac{A_1}{A_2} \overline{V}_1 \tag{7}$$

where A = conduit discharge area and $\overline{V}$ = mean velocity of flow at a cross section.

If it is assumed that there is a nonuniform distribution of velocity at the entrance to the contraction (V_1 as shown in Fig. 12) and the pressure

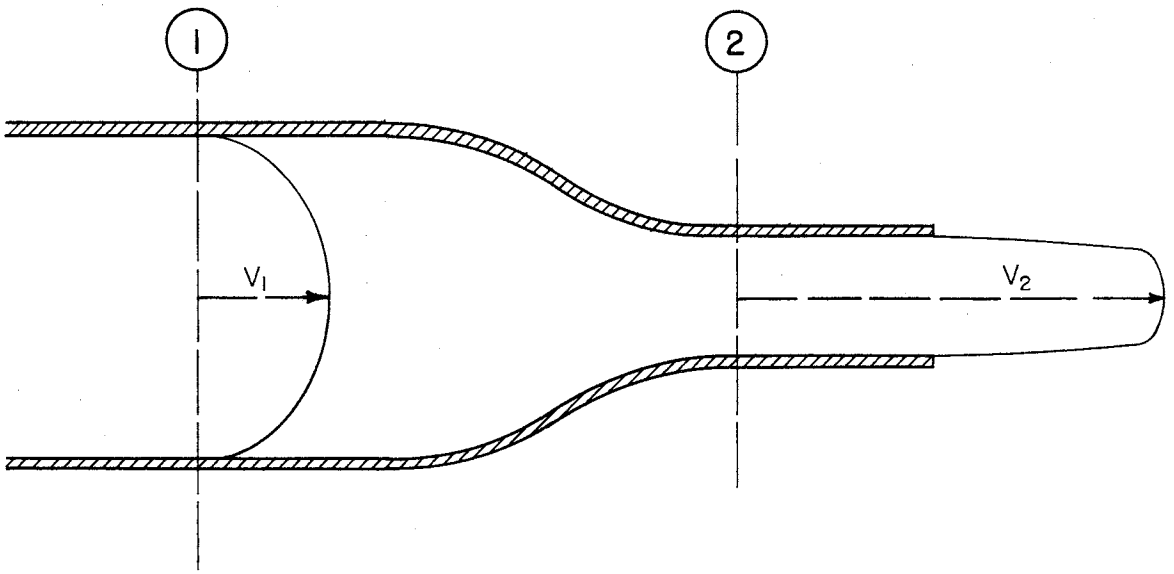

Fig. 12 - Velocity Profiles for a Contraction

drop is uniform, the graphic presentation of Eq. (6) as shown in Fig. 13 indicates that the velocity distribution at discharge from the contraction V_2 will be considerably improved in uniformity over that at entrance and that the degree of improvement is principally dependent on the magnitude of the area ratio of Eq. (7). A further analysis of the figure indicates the value of V_2 at various parts of the flow section is more or less independent of the corresponding value of V_1 because the kinetic energy represented by V_2 is largely supplied by the uniform differential pressure energy.

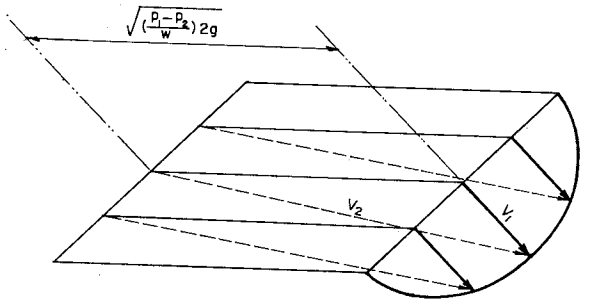

Fig. 13 - Graphical Summary of Velocities in a Contraction

In summary of the foregoing it may be said that a proper boundary contraction will serve as a powerful corrective to the velocity variations of a flow stream, provided that substantially uniform pressure distributions can be achieved in the flow sections preceding and following the contraction

by establishment of parallelism between flow filaments at these sections. Such parallelism in the upstream region is largely dependent on the design quality of the recirculating system while that of the downstream or test section region is dependent on the contraction boundary form. While this establishes the corrective possibilities of a boundary contraction with respect to velocity, it does not serve to point out the possible influence of the contraction on the turbulence characteristics of the stream. In view of the importance of this characteristic, it is appropriate that this influence be examined.

The turbulence characteristics of the open water conditions which the tunnel test stream attempts to simulate are not too well known, but observations in natural winds and in open air for aeronautical purposes indicate that, in general, a turbulence with equal strength in all directions (isotropic) and low relative values is to be expected in the usual natural flow field, except in boundary regions. Both theory and test for contracted air streams [1, 2, 3]* indicate that the following general relations apply to turbulence changes:

(1) Turbulence is considerably reduced by the contraction, provided it is made isotropic in character before being admitted to the contraction. Isotropic character may be approximately established by passing the flow through suitable screens or grids.

(2) While a general reduction occurs in the relative strength of turbulence, the contraction does serve to distort the initial isotropic character.

(3) The superimposed turbulent velocity component along the principal axis is reduced in magnitude in a ratio approximately inversely proportional to the area ratio A_1/A_2.

(4) The superimposed turbulent velocity components along the two lateral axes increased in proportion to $\sqrt{A_1/A_2}$.

In view of the above, it would appear that the most natural and satisfactory turbulence conditions will prevail in the tunnel test section when: the recirculating system minimizes production of turbulence, particularly that of large scale; space is provided upstream of the contraction to

---

*Numbers in brackets refer to the corresponding numbers in the reference list at the end of the chapter.

permit addition of screens or grids for turbulence control and decay, as dictated by eventual tests; and the contraction ratio is a maximum.

B. Design Studies

1. Selection of Area Ratio

Having established the general influence of area reduction on velocity distribution, it next becomes necessary to determine the magnitude of reduction for a specific tunnel performance.

Although test stream quality is largely dependent on achieving a maximum contraction ratio, it is obvious that economics and other factors may limit optimum values to more practical ranges. Fixed standards of quality are not available; but, it would appear from previous work in water and wind tunnels that a velocity variation across the test stream of less than 1 per cent is a prime objective for quality work. This, of course, recognizes that the velocity in the boundary layer must vary from zero to the velocity of the test stream core, but assumes that models tested in such a stream have dimensions sufficiently small to assure that the test section boundary layer does not influence the operation of the model mounted at the stream core.

A quantitative measure of the contraction influence on velocity variation may be arrived at in the following manner. If Eq. (6) is written along a streamline "a" and a streamline "b", the ratio of velocities on these same streamlines for a section downstream of the contraction will develop thus

$$V_{a_2}^2 = V_{a_1}^2 + \left(\frac{p_1 - p_2}{w}\right) 2g$$

$$V_{b_2}^2 = V_{b_1}^2 + \left(\frac{p_1 - p_2}{w}\right) 2g$$

$$\frac{V_{a_2}}{V_{b_2}} = \sqrt{\frac{V_{a_1}^2 + \left(\frac{p_1 - p_2}{w}\right) 2g}{V_{b_1}^2 + \left(\frac{p_1 - p_2}{w}\right) 2g}}$$

This may be translated to average conditions and established geometry by substituting the following:

$$V_{a_1} = K_a \bar{V}_1 \, , \; V_{b_1} = K_b \bar{V}_1 \, , \; \alpha = \frac{\sum \Delta A v^3}{A \bar{V}^3}$$

$$\frac{V_{a_2}}{V_{b_2}} = \sqrt{\frac{(K_a \bar{V}_1)^2 + \bar{V}_1^2 \left[\alpha_2 \left(\frac{A_1}{A_2} \right)^2 - \alpha_1 \right]}{(K_b \bar{V}_1)^2 + \bar{V}_1^2 \left[\alpha_2 \left(\frac{A_1}{A_2} \right)^2 - \alpha_1 \right]}}$$

$$= \sqrt{\frac{K_a^2 + \alpha_2 \left(\frac{A_1}{A_2} \right)^2 - \alpha_1}{K_b^2 + \alpha_2 \left(\frac{A_1}{A_2} \right)^2 - \alpha_1}} \qquad (8)$$

In order to gain some idea of the magnitude of A_1/A_2 necessary to keep the test stream velocity within the desired limits, it will be assumed that $V_{a_1} = 1.20 \, \bar{V}_1$; $V_{b_1} = 0.2 \, \bar{V}_1$; $\alpha_1 = 1.07$; and $\alpha_2 = 1.00$. These values have been arbitrarily selected as representing a severe demand on the reforming abilities of a contraction, inasmuch as they define an approach condition typical of a fully developed turbulent pipe flow. In this case $V_{a_1} = 1.20 \, \bar{V}_1$ is the maximum center velocity, and $V_{b_1} = 0.2 \, \bar{V}_1$ is an arbitrary limit such that values above 0.2 may be assumed to be part of the core flow which will be reformed, while values below 0.2 may be safely assumed to be contained within the boundary layer at section 2 and thus are not expected to be within the prescribed limits of variation. It might also be pointed out that $\alpha_2 = 1.00$ is an assumption on the conservative side, since values slightly greater than this will normally prevail. Since the above values relate to a flow system which probably will have considerably more distortion than is produced by the recirculating system of a well-designed tunnel, their application should lead to a conservative selection of the contraction area ratio.

Values of V_{a_2}/V_{b_2} obtained by substituting arbitrary ratios of end areas (A_1/A_2) in Eq. (8) are listed in Table II.

TABLE II

INFLUENCE OF CONTRACTION RATIO ON UNIFORMITY OF VELOCITY

Area Ratio $\frac{A_1}{A_2}$	Velocity Ratio $\frac{V_{a_2}}{V_{b_2}}$
5	1.020
6	1.014
7	1.010
8	1.008
9	1.006
10	1.005

In an effort to select an area ratio providing all necessary flow quality together with reasonable consideration of physical size and cost, the area ratios of existing wind and water tunnels were reviewed. The results of this comparison indicate that low turbulence wind tunnels with ratios as high as 25 have been employed, but the ratios for general purpose tunnels are more commonly restricted to the range from 5 to 10. In the case of water tunnels, ratios as large as 26 have been employed, but conventional designs lie between values of 6 and 9. Because of this and the desirability of obtaining a high velocity uniformity with low turbulence and reasonable construction costs, an area ratio of 9 has been arbitrarily elected for application in this case.

2. Selection of Boundary Curve

While the foregoing has summarized the general energy harness imposed on the velocity and pressure relations, it serves only to approximate the necessary ratio of areas without in any way defining the shape of the contraction boundary curve necessary to effect the transition between areas. In view of the fact that boundary forms can influence flow quality materially, the close proximity of the contraction to the test section necessitates a critical review of the available design methods. If the mechanics of flow through conventional forms of hydraulic contractions were examined, then the following

summary would approximate the order of complexity and possible benefits and detriments which might be derived from the use of each form.

a. The Plane Orifice in an Infinite Tank

While this form is not particularly applicable to the case of finite approach area, a wealth of related background information has been accumulated on its characteristics. For the case of the free liquid jet discharging into air, the characteristics of the flow in the plane of complete contraction (vena contracta) are a very high uniformity of velocity across the jet, with the exception of the outer layers which have been retarded by friction with the air and tank wall and parallel axial direction for all streamlines and all fluid particles at the uniform pressure of the surrounding atmosphere (except for a small constricting pressure from the peripheral surface tension).

An approximation of the pressure velocity transition is indicated in Fig. 14. In this it may be noted that internal pressures exist in the plane of the orifice as a result of the dynamics of the local curvilinear flow. Such internal pressures persist until parallelism is achieved at the vena contracta.

Where the jet discharges free and horizontal, the quality of flow is adversely affected, in that the lower filaments of the jet are subjected to a greater initial pressure than the upper filaments and accordingly will have a greater final velocity. This difference is, however, small when the orifice diameter is small relative to the head on the orifice. In addition to the above gravitational effect, a second effect is that the free horizontal jet will begin to show curvature of its axis as soon as the fluid particles leave the tank wherein buoyant effects are in force.

If the jet discharges when submerged, that is, into a still pool of the same liquid as constitutes the jet, certain important differences result in comparison with a free discharge. The most notable differences are: all filaments are subjected to the same differential head and accordingly both upper and lower filaments will have the same velocity; a horizontal jet is buoyed up in the still pool and is not subject to curvature as a result of gravity; there are no surface-tension forces effective in producing internal pressures; the liquid surrounding the jet offers a greater viscous shear than

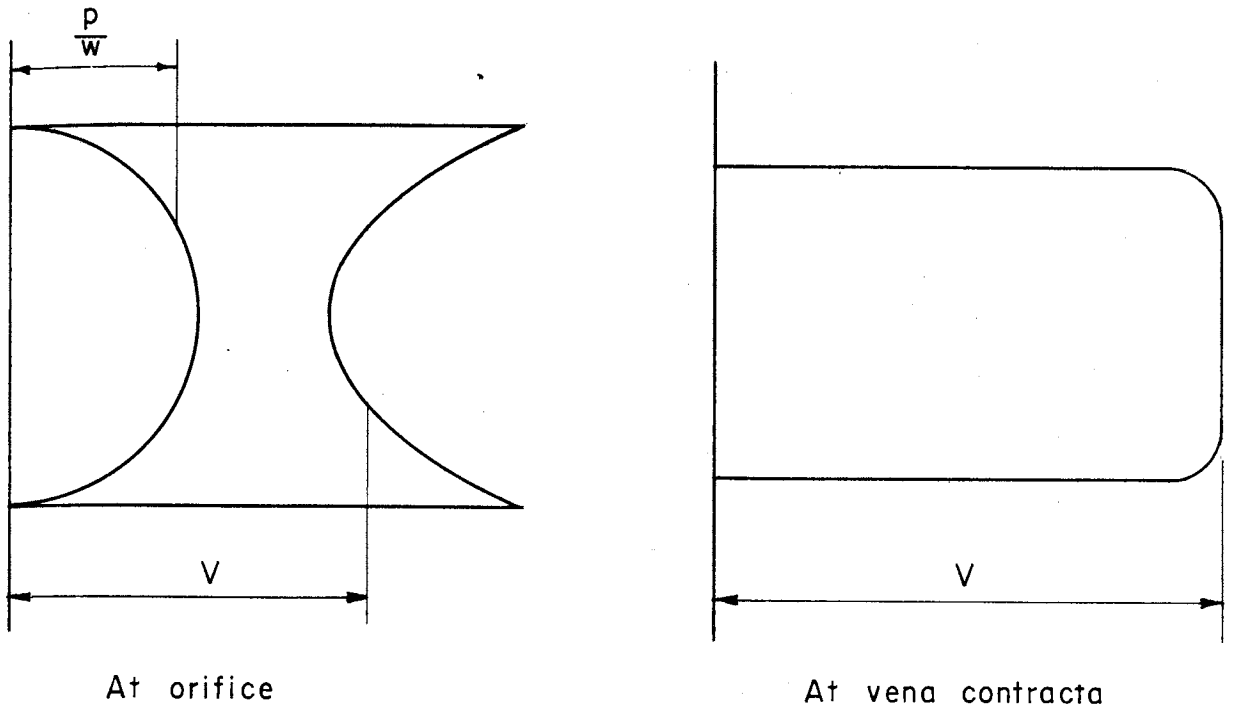

Fig. 14 – Pressure-Velocity Variations for a Plane Orifice Jet (After Daugherty)

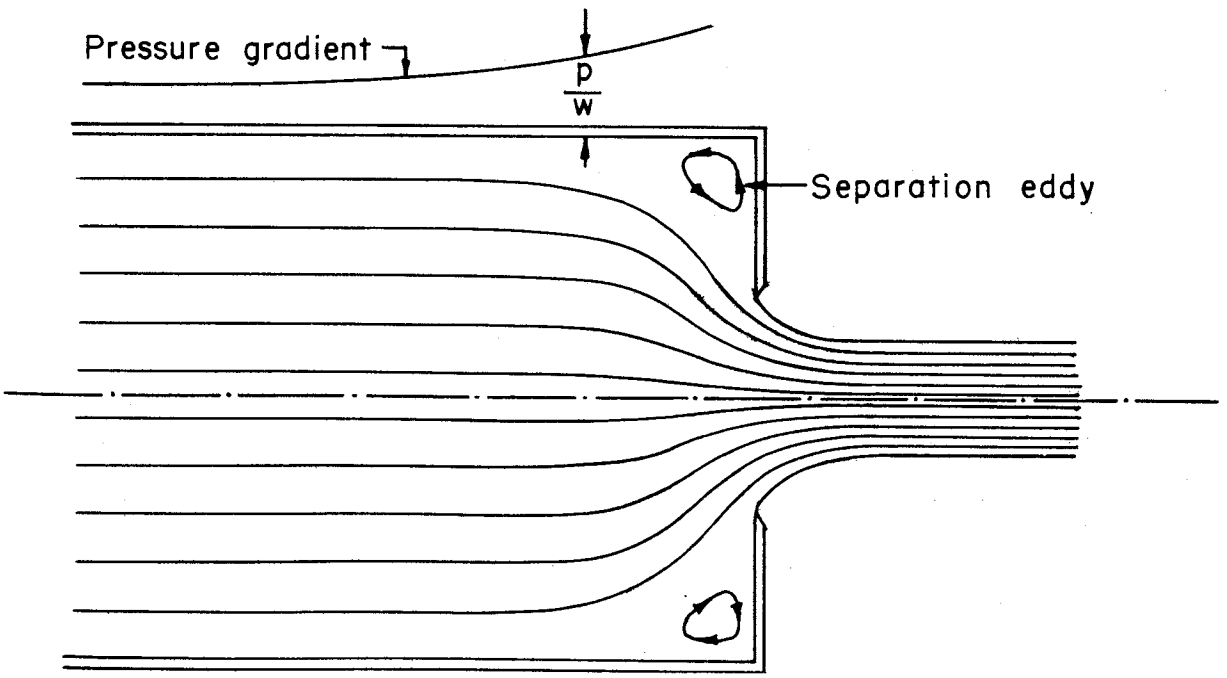

Fig. 15 – Eddy Pattern in the Plane Orifice Approach

is the case with gas and, accordingly, the jet periphery is eroded at a rapid rate due to the mixing action.

It is important to note that the dynamics of flow are such that both analytical and experimental studies establish the position of the vena contracta as being approximately 1/2 orifice diam downstream of the plane of the orifice irrespective of whether the jet is free or submerged.

b. The Plane Orifice Terminating a Cylindrical Conduit of Finite Diameter

The action of this flow boundary is very similar to that of the infinite tank, except that the presence of a boundary to the approach flow establishes a boundary layer which varies with the previous history of the flow and accordingly impresses a variation of velocity on the discharging jet. The magnitude of the discrepancy may be estimated by the method previously described under the section on the selection of area ratio, pages 39 to 41.

In addition to inducing the above velocity discrepancy, the flow confinement of the boundaries of the approach conduit establishes a streamline pattern which may be approximated by Fig. 15. It is to be noted that the balance of forces establishing the streamline curvatures just upstream of the orifice plate is of such nature that a stagnation pressure is approximated in the 90° boundary junction, with an increasing boundary pressure gradient as shown. The presence of such an adverse gradient in the path of the low velocity fluid particles approaching in the conduit boundary layer is such that an upstream motion is induced and a separation eddy begins to grow in the dead water area. It is the inherent nature of such eddies to grow progressively in size and peel off into the passing flow. This growth and peeling is intermittent and leads to detrimental time variations in the jet flow quality.

c. The Bell-Mouth Orifice Terminating a Cylindrical Conduit of Finite Diameter

The addition of a solid boundary to the curvilinear surface of the jet provides a means whereby the pressure on the outer filaments may be increased or decreased from that which prevails at the vena contracta, and thus provides some control over the streamline pattern. The solid boundary increases the viscous shear and promotes the establishment of a normal boundary layer rather than the mixing zone encountered with the submerged jet. While the boundary layer probably consumes greater energy, it is apparent that a more stable flow will result from the added constraint.

The geometry of the bell-mouth boundary may consist of a simple cone or a curve originating at either the conduit boundary (in which case no plane orifice would exist) or from the edge of the orifice. In either case, however, a dead water area is promoted in the angular corner of the boundary and separation eddies are to be expected.

d. The Ogee Orifice Terminating a Cylindrical Conduit of Finite Diameter

This flow boundary offers the same general control as the simple bell-mouth form, but has the advantage of providing no angular dead water area at the upstream end, thus reducing the possibility of separation eddies of large size.

e. Summary

A study of the shape of contraction curves employed in American and European water tunnels and discussions with a number of designers indicate that until quite recent date, water tunnel contraction curves were largely determined by adapting one of the foregoing forms of the plane orifice jet, with liberal usage of the arbitrary circular arc and intuitive French curve fairing as construction expedients. There is evidence that many low speed tunnels constructed by such methods operate successfully and with high flow quality, but there is also evidence that such designs, when employed in high speed tunnels, may be a source of trouble when a stable, low turbulence flow is the objective. Certain of these tunnels show the higher wall velocity and lower core velocity in the test jet apparent in the undeveloped flow of Fig. 14. This serves to indicate that such contractions are either improperly formed or excessively foreshortened to the extent that the contraction has not been fully accomplished within the cone and is still being completed in the test section.

An attempt to find a more rational and exact approach than is offered by intuitive fairing discloses that a number of related analytical solutions have been offered in the aeronautical literature of recent years. While all of these solutions do not have identical design emphasis, in general, the objectives seek a boundary form such that the boundary pressure gradient shall not possess regions having an adverse slope leading to separation of flow. A pressure gradient has been indicated in Fig. 15 and a partial solution offered in the form of a fairing for this dead water area. However, a more

detailed analysis of the flow mechanics indicates that application of an ogee boundary curve may eliminate the larger dead water areas but does not eliminate the basic, dynamic pressure effects which attend the reverse curvature of the streamlines. Thus, it is apparent that curvature of the approaching streamlines toward the conduit axis can be accomplished only if the solid boundary supplies the reaction pressure force necessary to achieve the flow curvature. The end result of such reaction pressures is a boundary pressure gradient which may be approximated by zone 1 of curve A on Fig. 16, rather than by curve B, which is the usual form arrived at by computing the pressure only on the basis of bulk values applied to a solution of the equation of continuity and a Bernoulli energy equation. Similar reasoning applied to the force pattern which must exist at zone 2 indicates that the reverse flow curvature can be accomplished only if dynamic pressures at the axis are higher than those at the wall. Accordingly, the presence of an excessive rate of curvature may produce a pressure dip as indicated on curve A. Obviously, a boundary pressure curve containing regions of adverse slope as shown in curve A will promote separation eddies in the areas indicated.

Further rationalizing as to the manner in which the pressure varies in a direction lateral to the axis indicates that in zone 1 the high dynamic pressures necessary to effect streamline curvature at the boundary must diminish to zero for the straight streamline along the axis. In accord with this transverse pressure gradient, Bernoulli energy relations along the various approaching streamlines will then require a velocity profile, the variation of which is approximated by the sketched curve. It is apparent from the nature of the approach flow that it is essential for an external force to be applied by the boundary if convergence is to be achieved.

If the same rationalizing is applied to the transverse pressure pattern that must exist in zone 2, it is apparent that a reversal of this transverse pressure gradient is in action, and accordingly, an inversion of the velocity profile must have occurred in flowing from zone 1 to zone 2. It also becomes apparent that the dynamic forces necessary to establish the flow curvature in this zone may, by proper design, be internally balanced to relieve the boundary wall of such excessively low pressures as are indicated by curve A. This possibility is established by the fact that the plane orifice jet, without solid boundary, normally discharges with a constant boundary pressure without the pressure dip indicated in curve A.

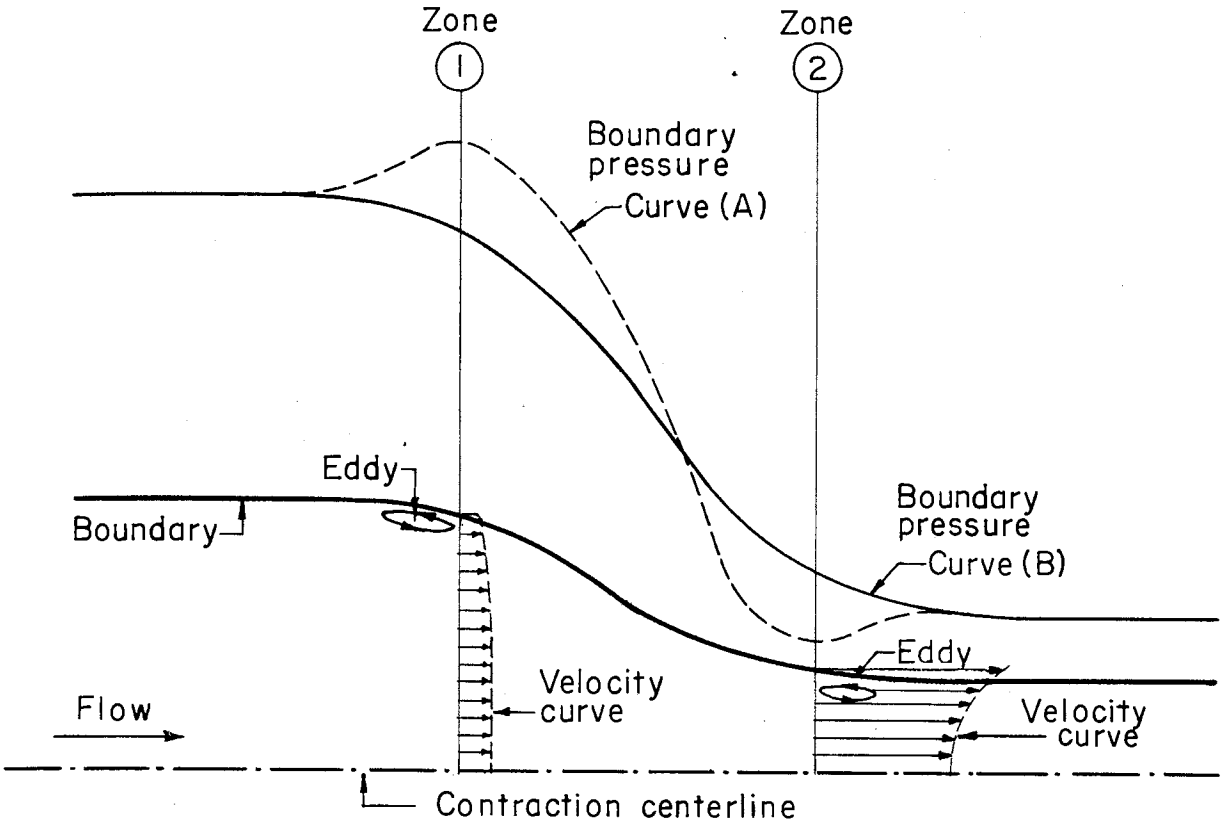

Fig. 16- Schematic Sketch of Pressure and Velocity Distributions for a Contraction

In view of the foregoing, the pertinent aeronautical literature was reviewed and the following general reactions were applicable to this case:

The analysis of H. S. Tsien [4] is founded on a desire to achieve a pressure gradient without adverse slope by determining a boundary streamline with a constantly increasing velocity. Tsien's solution applies particularly to determination of boundary curves which will eliminate the adverse gradient depicted in zone 2 of curve A on Fig. 16.

This analysis, based on potential flow theory, begins with a combination of the fundamental equation for irrotational flow and the equation of continuity to give series expansions for the axial and radial velocities that can be identified with the Laplace expression for the symmetric potential. These components may be combined to give the resultant velocity and the coordinates of the streamline. The solution to the mathematics of the original

equations and the exact shape of the resulting boundary streamline are dependent on the initial arbitrary selection of the velocity function along the axial streamline. For mathematical convenience in application to the series expansion, the velocity function was formulated consistent with reasonable physical velocity progression. The desired relation of entrance and exit velocity as determined by the area ratio is adjusted in the equation by suitable numerical constants. If this procedure is pursued, a family of stream-function curves of the form shown in Fig. 17 will result as a solution. Figure 18 shows the accompanying velocity curves for selected values of the stream function ψ. For such a family of curves, the following significant features may be noted: any of the continuous stream-function lines may serve as the geometric boundary of a contraction having the selected area ratio; the curves are asymptotic to the tangents formed by the upstream and downstream conduits; and, as indicated in Fig. 18, each stream function is accompanied by a boundary velocity curve of which the slope can serve to give evidences of the adverse pressure gradients previously shown in Fig. 16.

A very illuminating analysis by G. K. Batchelor and F. S. Shaw [5] leads to a set of stream-function curves very similar to those of Fig. 17. The analysis varies principally in the selection of the initial conditions, and in application of the mathematical method of relaxation rather than the series expansion of Tsien. It is noteworthy that the solution of Batchelor and Shaw pays particular attention to determination of a boundary curve which will minimize the adverse gradient depicted in zone 1 of curve A on Fig. 16.

Szczeniowski [6] also arrives at the same general curve but by still another mathematical approach. His solution is represented to be much simpler in computation than Tsien's and to have had successful application in a large Polish wind tunnel.

Goldstein [7], in his review of these three solutions, points out the deficiencies of these curves with respect to adverse velocity gradients near the inlet, and he presents theoretical treatments to improve the situation. The method is offered without experimental backing and depends on certain arbitrary selections.

Cheers [8], reasoning along lines quite different from any of the above, arrives at a radically new form of contraction which apparently offers

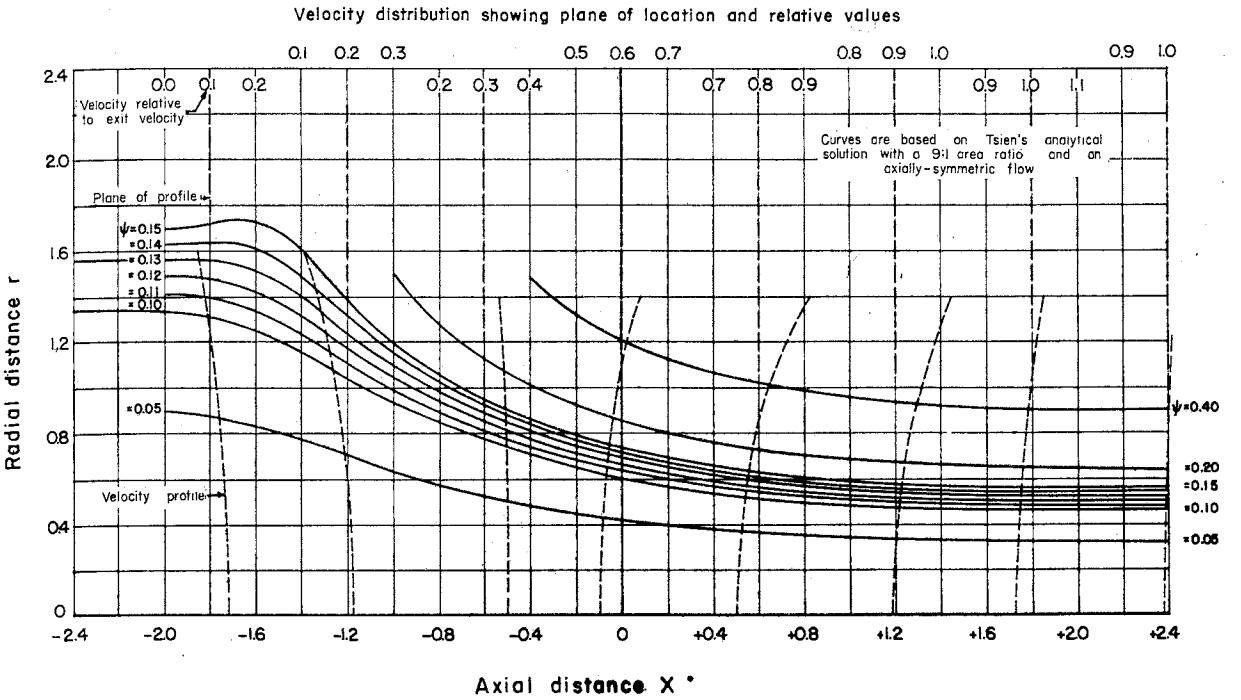

Fig. 17 - Contraction Boundary Curves

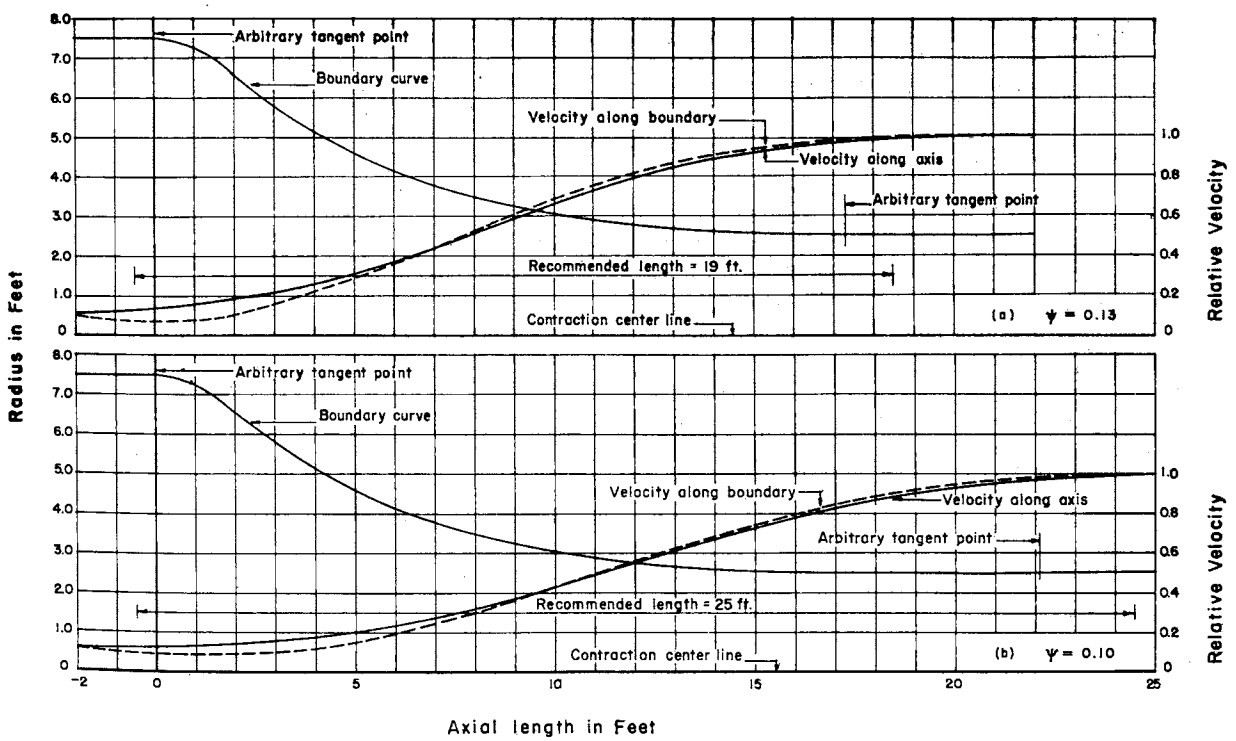

Fig. 18 - Selected Stream-Function Contraction Boundary Curves with Accompanying Velocity Curves

some benefits over the more accepted form. The method is offered without experimental support.

An overall review of these methods of arriving at a final design curve leads to the selection of Tsien's procedure as being the most suitable to this application. While the procedure appears to have certain drawbacks, the fact that its application led to successful results in the revised version of the California Institute of Technology high speed water tunnel seems justification for its use, as opposed to the untried theoretical offerings of the other methods. It should be noted, however, that the solution by Tsien's method is extremely lengthy and tedious and that substantially the same results might be obtained with less effort by employing one of the other methods. The comparison, being time consuming and of only academic interest, was not pursued in this case.*

It is also noteworthy that Tsien's method offers an indeterminate upstream solution for larger values of the stream function ψ. Such values are applicable where foreshortening of the cone is deemed necessary but must rely on intuitive fairing for the upstream curve with strong possibilities of separation conditions originating at this source. A detailed review of the Tsien data as summarized in Figs. 17 and 18 establishes the following salient findings with regard to the final boundary curve selection:

(1) The curve selection is founded on analytical procedure which takes no account of viscous action and is accordingly not wholly representative for the distortions occasioned by the boundary layer. Experience proves, however, that this omission is of minor significance in contracted flow except in the zone immediately adjacent to the boundary.

(2) The noticeable dip in the upstream end of the velocity curves as evidenced

---

*Rouse, Hunter, and Hassan, M. M., "Cavitation-Free Inlets and Contractions," Mechanical Engineering, Vol. 71, No. 3, pp. 213-16, March, 1949. This article describes a more recent and very promising approach to the contraction design problem, wherein a very material saving in time may be achieved through use of the electrical-analogy experimental method of determining boundary pressure distributions. The method permits rapid determination of values with a relatively inexpensive test setup. The method is somewhat limited in that it permits only physical testing of previously determined curves and does not permit an analytical design approach. However, cut-and-try tests of simple rational equations should approximate a suitable answer with greater economy than the tedium of Tsien's approach.

in $\psi = 0.13$ of Fig. 18 becomes progressively greater as the value of ψ increases, thus representing contractions of progressively shorter length.

(3) The dip in the velocity curve is directly associated with a rise in the pressure gradient and, accordingly, tends to promote separation; hence, decreasing values of ψ tend to suppress separation.

(4) Separation is a phenomenon complexly related to the previous history of the boundary layer entering the contraction and cannot be predicted on the basis of the idealized velocity curve alone. Therefore, in the interest of conservative design, the boundary curve represented by $\psi = 0.10$ in Fig. 18 has been arbitrarily selected for adoption in this application. While a slight decreasing velocity gradient still exists at the entrance, its magnitude is judged insufficient to produce serious separation effects.

(5) Selection of a curve of low ψ-value leads to long physical length and a thickened boundary layer on discharge.

(6) Since the ψ-curves are asymptotic to the upstream and downstream tangents, a practical contraction design must arbitrarily elect finite points at which tangency may be presumed to begin. The selected tangent points in this instance are shown on Fig. 18-b along with the recommended length of cone. It is to be noted that the downstream end of the contraction is beyond the point of tangency and gives a total contraction length of five times the jet diameter. This added length was considered necessary to achieve full development of the velocity distribution, which progressively improves with added length, as shown in Fig. 17. It is estimated that the velocity variation from center to boundary at the exit end of the "recommended length" is of the order of 0.75 per cent.

It is noteworthy that the procedure for selecting the boundary curve has included no evaluation of the turbulent conditions of the entering flow and no prediction of the turbulence to be expected at exit. While it would be highly desirable to be able to make such an analytical assessment, the complex and unknown state of the entering flow precludes any such possibilities. It is also unfortunate that the present state of knowledge of turbulence instrumentation does not permit making experimental evaluations in a model tunnel. Some consideration has been given to measurements employing the hot wire anemometer, but the complexities of its use in water are still unsolved. Consideration has also been given to use of the turbulence sphere but limitations of jet speeds and sphere sizes in practical model tests do not permit achieving

Reynolds numbers adequate to a proper study. Accordingly, as indicated in the section on general considerations, the control of turbulence will be restricted in this study to selection of the largest practical area ratio and provision of upstream space for screens or grids.

The computed coordinates for the curve represented by Fig. 18-b expressed in dimensions suitable for a model having a 6-in. jet diam are listed in Table III, together with the dimensions of the machined aluminum casting that was actually used for the contraction model studies. A later recomputation of the boundary coordinates by the David Taylor Model Basin disclosed some small errors; the recomputed coordinates are also listed in Table III.

Since the theoretical selection of contraction dimensions was based on a number of arbitrary evaluations and simplifying assumptions, it was deemed necessary that the design be checked experimentally to assure the desired flow quality in the tunnel test section. The prime objectives of model studies for such a purpose are the determination of the jet velocity distribution and the boundary pressure distribution. The following sections of this chapter deal with the experimental studies conducted in confirmation of the foregoing design considerations.

C. Experimental Studies

1. Apparatus and Procedures

The contraction cone for the model studies consisted of a single aluminum alloy casting smoothly machined and polished to provide a boundary transition between the 18-in. diam welded steel approach conduit and the 6-in. diam cast aluminum test section. The general relation of the contraction cone to the other tunnel elements is shown in Fig. 19 and the measured values of the cone coordinates are shown in Table III.

The interior finish of the surface was judged hydraulically smooth and was in dimensional agreement with the design values except in the region of $x = 24.5$, where a slight depression of 0.005 in. persisted as the result of an initial machining error.

Velocity traverses of the flow cross section were made in two planes, one located 6 in. upstream of the contraction beginning ($x = -6.0$) and the

TABLE III

COORDINATES OF THE CONTRACTION BOUNDARY*

Original Computed Values		Measured Values			Recomputed Values	
x (in.)	r (in.)	x (in.)	r** (in.)		x (in.)	r (in.)
0.00	8.999	0.00	9.00	Measured on template	0.00	9.000
1.33	8.932	1.50	8.95		1.34	8.955
2.67	8.699	3.00	8.75		2.68	8.781
4.00	8.366	4.00	8.47		4.02	8.382
5.33	7.699	5.00	8.11		5.36	7.754
6.67	6.986	6.00	7.62		6.70	7.021
8.00	6.199	7.00	7.08		8.04	6.299
9.33	5.699	8.00	6.50		9.38	5.658
10.67	5.166	9.00	6.02		10.71	5.111
12.00	4.733	10.00	5.58		12.05	4.644
13.33	4.333	11.00	5.21		13.39	4.286
14.67	4.000	12.00	4.88		14.73	3.994
16.00	3.746	13.00	4.56		16.07	3.736
17.33	3.586	15.00	4.04		17.41	3.521
18.67	3.400	17.00	3.68		18.75	3.360
20.00	3.300	19.00	3.41		20.09	3.239
21.33	3.200	21.00	3.25	Inside micrometer measurements	21.43	3.148
22.67	3.133	21.50	3.213		22.77	3.087
24.00	3.100	22.00	3.176		24.11	3.040
25.33	3.033	22.50	3.148		25.45	3.005
26.67	3.000	23.00	3.126		26.79	2.984
28.00	3.000	23.50	3.110		28.13	2.969
29.33	3.000	24.00	3.100		29.47	2.960
30.67	3.000	24.50	3.080		30.80	2.953
		25.00	3.070			
		25.50	3.049			
		26.00	3.033			
		26.50	3.020			
		27.00	3.013			
		27.50	3.006			
		28.00	3.003			
		29.00	3.002			
		30.00	3.002			

*Values of x are measured from the upstream end of the curve (point of tangency with cylindrical approach conduit). Values of r are radii measured from the axial centerline.

**When the cone was rebored, the boundary was shifted 1/2 in. downstream. Therefore, 1/2 in. must be added to the computed values of x before comparing the computed radii with the measured boundary radii after reboring.

other 1/2 in. downstream of the contraction end (x = 30.5). These traverse planes are designated as stations 12 and 1, respectively, in other sections of this report. The velocity traverses were made using a 3/8-in. diam "cantilever" Pitot cylinder in the upstream section and a 1/4-in. diam "long" Pitot cylinder in the downstream section. The details of this instrumentation are given separately in the appendix.

The casting was provided with 20 pressure measuring taps spaced along an axial line at the bottom of the cone, as shown in Figs. 19 and 20. It will be noted from Fig. 20 that three of these bottom taps were supplemented by side and top taps to yield manifold rings utilized as a part of the velocity measuring instrumentation of the tunnel. Details of this feature are described in the appendix. The pressure taps consisted of 1/32-in. diam holes, drilled normal to the wall and carefully deburred and chamfered at the inner end. The taps were connected by rubber tubing to 50-in. U-tube manometers filled with gage fluids of specific gravity suitable to the test velocity. Additional pressure data were obtained from a 3/8-in. tap used for velocity instrumentation in the plane x = -6.0 (see Fig. 19).

In order to determine the possible presence of separation zones which might not be detectable through the boundary pressure measurements, an experimental study of flow in the boundary layer was made by utilizing a flow streak technique [9]. This procedure consisted of painting the questionable boundary area with a thick mixture of white lead and turpentine and subjecting this dried surface to a stream of marking fluid, introduced through one of the pressure taps situated in the questionable area. The marking fluid consisted of a saturated water solution of hydrogen sulfide, which caused the white lead to turn to a visible black lead sulfide in the contact areas. The solution was fed into four taps in the contraction cone: the tap at the bottom at x = 1.5; the tap at the bottom at x = 4.0; the tap at the left side (looking downstream) at x = 17; and the tap at the bottom at x = 28.5. The solution was slowly admitted through the pressure tap holes with the tunnel operating at a test section velocity of 50 fps. The flow delineation accessories are shown in Fig. 20.

2. Velocity Distribution Studies

The upstream and downstream velocity distributions resulting from experimental measurements at the two traverse stations previously described

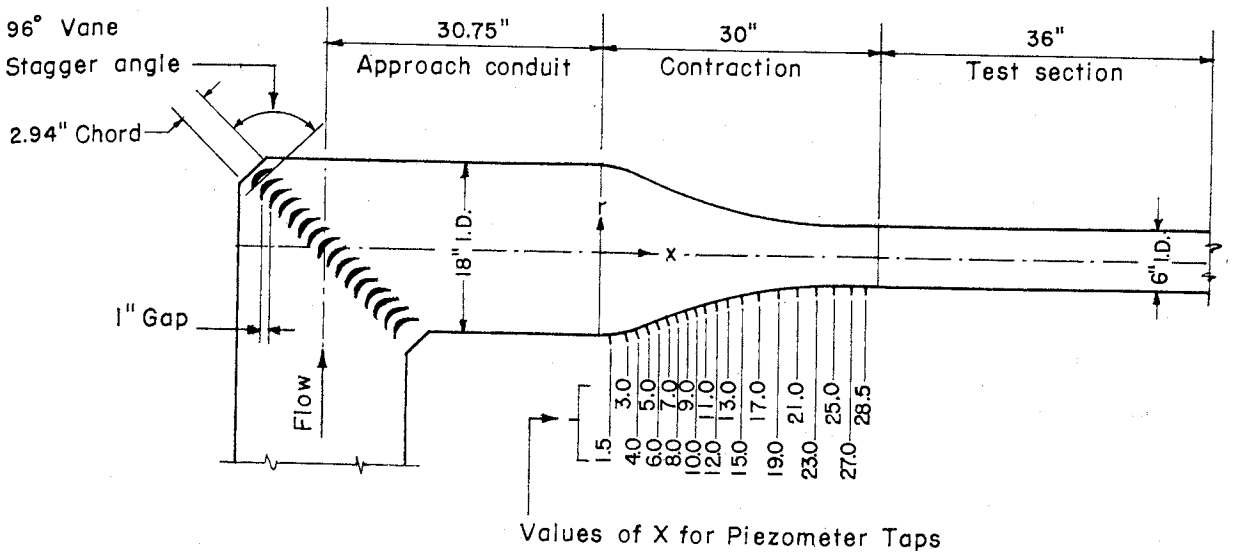

Fig. 19 – Sectional Elevation of Contraction Flow Circuit

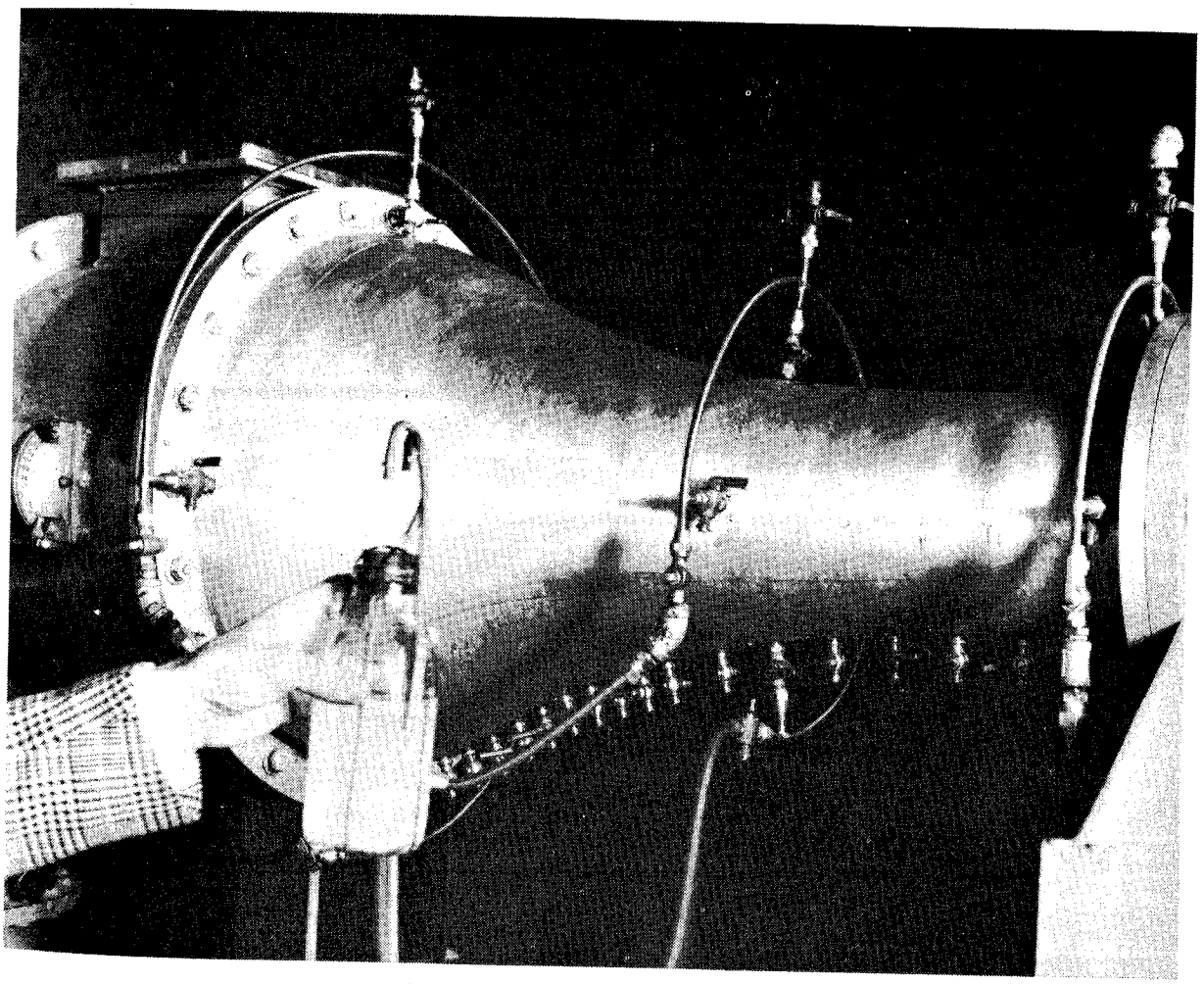

Fig. 20 – Contraction Cone with Piezometer Taps and Flow Delineation Accessories

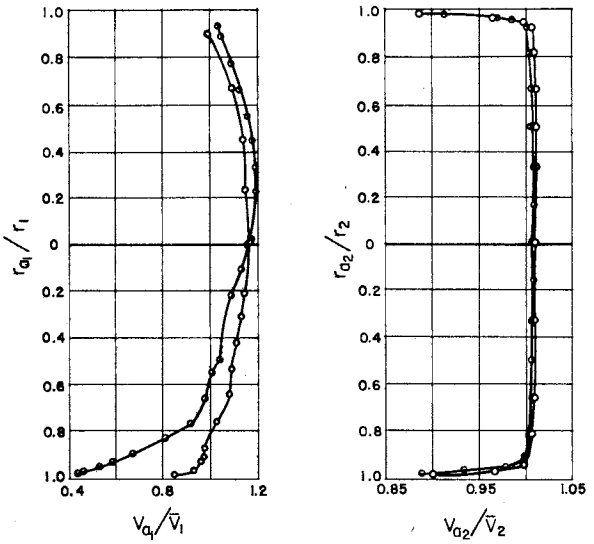

Entrance measurements were taken at x = −6.0 in. where r_1 = 9.0 in., while exit measurements were taken at x = 30.5 in. where r_2 = 3.0 in. Encircled (o) points were measured on a horizontal diameter which was parallel to the elbow vanes while (•) points were measured on a vertical diameter. Values were taken with $\bar{V}_2$ = 49.32 fps., corresponding to Re = 2.48 x 10^6.

Fig. 21 - Contraction Velocity Profiles

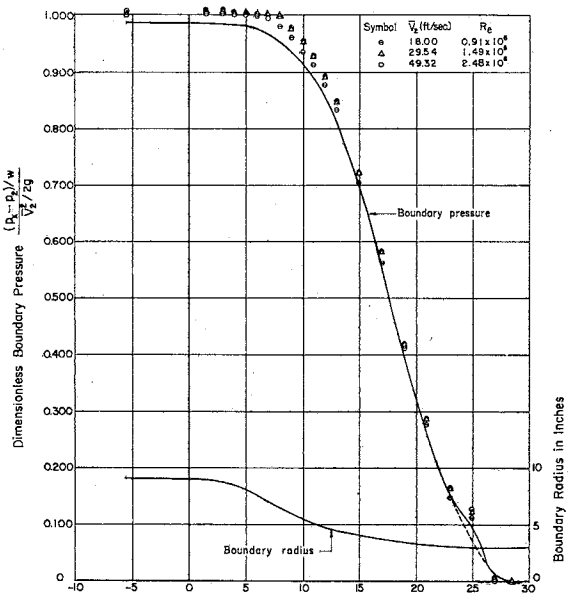

Measured pressure values are shown for three values of $\bar{V}_2$ and their corresponding Reynolds numbers. The solid line represents a simplified theoretical curve based on pure axial flow. The dotted line represents the theoretical curve for the contraction which would exist had no machining error occurred.

Fig. 22 - Contraction Boundary Pressure Measurements

are presented graphically in dimensionless form in Fig. 21 with the corresponding data given in Table IV. These data represent measurements made at the maximum (considered most critical) velocity attainable, which was about 50 fps. Other velocity distribution data taken at the exit station at lesser speeds are presented in the test section discussions of Chapter II but are not accompanied by the entrance distribution data, as in this case, because of the difficulty of accurately measuring the smaller velocities. It is noteworthy that the comparative exit velocity distributions are substantially the same regardless of mean velocity.

3. Pressure Distribution Studies

The distribution of pressure on the contraction boundary was determined by using the previously described pressure measuring taps during operation of the tunnel at three rates of flow. The data are presented graphically in Fig. 22 and tabularly in Table V and have been reduced to a more or less dimensionless base involving the test section velocity and pressure values. The solid line (theoretical) was added to demonstrate the discrepancy between a simplified axial flow assumption and the measured values. This line represents the same approximation as curve B of Fig. 16. The wavy portion of the line between x = 23 and x = 26 results from the aforementioned error in machining the contraction in this region.

TABLE IV

VELOCITY DISTRIBUTION 6 IN. UPSTREAM AND 1/2 IN. DOWNSTREAM OF CONTRACTION CONE

Velocity Distribution 6 in. Upstream of Contraction Cone

$\bar{V}_1 = 5.48$ fps $Re_1 = 0.83 \times 10^6$

Horizontal Diameter (Parallel to Vanes)				Vertical Diameter (Perpendicular to Vanes)							
Distance from Side Wall (in.)	$\frac{r_{a_1}}{r_1}$	Velocity (fps)	$\frac{V_{a_1}}{\bar{V}_1}$	Distance from Bottom Wall (in.)	$\frac{r_{a_1}}{r_1}$	Velocity (fps)	$\frac{V_{a_1}}{\bar{V}_1}$	Distance from Bottom Wall (in.)	$\frac{r_{a_1}}{r_1}$	Velocity (fps)	$\frac{V_{a_1}}{\bar{V}_1}$
0.9	0.900	5.44	0.993	0.10	0.988	2.43	0.444	13.00	0.444	6.47	1.181
2.9	0.678	6.01	1.097	0.20	0.978	2.52	0.460	14.00	0.556	6.37	1.162
4.9	0.456	6.26	1.142	0.35	0.962	2.92	0.533	15.00	0.667	6.18	1.128
6.9	0.233	6.33	1.154	0.60	0.933	3.18	0.581	16.00	0.778	6.01	1.097
8.9	0.011	6.39	1.167	1.00	0.888	3.68	0.672	17.00	0.889	5.75	1.049
10.9	0.211	6.27	1.143	1.50	0.833	4.46	0.815	17.40	0.933	5.70	1.040
11.9	0.322	6.24	1.138	2.00	0.778	5.06	0.924				
12.9	0.433	6.14	1.119	3.00	0.667	5.39	0.984				
13.9	0.544	6.01	1.097	4.00	0.556	5.53	1.008				
14.9	0.656	5.96	1.088	5.50	0.500	5.75	1.048				
15.9	0.767	5.60	1.022	7.00	0.222	5.99	1.093				
16.9	0.878	5.34	0.975	8.00	0.111	6.22	1.135				
17.25	0.916	5.34	0.975	9.00	0.000	6.37	1.162				
17.45	0.938	5.30	0.967	10.00	0.111	6.47	1.181				
17.75	0.972	5.11	0.933	11.00	0.222	6.53	1.192				
17.90	0.988	4.66	0.851	12.00	0.333	6.53	1.192				

Velocity Distribution 1/2 in. Downstream of Contraction Cone

$\bar{V}_2 = 49.32$ fps $Re_2 = 2.48 \times 10^6$

Horizontal Diameter (Parallel to Vanes)				Vertical Diameter (Perpendicular to Vanes)			
Distance from Side Wall (in.)	$\frac{r_{a_2}}{r_2}$	Velocity (fps)	$\frac{V_{a_2}}{\bar{V}_2}$	Distance from Bottom Wall (in.)	$\frac{r_{a_2}}{r_2}$	Velocity (fps)	$\frac{V_{a_2}}{\bar{V}_2}$
0.05	0.983	43.41	0.880	0.05	0.983	43.75	0.887
0.10	0.966	47.48	0.963	0.10	0.967	46.01	0.933
0.15	0.950	48.88	0.991	0.15	0.950	48.31	0.979
0.25	0.916	49.63	1.007	0.25	0.917	49.28	1.000
0.55	0.817	49.84	1.010	0.55	0.817	49.69	1.007
1.00	0.667	49.92	1.012	1.00	0.667	49.77	1.009
1.50	0.500	49.92	1.012	1.50	0.500	49.69	1.007
2.00	0.333	49.92	1.012	2.00	0.333	49.77	1.009
3.00	0.000	49.92	1.012	2.50	0.167	49.77	1.009
4.00	0.333	49.90	1.011	3.00	0.000	49.77	1.009
5.00	0.667	49.77	1.009	3.50	0.167	49.77	1.009
5.45	0.817	49.71	1.008	4.00	0.333	49.77	1.009
5.75	0.917	49.36	1.001	4.50	0.500	49.69	1.007
5.85	0.950	49.02	0.994	5.00	0.667	49.69	1.007
5.90	0.967	47.69	0.968	5.45	0.817	49.56	1.005
5.95	0.983	44.38	0.900	5.75	0.917	49.28	1.000
				5.85	0.950	48.59	0.986
				5.90	0.967	47.75	0.968
				5.95	0.983	44.97	0.912

Note: The use of values carried to the fourth significant figure is a calculating and reference expedient and is not indicative of the order of accuracy of the experimental work which, in general, can only justify the third significant figure.

TABLE V

CONTRACTION BOUNDARY WALL PRESSURE DATA

Boundary Coordinates (See Fig. 19)		Theoretical Boundary Pressure*	Experimental Boundary Pressure**		
			For $\bar{V}_2$*** = 18.00 fps and Re = 0.91 x 10^6	For $\bar{V}_2$ = 29.54 fps and Re = 1.49 x 10^6	For $\bar{V}_2$ = 49.32 fps and Re = 2.48 x 10^6
x (in.)	r (in.)	(1 - K)			
-6.00	9.00	0.988	1.012	1.0255	1.0268
0.00	9.00	0.988			
1.50	8.95	0.987	1.012	1.0264	1.0284
3.00	8.75	0.986	1.012	1.0256	1.0269
4.00	8.47	0.984	1.010	1.0246	1.0262
5.00	8.11	0.981	1.009	1.023	1.024
6.00	7.62	0.976	1.006	1.019	1.020
7.00	7.08	0.968	0.997	1.011	1.012
8.00	6.50	0.955	0.981	0.995	0.998
9.00	6.02	0.938	0.962	0.977	0.978
10.00	5.58	0.916	0.938	0.953	0.955
11.00	5.21	0.890	0.913	0.927	0.928
12.00	4.88	0.857	0.879	0.895	0.893
13.00	4.56	0.813	0.834	0.847	0.849
15.00	4.04	0.696	0.706	0.722	0.721
17.00	3.68	0.558	0.562	0.583	0.583
19.00	3.41	0.401	0.411	0.417	0.417
21.00	3.25	0.274	0.276	0.287	0.286
23.00****	3.13****	0.156	0.147	0.157	0.166
25.00	3.07	0.099	0.112	0.119	0.128
27.00	3.01	0.013	0.013	0.011	0.011
28.50(2)	3.00	0.000	0.000	0.000	0.000
30.00	3.00				

*Assuming pure axial flow with uniform velocity distribution and no head loss: if

$$K = \frac{\bar{V}_x^2}{\bar{V}^2} = \frac{\frac{Q^2}{\pi^2 r_x^4}}{\frac{Q^2}{\pi^2 r_2^4}} = \frac{r_2^4}{r_x^4} = \frac{(3.00)^4}{r_x^4}, \text{ then } \frac{p_x - p_2}{w} = (1 - K)\frac{\bar{V}_2^2}{2g}, \; 1 - K = \frac{\frac{p_x - p_2}{w}}{\frac{\bar{V}_2^2}{2g}}$$

**All experimental pressure differences between x and 2 are divided by the velocity head at 2:

$$\frac{\frac{p_x - p_2}{w}}{\frac{\bar{V}_2^2}{2g}}$$

***$\bar{V}_2$ is the average velocity at the contraction throat of 6-in. diam while Re is the Reynolds number based on this diameter.

****Error in machining from x = 23.5 to 25.5.

Note: The use of values carried to the fifth significant figure is a calculating and reference expedient and is not indicative of the order of accuracy of the experimental work which, in general, can only justify the third significant figure.

It will be observed from the experimental data of Table V that a very slight adverse pressure gradient exists at the higher velocities in the region x = -6.0 to x = 1.5 in a manner generally consistent with the rationalizations of Fig. 16 and at a rate comparable to that expressed by the boundary velocity curve of Fig. 18.

The boundary pressure data of Fig. 22 show no evidence of the low pressure values indicated in zone 2 of curve A, Fig. 16, although a marked deviation of the data is evident in the region of the machining error at x = 25.0. It is particularly unfortunate that the machining error occurred in the region it did, as this portion of the boundary might otherwise be suspected of producing separation conditions. However, the very gradual easement of the general radius of curvature at this point would indicate that a boundary without machining error should produce a pressure curve corresponding to the dotted line faired-in between the points taken at taps x = 25.0 and x = 27.0.

As a follow-up on the boundary pressure measurements, the possible separation areas were subjected to the flow delineation procedure previously described and the cone was then removed from the tunnel and photographed. The significant data are shown in Figs. 23 to 26. In examining these figures, the following factors may be noted:

(1) Black strings representing axial traces have been taped to the boundary to define the axial flow direction. The principal flow direction may be observed to have a slight spiral in a counter-clockwise direction (looking downstream) but is not judged serious since it is not present to a noticeable degree in the test section. The source of a spiral in this direction is unaccountable as it is contrary to the slight spiral evident in the region of the pump discharge. (The pump would normally be considered the only source of asymmetric flow.)

(2) The flow streak originating from the tap at x = 1.5 shows definite indications of upstream boundary flow but the limited extent in the upstream direction and the strong trace downstream give evidence that the separation effect is weak and confined to the immediate boundary layers. It is considered unlikely that separation eddies of any significant strength could be generated in this region.

(3) No trace of reverse flow is evident in the streaks originating at taps x = 4.0 and x = 17.0.

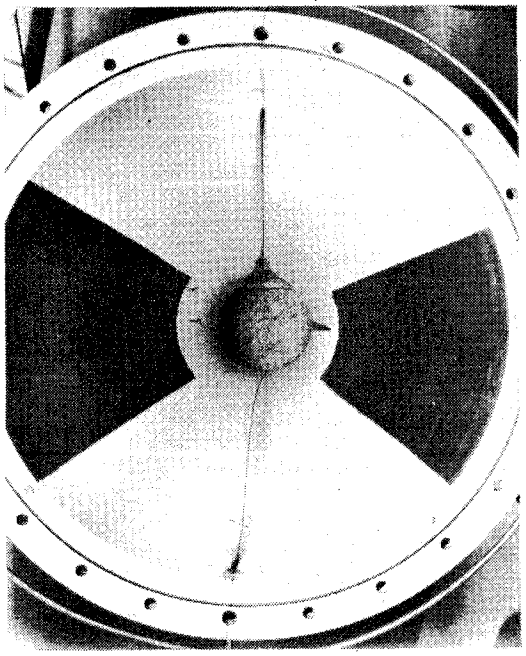

Fig. 23 - Contraction Boundary Wall Flow Streaks. (Black strings represent axial traces)

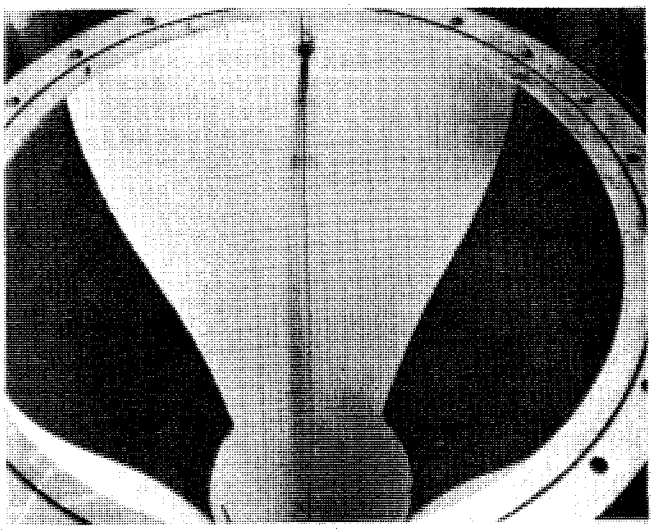

Fig. 24 - Contraction Boundary Wall Flow Streak from Tap at Station x = 1.5

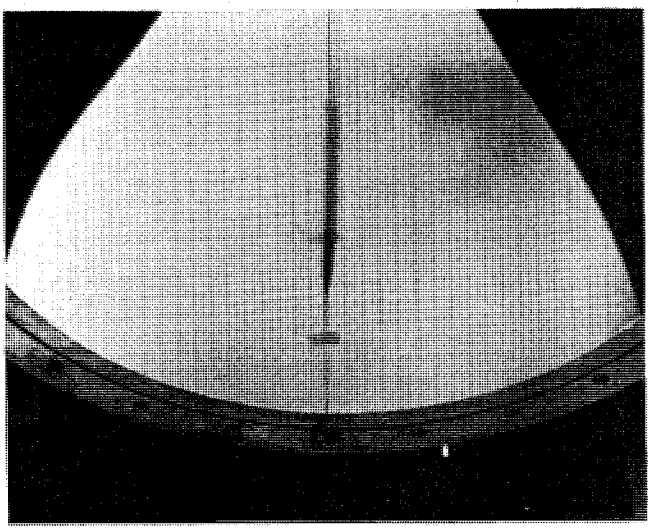

Fig. 25 - Contraction Boundary Wall Flow Streak from Tap at Station x = 4.0

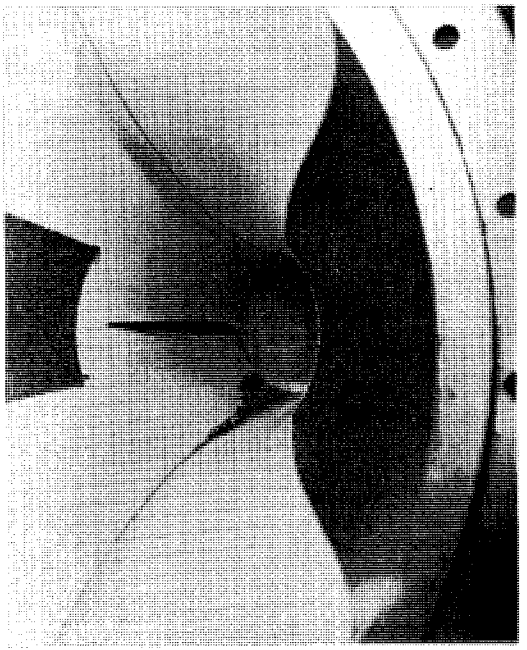

Fig. 26 - Contraction Boundary Wall Flow Streak from Tap at Station x = 17.0. (The position of the side tap at x = 28.5 is defined by the inserted pin.)

TABLE VI

CONTRACTION HEAD LOSS DATA

Test Section Velocity $\bar{V}_2$	$\frac{p_1 - p_2}{w}$	$\frac{\bar{V}_2^2}{2g}$	$\frac{\frac{p_1 - p_2}{w}}{\frac{\bar{V}_2^2}{2g}}$	$\frac{h_f}{\frac{\bar{V}_2^2}{2g}}$
fps	ft of water	ft		
9.478	1.43	1.3949	1.0252	0.0414
9.539	1.47	1.4129	1.0404	0.0566
14.989	3.59	3.4887	1.0290	0.0452
14.998	3.56	3.4929	1.0192	0.0354
19.695	6.10	6.0232	1.0127	0.0289
22.684	8.07	7.9901	1.0100	0.0262
25.124	9.87	9.8015	1.0070	0.0232
25.692	10.33	10.2497	1.0078	0.0240
26.249	10.75	10.6989	1.0048	0.0210
29.888	14.00	13.8710	1.0093	0.0257
30.634	14.72	14.5720	1.0101	0.0263
30.762	15.02	14.6941	1.0222	0.0384
35.371	19.72	19.4271	1.0151	0.0313
39.491	24.58	24.2114	1.0150	0.0312
47.411	34.96	34.9038	1.0016	0.0178

Note: The use of values carried to the sixth significant figure is a calculating and reference expedient and is not indicative of the order of accuracy of the experimental work which, in general, can only justify the third significant figure.

respectively evaluated as $\alpha_1 = 1.07$ and $\alpha_2 = 1.00$, from integration of the velocity profiles shown in Fig. 21.

If the value of the head loss is made dimensionless by expressing it in ratio with the test section velocity head then

$$\frac{\frac{h_f}{\bar{V}_2^2}}{\frac{\bar{V}_2^2}{2g}} = \frac{\frac{p_1 - p_2}{w}}{\frac{\bar{V}_2^2}{2g}} - \alpha_2 + \alpha_1 \left(\frac{d_2}{d_1}\right)^4$$

Values for the expression given above are listed in the last column of Table VI. While there is evidence of appreciable scatter in the data, the general trend indicates a decreasing percentage head loss with increasing velocity, or

Reynolds number, as is consistent with the usual evidence in friction loss studies. A later analysis of the data of Table IV gave some reason to believe that a laminar, turbulent boundary-layer transition may have occurred for the range of velocities covered. This could account for the scatter in the pressure coefficient values in the fourth column of the table.

For the range of velocities employed in the calibration, an average value of 0.031 results. For the larger Reynolds number values of the prototype, it is probable that 0.02 would be quite representative for design purposes although the above mentioned influence of a laminar-turbulent critical introduces obscuring scale effects preventing a refined assessment.

D. Conclusions

On the basis of these design studies and experimental investigations, the following general and specific conclusions are drawn with regard to contraction design procedures:

(1) The area ratio of a contraction is the simplest and most powerful control which can be used to improve a distorted velocity profile. Measured values of the velocity distribution indicate the generalized relation between desired jet velocity variations and selected area ratios as expressed by Eq. (8) may be used for the purpose of specific design approximations.

(2) Excessive shortening of the contraction length inhibits full development of a flat jet velocity profile while excessive lengthening promotes such flatness but only at the expense of a thickened boundary layer and reduced jet core area. Analytical procedures which might be employed to predict the boundary-layer thickness are considered too complex and inexact to justify their extended use.

(3) In the case of a 6-in. jet issuing from a model contraction having a length of 5 jet diam and an area ratio of 9 to 1, the boundary layer at Re = 2.5×10^6 was observed to have a thickness of about 4 per cent of the exit diameter and a core flow in which 85 per cent of the area had a velocity variation of less than 0.5 per cent.

(4) The contraction of a stream of finite diameter may be achieved with greatest flow stability by use of an ogee shape of boundary transition.

(5) Excessive shortening of the length of an ogee contraction will be accompanied by a sharp radius of curvature of the boundary, which may establish

adverse pressure gradients along the boundary wall leading to separation eddies and pulsations in the discharge flow. The adverse gradients are most likely to be found in a region at or upstream of the upper point of tangency and slightly downstream of the point of curve inflection.

(6) The analytical development by Tsien defines a boundary curve which in the ideal case can be made free of adverse pressure gradients in the region downstream of the inflection point and permits arbitrary selection of a tolerable gradient near the upstream point of tangency.

(7) Model studies of a contraction based on the above idealized analytical approach gave experimental boundary pressure values in agreement with the analysis in the case of a 6-in. jet issuing from a model contraction having a length of 5 jet diam and an area ratio of 9 to 1. This agreement is of such nature that the model findings with regard to boundary pressures should be applicable to prototype sizes with a minimum of scale effects.

(8) Lack of suitable instrumentation prevented experimental measurement of the turbulence strength and scale or the detection of separation eddies in the model contraction. There was, however, no evident indication or reason to believe that significant values were present.

(9) The experimental boundary pressure data give evidence that the energy head loss for the contraction may be conservatively approximated by the expression $h_f = 0.02\ \overline{V}_2^2/2g$ for the prototype under consideration where $\overline{V}_2$ is the average velocity at the discharge end of the contraction.

References

[1] Goldstein, S. Modern Developments in Fluid Mechanics. London: Oxford University Press, 1938, Vol. I, pp. 201-03.

[2] Fage, A. The Effect of Contraction on the Turbulence in a Fluid Stream. Aeronautical Research Committee Reports and Memoranda No. 1584, Vol. 1 (British), 1933-34.

[3] Hall, A. A. Measurement of the Intensity and Scale of Turbulence. Aeronautical Research Committee Reports and Memoranda No. 1842 (British), 1938.

[4] Tsien, H. S. "On the Design of the Contraction Cone for a Wind Tunnel." Journal of Aeronautical Sciences, Vol. 10, pp. 68-72. February, 1943.

[5] Batchelor, G. K., and Shaw, F. S. A Consideration of the Design of Wind Tunnel Contractions. Australian Council for Aeronautics Report ACA-4, 1944.

[6] Szczeniowski, B. "Contraction Cone for a Wind Tunnel." Journal of Aeronautical Sciences, Vol. 10, pp. 311-12. October, 1943.

[7] Goldstein, S. Notes on the Design of Converging Channels. Aeronautical Research Committee Reports and Memoranda No. 8495 (British), 1945.

[8] Cheers, F. Notes on Wind Tunnel Contractions. Aeronautical Research Committee Reports and Memoranda No. 8535 (British), 1945.

[9] Hutchinson, J. F. The Delineation of Surface Lines of Flow and Wave Profiles at the David Taylor Model Basin. United States Department of the Navy David Taylor Model Basin Report No. 535, 1944.

P 66

(blank)

CHAPTER IV. DIFFUSER STUDIES

A. General Considerations

The purpose of the diffuser of a water tunnel is to reduce the large discharge velocity of the test section to a value more compatible with the functional requirements of the remainder of the tunnel recirculating system. The velocity reduction or area expansion is necessary for the following reasons:

(1) It is not economically feasible to return the water stream from the discharge end of the test section to the entrance without reduction of velocity. This condition prevails because such a return necessitates a 360° directional diversion of the flow plus a considerable straight travel distance, all of which entails a frictional energy loss that is a function of the square of the velocity. Obviously, with the extremely high velocities proposed for the test section (84.5 fps), any increase in cross-sectional area of the return circuit will markedly reduce the energy losses and required pumping power costs.

(2) If a constant area of cross section is used in the return duct, the inherent internal mechanism of fluid flow tends to destroy any initial uniformity of direction or velocity and returns to the test section a flow having definitely disturbed quality. Numerous corrective devices and methods have been employed but none is more simply effective than the contracting or accelerating cone. Accordingly, the benefits of contracting into the test section can be available only if the return circuit has provided expansion after leaving the test section.

(3) Among the fundamental operating specifications for the proposed tunnel was a requirement for testing conditions having a minimum of background noise. Operations in existing tunnels indicate that a large source of such noise is the cavitation produced in passage through the vaned elbows and the pump of the return circuit. This cavitation is enhanced by an increase in velocity and suppressed by an increase in pressure; therefore, an increase in return duct area can automatically contribute dual benefits with respect to noise abatement and the related vibration, pitting, and energy loss.

A superficial study of the diffuser problem leads to the conclusion that a simple expansion of area should provide the desired velocity reduction; however, actual tests and a more thorough analysis have proved that simple area expansion can achieve reasonable efficiency only under limited conditions.

Unlike the favorable pressure gradient generally encountered in a flow contraction, an adverse or increasing pressure gradient accompanies the velocity change produced in an expansion. This increasing pressure gradient is applied to a boundary layer, which is simultaneously being retarded by wall drag and accelerated by shear and momentum transfer with the faster core flow. If the momentum transfer is inadequate, the pressure gradient may induce a complete reversal of the boundary flow. Such a reversal of boundary flow direction serves as a wedge to separate the core flow from adherence to the wall geometry and sets up a large turbulent eddy or dead water zone. This dead water not only prevents the desired geometry of flow but irreversibly absorbs a large amount of energy and incites flow instability. It is the purpose of proper diffuser design to suppress this separation with a boundary geometry or auxiliary facilities of least cost.

B. Design Studies

1. Diffuser Shape

a. Simple Expansions

The first consideration in selecting a flow expansion is quite naturally a simple tapering duct. This solution is so direct that it has been and is used wherever simplicity governs the design. The geometry of construction offers an infinite number of variations from abrupt step transitions to long tapers, together with a variety of cross-sectional forms.

In an attempt to establish the proportions giving optimum flow conditions, a number of investigators have made tests on straight and curved tapers having circular, square, and rectangular cross sections. An analysis of these data indicates that a straight walled cone of circular section and small angle is most efficient in effecting the desired expansion. A minimum head loss is usually observed with an included angle of about 6° to 8°. Angles larger than this tend to increase the loss induced by wall separation, by reason of a steeper adverse pressure gradient, while smaller angles increase the physical length required to effect the desired area expansion and, accordingly, increase the loss by increasing the frictional area exposed to high velocity drag.

b. Expansion by Boundary-Layer Removal

It was early recognized that the retarded boundary layer of a large angle, simple diffuser served as a wedge to separate the flow from the

wall, thus changing the desired flow condition. Prandtl [1]*, in 1904, performed elementary academic experiments serving to show that separation could effectively be prevented by suction removal of that part of the boundary layer which was beginning to reverse. Ackeret [2], in 1926, made quantitative measurements of suction removal on diffusers with rapid expansions by withdrawing fluid through holes or slots in the boundary wall. Although his work was not comprehensive, it did indicate that the stream could be made to follow the diffuser shape by removing 1 or 2 per cent of the total flow at an expenditure of suction energy amounting to 1 or 2 per cent of the kinetic energy of the test jet. If these percentages are applied to the large flow and energy of the proposed prototype, it is apparent that very substantial auxiliary equipment would be necessary to implement flow expansion by this method.

In addition to the energy and flow handling problems occasioned by this method, it would encounter additional complications in application to a water tunnel diffuser where the suction region would be very close to that in which minimum cavitating pressures may already be in effect. The application of suction would then promote rather than suppress harmful cavitation. In view of these disadvantages, the suction diffuser was considered insufficiently developed to warrant use in the proposed application.

c. Expansion by Boundary-Layer Acceleration

While suction removal of dead water having insufficient kinetic energy can effectively prevent separation phenomena, it is apparent that original prevention of the dead water by energizing it to maintain its forward motion should be equally effective. An obvious method of doing this is to jet into the boundary flow additional fluid carrying kinetic energy from an outside source. For most effective action, this should be done at the beginning of the zone of energy deficiency with the kinetic energy jet directed parallel to the boundary. The additive energy may be supplied by external pumping systems but it is also possible in some cases to convey fluid from high pressure sources elsewhere in the parent flow system. The latter method has met with some success in suppressing separation on the low pressure side of airfoils in what is known as the slotted wing. This device operates by conveying pressurized air from the high pressure leading edge of a wing back through a slot that jets into the boundary layer in the separation zone. The method also shows some energy gains when applied to the conical draft tube diffusers of hydraulic turbines in a system developed by Professor L. F. Moody [3].

---

*Numbers in brackets refer to the corresponding numbers in the reference list at the end of the chapter.

An analysis of the information on this general method of expansion leads to the conclusion that considerable physical complexity will be encountered in its use. If a separate source of energy were used, it would involve a rather substantial pumping plant and control system. If high pressure points of the return circuit were used for energy supply, a complex piping system would be involved. In view of the complications of and the lack of specific information on this system of expansion, it was not considered applicable to the proposed design.

d. Expansion by Flow Rotation

If the flow through a diffuser has a rotation about its axis in addition to its motion of translation, the efficiency of energy transfer may be materially increased in some cases. The efficiency increase is probably due to a complex combination of the radial pressure gradient countering the adverse axial pressure gradient and to an increase in momentum transfer through radial flow.

Since rotation could be induced only by introduction of blading systems at the diffuser entrance, it would be difficult to induce rotation in a water tunnel diffuser without creating the possibility of cavitation on the vaning or prerotation effects in the test section flow. Both of these effects tend to destroy the desired flow quality and thus eliminate this method from further design consideration.

e. Expansion by Deflectors or Vanes

As in the case of several of the other expansion systems, this one attempts to achieve diffuser efficiency through accelerating the dead water. This is accomplished by increasing the momentum transfer through provision of suitable deflector vanes serving to scoop the high energy core flow into the dead water zones. While the method offers some possibilities for diffusers operating at nominal speeds and pressures, it must be dropped from consideration in this design because of the cavitation which would occur on the deflector vanes under low pressure conditions.

f. Comparison

An analysis of the diffuser types previously discussed indicates that the small angle, simple, conical expansion is most likely to produce the desired results. It is fully appreciated that this system is not necessarily

the most economical, in view of its very large physical size and its appreciable energy losses; but it is simple, free of maintenance and adjustment problems, and should minimize the possibility of cavitation.

Previous investigators have found straight, tapered walls to be just as effective as complex, curved walls for the small angle under consideration except where a curved junction is judged necessary at the test section transition. Numerous studies indicate that a minimum energy loss will occur for an included wall angle of 6° to 8°. However, because of the very low pressures and high velocities which may exist at the entrance to the tunnel diffuser, a conservative value of 5° was arbitrarily proposed.

2. The Diffuser Transition Curve

A parabolic transition having a length of 1/2 test section diam was provided to avoid a sharp break in the boundary at the intersection of the test section cylinder and the diffuser cone. Since the transition curve is intimately associated with the test section performance, the design studies for this element have been included with those of the test section in Chapter II. The general arrangement of the diffuser and the transition is shown in Fig. 27.

3. The Pump Diffuser

The short diffuser following the pump is not analyzed in this section since its performance is so intimately dependent on the characteristics of the pump impeller, hub fairing, and straightening vanes; these are primarily the responsibility of the pump builder.

For the purpose of constructing the model tunnel, the pump diffuser was built as a simple cone with an 8° included angle. This angle is in a range which should provide nearly maximum efficiency yet it is of minimum length, thus allowing the maximum length of stilling section in the lower leg of the tunnel.

C. Experimental Studies

1. Apparatus and Procedures

The main diffuser in the model water tunnel was made in three sections. The upstream section was an aluminum casting bored to provide the necessary transition curve between the cylindrical test section and the conical diffuser. The two downstream sections of the diffuser were fabricated from 3/16-in. thick sheet steel rolled to the proper shape and welded to steel flanges. Minor

joint discrepancies resulting from the rolling were removed by hand grinding the subassemblies. Minor discrepancies in the curve form of the transition casting are described and illustrated in Chapter II.

The interior of the cast section was smoothly polished with emery cloth while the steel sections were roughly filed and polished with emery cloth to remove the surface irregularities resulting from galvanizing.

Velocity profiles were determined at stations 3, 4, and 5 (see Fig. 27) using the 3/8-in. diam "cantilevered" Pitot tube and at station 2 using the 1/4-in. diam "long" Pitot tube, both of which are described in the appendix. The profiles were taken on both horizontal and vertical diameters of the section.

Boundary pressure measurements were made at taps in the plane of the velocity traverse stations.

2. Velocity Distribution

The velocity distribution in the diffuser is an important index of the energy exchange in the diffuser proper and reflects also on the energy conditions in the tunnel components following the diffuser. The significant velocity traverses shown in Fig. 28 consist of readings taken at the highest or most critical speed, approximately 50 fps, with some supplementary traverses at 30 fps to serve as a check on the asymmetry evident at stations 3 and 4. While this quantitative treatment of the data will be interpreted in a later section to give prototype energy loss values, the qualitative nature of the prototype profiles will be examined at this point.

It is evident in Fig. 28 that there is a marked lack of symmetry in the diffusing stream with low velocities predominating on the diffuser bottom or inside of the tunnel loop. Since the presence of a considerable low velocity region could serve to initiate separation, it is important tc rationalize as to the cause and influence of the asymmetry condition observed to exist in the model. In an effort to determine whether the asymmetry was a product of the flow deficiencies of other components of the tunnel or whether it was inherent to the diffuser, the velocity distributions described in the chapters on the elbow, contraction, and test section were examined and found to give general evidence of a slightly lower velocity on the inside of the tunnel loop. While it is possible the difficulty may originate in the diffuser, an examination of the vane-elbow data indicates the elbow component may contribute considerably, since the major part of all tunnel studies was made with a vane angle setting of 96°.

Rather extensive studies of the vane geometry as described in Chapter V establish that flow symmetry and component performances could be improved materially by changing the vane angles to 101°. Since these diffuser studies were conducted in parallel with the early vane studies, no opportunity was presented to include diffuser tests with the optimum vane setting. However, a subsequent program of testing this tunnel when rebuilt as an open-jet tunnel with an alternate closed-jet sleeve, gave evidence that the earlier 5° diffuser performance was quite abnormal. In the rebuilt tunnel having vanes set at 101°, separate tests with a 6° 40' and a 9° cone gave greater symmetry and relatively higher wall velocities than evidenced in Fig. 28. Similar tests conducted at the Ordnance Research Laboratory, Pennsylvania State College [4], also showed satisfactory symmetry at angles of 7.5° and 10°.

A general study of the work of other diffuser investigators with a view to their findings on the presence of asymmetry disclosed that Nikuradse [5] had measured related phenomena and quantitatively determined the influence of the cone angle. While Nikuradse's numerical values taken from a rectangular two-dimensional diffuser are not directly applicable to the circular cone under consideration here, the trend of the progressive change in velocity distribution with change in diffuser angle is judged comparable. This trend for the diffuser tested by Nikuradse may be summarized: (1) for small expansion angles (8° total angle) the flow profile is symmetrical and stable; (2) for somewhat larger angles (10° total angle) the flow becomes unsymmetrical but without evidence of reverse boundary flow or instability; (3) for still larger angles (12° total angle) the unsymmetrical flow has apparent separation on one side but is still stable; (4) for still larger angles (16° total angle) the asymmetric flow stream switched slowly from one side to the other in an unstable manner.

In view of the above data, but with full awareness of the form discrepancies between the rectangular diffuser and the model tunnel and the possible deficiencies of the vane setting, it would appear that the velocity profiles of Fig. 28 represent a flow pattern which in the worst case might be considered analagous in form to that of item (2) of the foregoing. If this is assumed to be the case, it would then appear that a decrease in total cone angle would tend to give a more symmetrical pattern, while only a slight increase in angle would produce definite separation. It is, therefore, indicated that use of a 5° diffuser cone in the model is definitely on the side of

conservatism, and if economic considerations dictate more radical procedures, an angle of 6° or 7° could be employed with no great risk of adverse effects.

While there are insufficient data in these tests to indicate any trends in performance differences between the model and the prototype, it seems safe to say that increasing the size by ten times and the velocity from 50 to 85 fps should serve to improve the efficiency and separation conditions. This seems rational since the flow pattern is principally dominated by viscous forces which for high Reynolds numbers, as in this case, normally produce improved flow and separation suppression with increased values.

It should be noted that the discussion of flow quality applies only to the case of flow in the unoccupied tunnel. If a test body is mounted in the test section, the flow may of course be profoundly influenced by the nature of the body. Since the nature of the body will be widely variable in a general purpose tunnel, it will be impossible to predict the range of diffuser performance. It seems reasonable to assume, however, that the simple conical diffuser will perform as well or better than the other diffuser types suggested -- which are, in general, rather sensitive to changes in the design variables. It is also worthy of note that these tests take no account of the basic level of turbulence in either the model or the prototype tunnel. It is probable that this has some effect on the diffuser separation conditions, but lack of suitable instrumentation prevents evaluating the turbulence. It is doubtful that turbulence would produce significant scale effects because the turbulence values in the model and the prototype are probably comparable.

3. Energy Losses

The total energy lost in a diffuser action is normally evaluated by measuring the change in the sum of the pressure and the kinetic energy as the flow progresses from the inflow to the outflow. In the model tunnel studies, this change in energy is measured by boundary pressures and velocity traverses, as described elsewhere. The kinetic energy data as represented by the velocity traverses of Fig. 28 are converted to a more useful form by applying an integration of the plotted profile to the expression

$$\alpha = \frac{\Sigma \triangle A V^3}{A \overline{V}^3}$$

where $\overline{V}$ is the mean velocity of the section. The value of α may then be used in the form $\alpha \overline{V}^2/2g$ to express the mean velocity head of the total stream.

Three values of α_2, corresponding to the three different rates of flow at which the pressure gradient was measured, were computed from velocity traverses taken at station 2, and one value of α_5 was computed from the velocity traverses at station 5. Only the single traverse at high speed was taken at station 5 because of the difficulty in accurately measuring the lower velocities. The α, $\bar{V}$, and pressure gradient values for the tests are listed in Table VII.

The overall efficiency of the diffuser in conversion of kinetic energy to pressure energy can then be represented by the following equation in which the subscripts represent the station numbers:

$$\eta = \frac{\frac{p_5 - p_2}{w}}{\frac{\alpha_2 \bar{V}_2^2 - \alpha_5 \bar{V}_5^2}{2g}}$$

The percentage of energy lost may be written as $(1 - \eta)\ 100$. Values of η for $\bar{V}_2$ = 18.0, 30.0, and 49.62 fps are tabulated in Table VII. Since these values apply to the model tunnel, extrapolation to the proposed prototype will require a consideration of the makeup of the losses and the possible scale effects involved.

It has been established that the makeup of total energy loss in a conical diffuser can, for convenience of analysis, be considered composed of two principal parts, as follows:

(1) The shearing friction loss caused by the interaction of the solid boundary and the flowing stream. This assumes that the flow expands in an orderly manner and that the shearing action is similar to that occurring in straight pipe flow.

(2) The form loss which measures the friction of the extra turbulent eddying resulting from the inability of the flow to conform to the boundary. This is, of course, the measure of the effect of separation phenomena and increases with the degree of separation.

If the two parts of the total are examined as to the influence of scale effects, it is apparent that the first part must be corrected for the usual variables relating to pipe flow friction, namely, size, roughness, and the Reynolds number. Experience has established that the second part is relatively oblivious to scale effects.

TABLE VII

DIFFUSER ENERGY LOSS DATA

		Test Sec Vel = 18.0 fps		Test Sec Vel = 30.0 fps		Test Sec Vel = 49.62 fps	
		Station 2	Station 5	Station 2	Station 5	Station 2	Station 5
model	Velocity (fps)	18.00	3.72	30.00	6.19	49.62	10.25
	α	1.0185	1.812	1.0144	1.812	1.0151	1.812
	α $(\bar{V}^2/2g)$ (ft)	5.12	0.39	14.18	1.07	38.81	2.96
	Re = V (d/ν)	0.9×10^6	0.4×10^6	1.5×10^6	0.7×10^6	2.5×10^6	1.1×10^6
	f	0.0198	0.0178	0.0198	0.0172	0.0195	0.0170
	$p_5/w - p_2/w$ (ft)	4.34		11.81		32.31	
	p_f/w (ft)	0.25		0.67		1.72	
	η	0.9164		0.9007		0.9012	
	η_o	0.9683		0.9518		0.9490	
prototype	η'	0.9280		0.9280		0.9280	
	η'*	0.8780		0.8780		0.8780	

*With test installation in test section.

Note: The use of values carried to the fourth and fifth significant figure is a calculating and reference expedient and is not indicative of the order of accuracy of the experimental work which, in general, can only justify the third significant figure.

The expression for the evaluation of the friction loss is the conventional

$$h_f = \frac{fL}{d} \frac{\overline{V}^2}{2g}$$

which is arranged to account for the variable geometry by the following integration form

$$d\left(\frac{p_f}{w}\right) = \left(\frac{f}{d} \frac{\overline{V}^2}{2g}\right) d\ell$$

The integration is accomplished by the following procedure with reference to Fig. 29:

$$d = d_2 + 2\ell \tan\theta \quad , \quad d\ell = \frac{d(d)}{2 \tan\theta}$$

$$d\left(\frac{p_f}{w}\right) = f \frac{d(d)}{2 \tan\theta \cdot d} \left(\frac{V^2}{2g}\right) \quad , \quad V^2 = V_2^2 \left(\frac{d_2}{d}\right)^4$$

$$\frac{p_f}{w} = \int_{d_2}^{d_5} \frac{f \overline{V}_2^2 d_2^4}{2 \tan\theta \cdot 2g} \left[\frac{d(d)}{d^5}\right] = \frac{f \overline{V}_2^2 d_2^4}{8 \tan\theta \cdot 2g} \left[\frac{1}{d_2^4} - \frac{1}{d_5^4}\right]$$

$$= \frac{f}{8 \tan\theta} \left[\frac{\overline{V}_2^2 - \overline{V}_5^2}{2g}\right]$$

and for $d_2 = 6$ in., $d_5 = 13.2$ in., $\theta = 2^\circ 30'$

$$\frac{p_f}{w} = 2.60f \frac{\overline{V}_2^2}{2g}$$

The conventional friction factor f was evaluated for the model using the published data from page 211 of reference [6] and the Reynolds number shown in Table VII, with the surface considered as galvanized iron. The resulting f-values are shown in Table VII along with the value of the wall-friction head loss p_f/w.

On the basis of this method of isolating the frictional effects, the efficiency of the form loss alone may be written as:

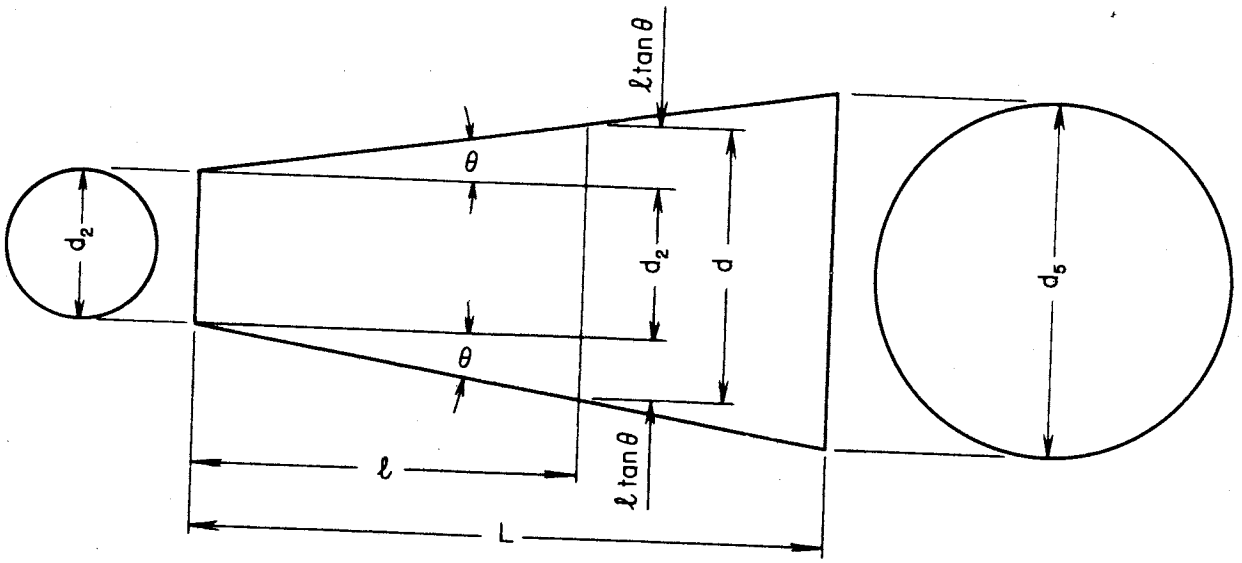

Fig. 29 - Designation for Diffuser Geometry

$$\eta_o = \frac{\frac{p_5 - p_2}{w} + \frac{p_f}{w}}{\frac{\alpha_2 \bar{V}_2^2 - \alpha_5 \bar{V}_5^2}{2g}}$$

Values of this expression for the model tunnel tests are shown in Table VII. It may be noted that these values vary somewhat, which is reasonable in view of the assumptions for the derived expressions and the accumulated experimental error. As a representative approximation, η_o will be assumed at 0.950 for computing the prototype extrapolation.

The total efficiency of the prototype diffuser energy conversion is then computed as follows:

$$\eta' = \eta_o - \left[\frac{\frac{p_f}{w}}{\frac{\alpha_2 \bar{V}_2^2 - \alpha_5 \bar{V}_5^2}{2g}}\right] = \eta_o - \left[\frac{2.60 f \bar{V}_2^2}{\alpha_2 \bar{V}_2^2 - \alpha_5 \bar{V}_5^2}\right]$$

In the prototype evaluation the last term will be assumed to have α-values, the same as in the model, while $f = 0.0085$. The latter value was chosen from measurements made by the Tennessee Valley Authority [7] on a flow conduit of approximately the same size and surface as the proposed prototype. Values of η' for the velocities used in the tests are shown in Table VII.

Comparison of the foregoing values with those of other investigators indicates agreement but with no exactness. Peters [8], who carried out the most comprehensive experiments, came to the conclusion that inherent sensitivities made experimental determinations of efficiencies of small angle diffusers vary widely. This is confirmed, since values of η_o varying from 0.89 to 0.97 have been found by various experimenters for θ in the region of 2° 30'. He found the nature of the inflow to the diffuser had a powerful influence on the efficiency and losses; accordingly, it may be expected that the previously computed η' values will vary materially with the nature of bodies mounted in the tunnel test section. In order to attempt some evaluation of this influence, a conservative estimate based on Peters' work will assume that the form loss $1 - \eta_o$ is doubled. Values of η'^* calculated on this basis are listed in Table VII.

Peters also found that in most cases energy measurements restricted to the diffuser cone proper did not give a true picture of the diffuser losses, since alterations of the velocity profile and eddy decay continue for some distance downstream of the cone length. These abnormalities in the duct following the cone produce losses which properly belong to the diffuser but which are in many cases necessarily assigned to the following duct component. In view of this, it must be recognized that the η' values tabulated in Table VII are for the diffuser alone and that the abnormally high losses (see Chapter V) occurring in the vane elbow following the diffuser are due to reformation or normalizing of the diffuser energy discharge rather than the usual performance losses of the vane elbow itself.

While the use of η as an expression of the conversion efficiency of the diffuser is a useful value for comparative studies of the diffuser alone, it will be necessary to convert this value if the head loss for the diffuser is to be compared and totaled with the loss for other parts of the tunnel. In keeping with the expression for head loss of other tunnel components, the value for the diffuser should then be $K\ (\bar{V}_2^2/2g)$.

An expression for K may be derived by writing Bernoulli's equation along the diffuser and expressing the head loss as $K\ (\bar{V}_2^2/2g)$. If this is solved for K by using the original η equation for substitution, the following expression will result:

$$K = (1 - \eta)\left[a_2 - a_5\left(\frac{d_2}{d_5}\right)^4\right]$$

Evaluating this by using the high velocity data of Table VII, the prototype K-value corresponding to η' will be 0.067 and that for η'^* will be 0.114.

D. Conclusions

On the basis of these design studies and experimental investigations, the following conclusions are drawn with regard to the proposed diffuser design procedures:

(1) On the basis of available general diffuser information and the tests herein described, a simple conical diffuser of 5° total angle appears to offer very conservative performance characteristics for the proposed prototype. While the tests cover only the 5° angle, it is believed that an angle up to 7° may be used without adverse effect.

(2) The 5° cone gave evidence of conditions approaching separation along one side. It is believed that the major portion of this asymmetry would be removed by a slight change in the angular setting of the elbow vanes, as discussed in Chapter V. In view of the high energy efficiency obtained in the tests there is reason to believe that the observed asymmetry did not produce separation.

(3) The energy loss in the 5° diffuser is satisfactorily low in comparison with values of efficiency of energy conversion as determined by other investigators. It is estimated that the efficiency of the diffuser will be 0.88 with a test body installed in the test section and 0.93 with no test body installed in the test section. Corresponding total energy losses may be expressed as $h_f = 0.114\ \overline{V}_2^2/2g$ with test body and $h_f = 0.067\ \overline{V}_2^2/2g$ without test body, where $\overline{V}_2$ is the average velocity at the entrance to the diffuser. Sensitivity to a variety of causes precludes using these values for precise calculations.

(4) Energy disturbances created in a diffuser persist for a considerable distance downstream of the diffuser cone. The evaluations of item (3) pertain only to the energy conversions and losses within the cone proper and do not include the subsequent losses resulting from normalizing the disturbances of the diffuser. Such losses are treated in other chapters of this paper.

Conclusions relating to the diffuser transition characteristics are discussed in Chapter II.

References

[1] Prandtl, L., and Tietjens, O. G. Applied Hydro- and Aero-Mechanics. New York: McGraw-Hill Book Company, 1934, p. 31.

[2] Ackeret, J. "Sucking of the Boundary Layer." Zeitschrift des Vereins Deutscher Ingenieure, Vol. 35, pp. 1153-58, 1926. (Translated from the German in National Advisory Committee for Aeronautics Technical Memorandum No. 395.)

[3] Kerr, S. L. "The Moody Ejector Turbine." Transactions of the American Society of Mechanical Engineers, Vol. 43, No. 1828, pp. 1201-17, 1921.

[4] Robertson, J. M., and Ross, D. Unpublished work relating to diffuser studies for a water tunnel. (More specific information concerning publication of this comprehensive and valuable work unavailable at this time.) Pennsylvania State College Ordnance Research Laboratory.

[5] Goldstein, S. Modern Developments in Fluid Mechanics. London: Oxford University Press, 1938, Vol. II, pp. 371-76.

[6] Rouse, Hunter. Elementary Fluid Mechanics. New York: John Wiley and Sons, 1946.

[7] Hickox, G. H., Peterka, A. J., and Elder, R. A. "Friction Coefficients in a Large Tunnel." Proceedings of the American Society of Civil Engineers, Vol. 73, pp. 451-70. April, 1947.

[8] Peters, H. "Conversion of Energy in Cross-Sectional Divergences under Different Conditions of Inflow." Ingenieur-Archiv, Vol. II, pp. 92-107, 1931. (Translated from the German in National Advisory Committee for Aeronautics Technical Memorandum No. 737.)

CHAPTER V. VANED ELBOW STUDIES

A. General Considerations

The function of the elbows in the proposed water tunnel is to assist in recirculating the test jet from the discharge end of the test section around and back to its contracting entrance. This is to be accomplished with a minimum loss of energy and a minimum final disturbance of the uniform parallel flow desirable in the test section. While a variety of physical forms might be conceived to accomplish this function, analysis of the experience available in the literature of the subject and consideration of fabrication methods pointed the selection of the form of recirculating conduit toward a system composed of four 90° elbows joined by straight ducts. It is the intent of this chapter to clarify the detailed design procedure relating to these 90° elbows.

The first consideration in selecting such 90° elbows is quite naturally the conventional radius elbow, which seemingly offers a smooth directional flow transition with standard fabricating practices and attendant economies. However, a study of the internal flow in such elbows and an analysis of the quantitative values obtained from extensive tests, as given in references [1]* to [6] and summarized in [7], indicate the following marked shortcomings for the proposed application:

(1) To permit the water stream to conform smoothly to the duct curvature the mean radius of sweep must be at least 2 duct diam in size and preferably 4 diam. Use of such long radii on prototype installations of large duct diameter will lead to very substantial distances between the legs of the loop; their use necessitates consideration of more compact design forms.

(2) If a sweep radius of less than 2 duct diam is employed, the stream no longer conforms to the sweep because of the manner in which the kinetic energy of the approaching core flow impinges against the outer wall under the centrifugal force of curvature. The result is a high pressure on the center of the outer wall and a low pressure on the inner wall. As a consequence of this pressure differential, a flow transverse to the duct axis takes place along each side wall and produces two large, high speed vortices trailing from the elbow exit. In addition to this, an adverse boundary pressure gradient of axial direction is created on the outer wall just upstream of the miter

*Numbers in brackets refer to the corresponding numbers in the reference list at the end of the chapter.

line and another is created on the inner wall somewhat downstream of the miter. These adverse gradients are productive of separation eddies which may be of sufficient strength to consume appreciable energy and to produce pulsations in the exit flow. In addition to these powerful flow distortions, another lack of symmetry is created in the discharge flow by the tendency of the rotating fluid mass to distribute itself in accord with the energy conserving principles of the free vortex, which produces high velocities along the path of short radius (along the inside of the bend) and low velocities along the path of long radius (along the outside of the bend). Use of short radius plain elbows will, accordingly, lead to energy losses and intolerable flow distortions.

A further analysis of a possible combination of the desirable flow properties of the long radius elbow with the desirable dimensional properties of the short radius turn leads to a compromise form which has found favor in many applications. This solution consists of disposing the cross-sectional duct area in such fashion that the width of area (dimension perpendicular to the plane of the bend) is increased and the depth is decreased. The improvement traceable to this change occurs because an increasing width-depth ratio (hereafter called the aspect ratio because of its similarity to the aeronautical term) reduces the percentage of total flow influenced by side wall vortices and leaves a core with a curved two-dimensional flow which can be maintained with losses only slightly greater than those which would be encountered in a similar straight duct. Decreasing duct depth produces decreasing differences in the centrifugal pressures on the inner and outer walls and consequent decreases in transverse flow. It is obvious, however, that increasing the aspect ratio will eventually increase the total wall area and consequent friction drag to the point where the incident losses transcend those of the normal side wall vortices. Test of rectangular sections with varying aspect ratios established that energy losses decreased rapidly with increasing aspect ratios up to a value of about 6 [3].

Disposing the duct area to a high aspect ratio is not as favorable a solution for the proposed tunnel design as it is in many other duct problems. The prime objection in this case is the severe shape transition required between such a duct and the connecting circular test section. Such transitions contribute undesirable flow irregularities and are to be avoided. In addition, the high aspect ratio requires large plane areas in fabricating the boundary walls; these are costly when designed for pressure loadings.

A digest of the foregoing indicates the large reductions in energy loss attending larger corner radii and aspect ratios cannot be taken advantage of in direct application to the external elbow proportions. However, a further analysis of the principle shows that internal addition of splitter partitions to an elbow of low aspect ratio and short radius effectively divides the flow into separate elbows individually having increasing radii and aspect ratios as the number of partitions increases. The benefits gained by this approach are soon limited as the addition of the splitters contributes increasing area for frictional drag. Tests of these compensating effects [3] indicate, in general, the use of two splitters yields a minimum loss for this type of elbow. The advantages of this type of construction led to its use in a number of early water tunnels.

A further refinement of the principles of the previous paragraph is accomplished by redistribution of the elbow elements into a mitered elbow fitted with a large number of short-length formed partitions or vanes. Proper design in this direction can divide the flow into a large number of cellular units operating at most favorable ratios yet without the large friction areas occasioned by the similar use of full length splitters. The measured losses in such an elbow are only about one-half to two-thirds of those in splitter elbows and are accompanied by a more uniform velocity distribution and less turbulence. Because of their low losses and flow quality these assemblies, known as vaned elbows, have been extensively used in wind tunnels since the first Göttingen tunnel of 1909 and are the accepted answer in wind tunnel designs. The structure and corrosion problems attending the use of such vanes in water retarded their acceptance in general water flow elbow applications until more recent flow quality requirements necessitated such acceptance. Their use in water tunnels has become quite general since 1938 and is considered the preferred approach to the proposed design.

The following summarizes the benefits attending proper use of vane type elbows in the proposed application: (1) minimum distortion of the velocity distribution; (2) minimum energy losses (as low as 10 per cent of the local kinetic energy of translation); (3) minimum strength and scale of such turbulence as is created; (4) minimum external physical dimensions; and (5) sensitive control of the velocity distribution through provision of adjustable vanes. It is the purpose of the remainder of this chapter to describe the detailed design of the vane geometry and the experimental tests conducted thereon.

B. Design Studies

Having determined the desirability of the vane type elbow for the application in question, the problem resolves itself into a selection of specific dimensional values which will produce an optimum flow condition consistent with practical forms for fabrication. The first significant dimensional value in the selection of the vanes is the spacing or number of vanes to be employed in the given elbow. This value is determined by a combination of the structural and hydraulic limits imposed.

Hydraulically, the only serious consideration is that the vanes shall reduce the area of the circular duct section to a group of approximate rectangles whose proportions or aspect ratio exceed a value of 6:1. Graphical division of a circular area into strips of equal width indicates that at least six or eight vanes are required to provide this aspect ratio for the rectangles forming the bulk of a circular section. An increase in the number of vanes will give even greater aspect ratios and will materially improve the discharge flow quality.

The number of vanes or spacings has a material influence on the structural properties of the vane when the vane is loaded as a beam since increasing numbers result in decreasing individual vane size and greater relative span lengths. While the reduction in vane size results also in a reduction in exposed load area, the beam strength decreases more rapidly than the load, and reduction in structural rigidity carried to an extreme may lead to deflection, vibration, and noise under high dynamic water loads. This can be alleviated by tying adjacent vanes together at points between the end supports, thus reducing the free span. It should be remembered, however, that such webs, struts, or tie plates, even though faired, introduce the same type of disturbance as a side wall and thus necessitate that aspect ratios be computed only on the basis of clear spans.

It therefore appears that the optimum number of vanes in an elbow is a unique compromise between the structural and hydraulic functions involved. These considerations have apparently been applied to previous water tunnel designs as the number of vanes of existing units appear to vary from 6 to 15, with ties being used with the larger values. Since the selection of vane number or spacing is intimately associated with the vane structural properties,

it becomes apparent that the size of the vane section is a necessary part of this selection and that certain definitions are necessary to the comparative description of vane properties. The most significant terms are defined in the following paragraphs and are shown in Fig. 30.

The vanes of a cascade are assumed to be of uniform cross section throughout so that the vanes may be replaced by their profile in a plane. The vane profile is defined by its chord length c and certain relative shape characteristics, such as maximum camber and maximum thickness. Only the chord is of importance at this time. The chord line is defined as the line obtained by placing a straight edge against the pressure side of the vane profile; it is tangent to the leading and trailing edges. The chord length is the distance between the projections of the extreme ends of the vane on the chord line.

A cascade of vane profiles is obtained by first selecting a straight line as a cascade axis. To form the cascade, vane profiles are placed on the cascade axis so that corresponding points on the profile fall at regular intervals along the axis and so that the chords of all the profiles make the same angle with the cascade axis. The distance between corresponding points on the axis is then the vane spacing s and the angle between the chord and the axis is the vane stagger θ. A given cascade is defined by the profile of the vanes, the chord length, the dimensionless spacing-chord ratio s/c, and the stagger angle θ. In place of the spacing-chord ratio, other investigators sometimes use the gap-chord ratio, where the gap is the projection of the spacing in the direction of approaching flow.

A cascade of vanes is installed in an elbow so that the cascade axis falls in a plane parallel to the miter plane of the elbow, where the miter plane is that plane formed by the intersection of the elbow walls. For a 90° bend, the cascade axis is placed at 45° to the direction of the approaching flow. The angle of attack between the approaching flow and the chord, designated by the symbol α, is then 45° less than the stagger angle; $\alpha = \theta - 45^{\circ}$.

An analysis of the limited amount of data available to justify a particular choice of dimensions disclosed that the most significant findings are those of Klein, Tupper, and Green [8], which indicate that vane turns for minimum energy loss should possess a spacing-to-chord ratio of about one half.

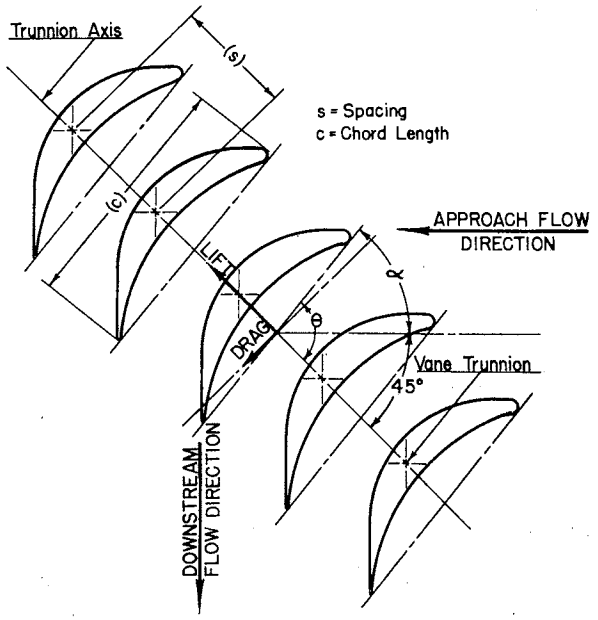

Fig. 30 - A Cascade of Vanes

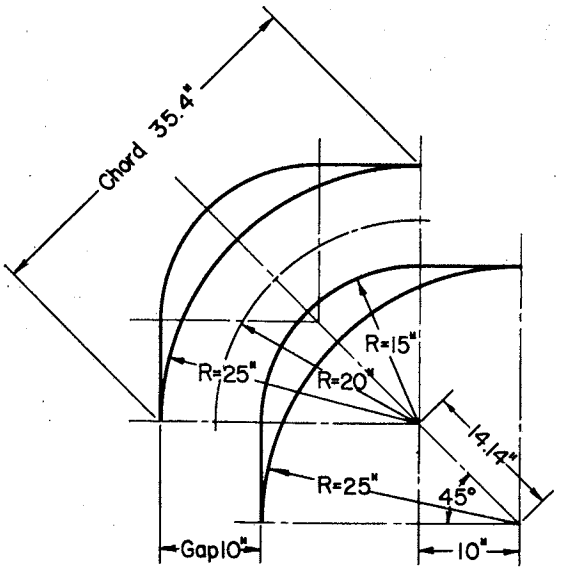

Fig. 31 - The Preliminary Vane Selection (Prototype Size)

On the basis of this and a preliminary analysis of dynamic loads and associated structural problems, a vane of the shape and the spacing shown in Fig. 31 was selected as a first approximation to the proposed design. This design is founded on arbitrary selection of a prototype vane gap of 10 inches. This dimension requires 18 gap units in the 15-ft diam of the prototype duct, a number larger than that used in other water tunnels but still not so large as to produce vanes of weak cross section. The chord is of convenient fabricating size, and the velocity profile should have a fine-tooth pattern.

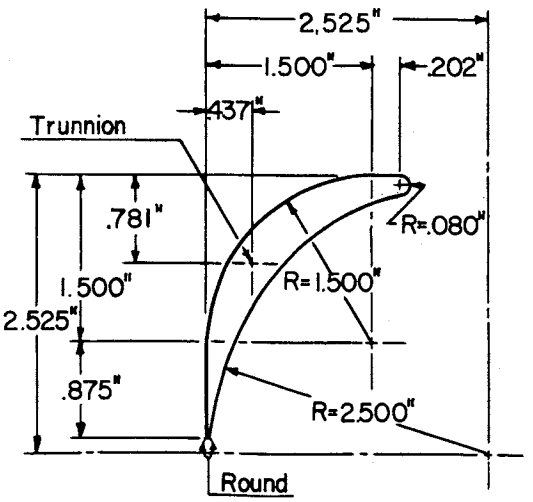

Fig. 32- The Proposed Vane Selection (Model Size)

It is apparent from Fig. 31 that the selected vane is of thickened cross section similar to wind tunnel vanes rather than the bent single plates used in most existing water tunnels. The thickened section was adopted because of its greater inherent structural rigidity and because it permitted a uniform gap (constant area) for flow passage through the vane. The former feature was important in view of the structural failures of single plate vanes

occurring in some water tunnel applications in this country; the latter feature was desirable in reducing separation eddies and the resulting energy loss and in providing directional stability, as evidenced by Collar's [9] findings.

The vane was formed with a minimum number of simple, circular arcs. For practical fabricating reasons this was considered preferable to the complex theoretical curvature of Krober [10] or the bent airfoils of Klein, Tupper, and Green [8] even though these refined forms offered slightly less energy loss.

In reducing the first approximation of Fig. 31 to a more practical form, Fig. 32, modifications were made similar to those used by Collar [9]. These consisted of a slight displacement of the surfaces to provide a finite and arbitrary prototype edge thickness of 1/4 in., a foreshortening of the fragile trailing edge, and a rounding of the leading edge in accordance with conventional aerodynamic practice. It has been contended by some authorities that the rounded leading edge satisfactory in aeronautics is subject to low pressure zones which could produce cavitation when employed with hydraulic blading, as in pumps or turbines. Accordingly, these designs sometimes employ sharp or hatchet edged blades to minimize the low pressure areas. This artifice might have been given further consideration if Collar's [9] work had not indicated that an angular adjustability of as much as 5^{o} might be necessary to permit determination of the optimum vane setting. The relative insensitivity to cavitation and separation of the rounded edge under angular changes in vane setting therefore dictated its use for the proposed design.

A thorough analysis of all earlier vane literature available indicated that the foregoing vane selection might serve as a suitable general approach to the problem but clearly indicated that refined performance characteristics could not be fully anticipated for the proposed prototype and that experimental studies directed toward the particular needs of this installation were imperative if the desired flow quality were to be achieved. Therefore, it was decided that a full model study of the proposed elbow should be undertaken.

Analysis of the model problem established that the one-tenth scale model proposed for study of other tunnel components would also be adequate to produce workable values for certain overall phases of the elbow tests but that

certain other phases could be more effectively examined by detailed studies on a separate flow diversion test bend. A flow diversion test bend was assembled and vaned elbows of one-tenth scale were fabricated for the model tunnel to accomplish these studies. The one-tenth scale vane profiles employed in both of these facilities were as shown in Fig. 32 and tests were arranged to supply these necessary design data:

(1) The angular setting of the selected vane which would provide the best discharge flow quality and least energy loss.

(2) The pressure distribution on the vane profile, with a view to clarifying the probability of cavitation and the magnitude and location of the dynamic structural loading.

(3) Scale relations between the model and the prototype.

C. Experimental Studies

1. Method

a. Apparatus

The experimental studies were conducted in two separate facilities. The first setup consisted of a small square duct (90° elbow) containing cast Cerrobend vanes; it was tested with both air and water as fluids. The second setup was a model tunnel elbow containing extruded aluminum vanes; it was tested only with water. The elbow was installed in the test stand with the bend in the horizontal plane. The entrance to the upstream tangent of the elbow was bolted to a plate on the end of a 12-in. diam supply pipe. A 6-in. square hole was centered in the plate to match the cross section of the Lucite pipe. Bolts through this plate served to hold a bell-mouthed contraction and a distributor ring in place in the 12-in. pipe. This distributor ring was used in conjunction with a supply of compressed air to introduce dyes or air bubbles into the flow.

For making measurements of the velocity and pressure in the elbow, three measuring stations (D-D, K-K, and M-M of Fig. 34) as well as two measuring discs and many separate piezometer taps were provided. The discs were used to permit traversable insertion of a Pitot cylinder to obtain

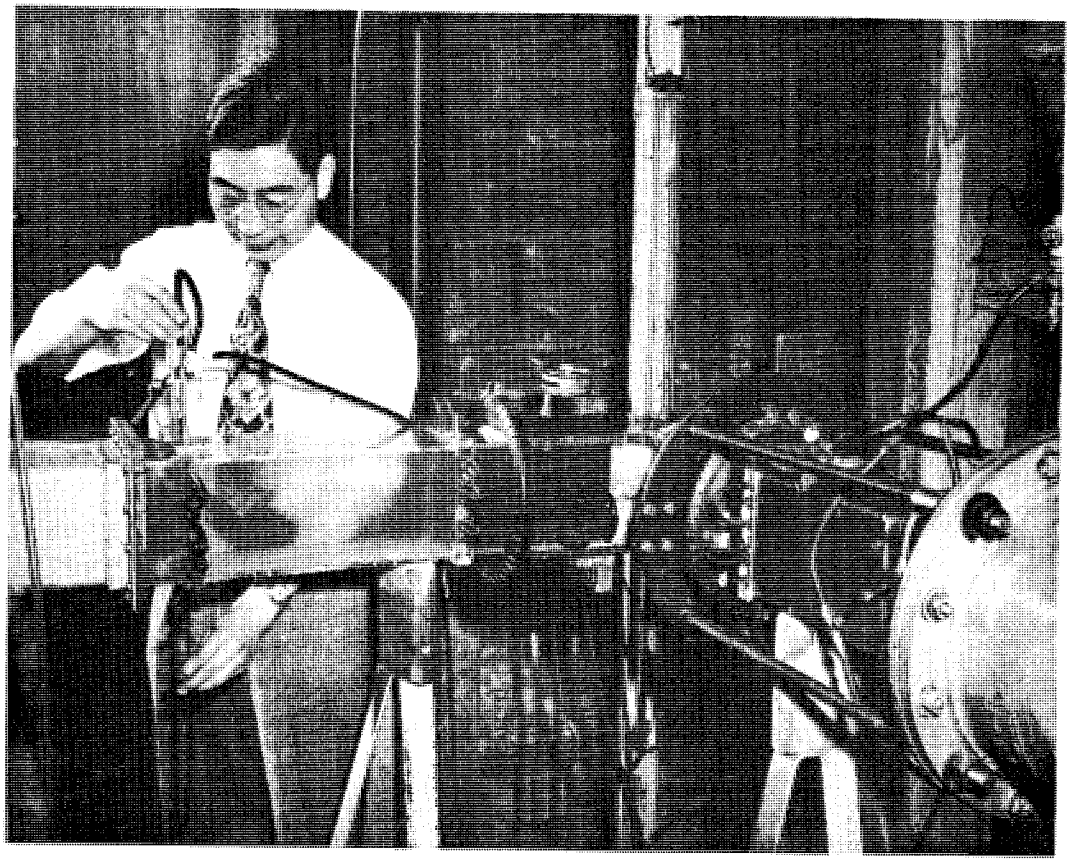

Fig. 33 – Flow Diversion Test Bend (Duct Elbow)

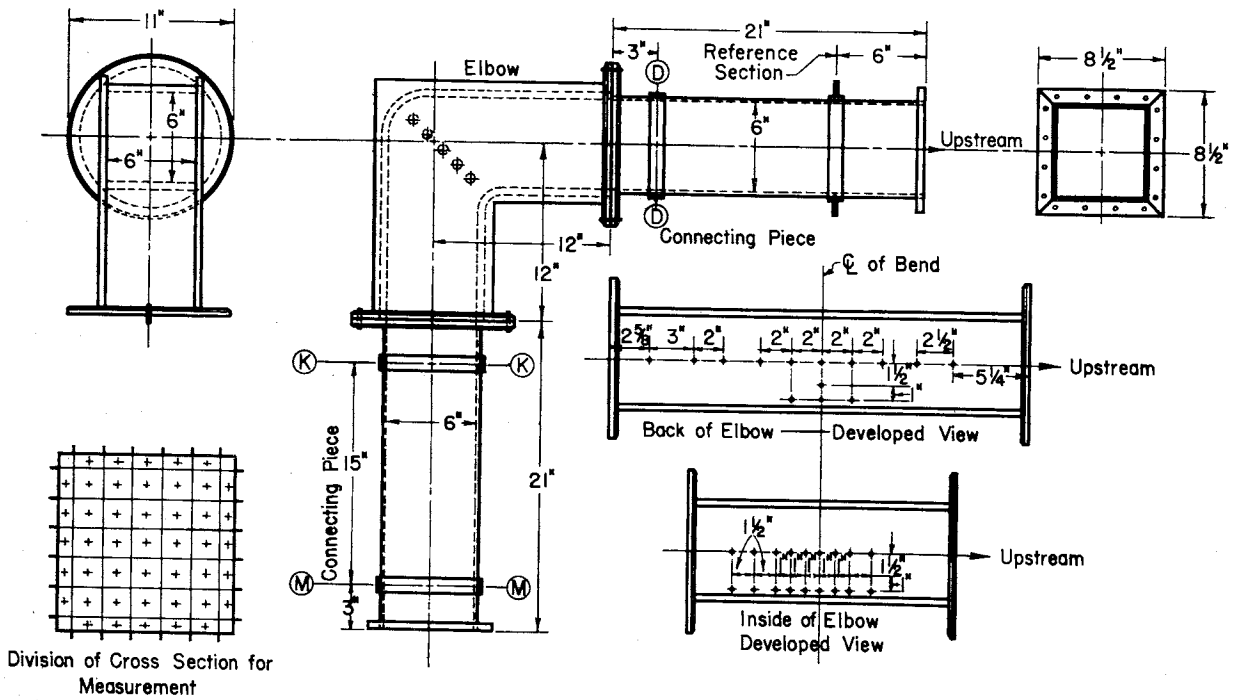

Fig. 34 – Duct Elbow Details

velocity and energy measurements immediately before and after the vanes, while the separate piezometer taps were used to obtain wall pressure measurements at many points around the bend. To remove all burrs, all 1/16-in. holes designed for wall pressure readings were carefully rounded at the inside edge to about 1/64-in. radius. At the measuring stations, the 1/4-in. holes allowed entry of a Pitot cylinder into the flow. These measuring sections made possible the obtaining of wall pressure readings at 24 points and velocity and energy readings at 45 points within the section in the course of a normal traverse.

The 12-in. diam supply pipe carrying fluid to the test elbow was connected to an air blower, and alternately to the main Laboratory supply channel, drawing water directly from the Mississippi River. This arrangement is shown in Fig. 35. The regulating valves in the 12-in. line were placed about 40 ft upstream from the elbow. A long honeycomb in the entrance pipe rectified the flow before it entered the bell mouth of the 6-in. duct. Flow of water through the elbow up to 4.5 cfs was measured by a discharge measuring flume, while the alternate capacity of the blower limited the flow of air to 30 cfs. The variations of the flow from either source were sufficiently small to be neglected entirely in the analysis and computation.

The discharge from the downstream tangent of the Lucite duct was led through a diffuser and a short length of 12-in. round pipe into a vertical pipe. The portion of this vertical pipe above the elevation of the Lucite duct served as a standpipe, and the lower portion conducted the water flow to the previously calibrated measuring flume. A valve in this lower pipe regulated the pressure in the Lucite duct while the standpipe protected the duct from an excess of pressure. The elbow was designed to receive a bank of five vanes of the form of Fig. 32 at the selected spacing of 1.414 inch. The free span of the vanes was 6 in., the full height of the duct. Thus the spacing-chord ratio is 0.48, the gap between the vanes is virtually 1 in., and the aspect ratio is 6 for these experiments. The aspect ratio of 6 assured two-dimensional flow near the centers of the vanes where measurements were to be made.

Two sets of vanes were used in the test bend, one consisting of pieces cut from the extruded aluminum stock adopted for use in the model water tunnel construction and the other consisting of specially prepared vanes of cast Cerrobend, a low melting temperature alloy. The Cerrobend vanes were

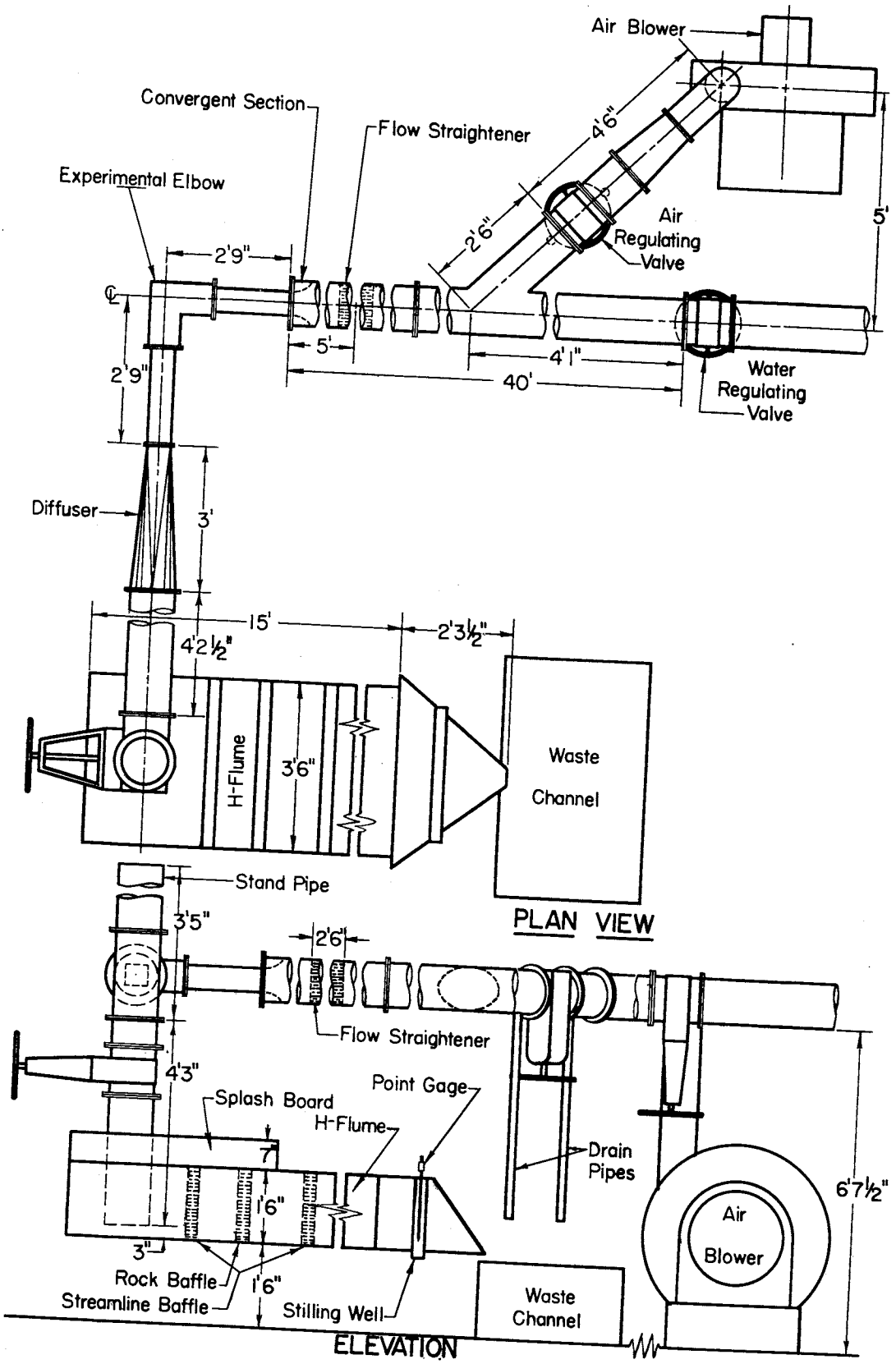

Fig. 35 - Duct Elbow Assembly

used because they permitted fabrication of "cast in" pressure taps and lines. The alternate set of extruded aluminum vanes was used for checking since it was discovered that the extruded vanes could not be produced with as great profile accuracy as could be done with the Cerrobend.

A final check of the shape of the experimental vanes disclosed a very close adherence of the Cerrobend vanes to all of the specified dimensions but it also revealed certain significant discrepancies in the shape of the extruded aluminum vanes. These differences were found to be at the leading edges and the region near the trailing edges of the aluminum vanes; the thicker sections of the vanes satisfied the specifications. The leading edge appeared to vary somewhat at different points along the spans but, in general, the nose was slightly more pointed than the radius of 0.08 in. specified. The tail of the vane was thinner than the design called for with a small ridge at the trailing edge. This thin section was bent around towards the center of curvature so that the profile presented a turn of about 95°. The overturning of the geometrical profile and the ridge were corrected before the installation of the vanes in the cascade frames. The verification of the performance of the aluminum vanes in relation to the dimensionally correct Cerrobend vanes was substantiated in the experimental data.

The Cerrobend vanes were polished smooth and then waxed before they were tested, but a slight roughness could be detected on the surface of the aluminum vanes. The effect of any differences in roughness between the vanes was not apparent in the evaluation of energy loss in the cascades nor in the observations of the flow on the surfaces of the vanes, as interpreted in a later section.

Pressure lines of 1/8-in. OD copper tubing were cast into all five of the vanes and were extended out through the end trunnions to provide a connection outside the duct for attaching the tubes to the manometers. Wall mounted, set screws bearing on the end of the vanes prevented the vanes from turning about the vane trunnions. This arrangement provided a rigid but adjustable support for the vanes in the simplest manner possible without disturbing the flow. It should be noted that the position of the trunnion as shown in Fig. 32 was selected to approximate the force center for the gravity and dynamic loads in order that torsional restraint and stability about the trunnion might be optimum. The center of dynamic forces was approximated by integration of a measured pressure diagram as obtained by Klein, Tupper, and Green [8] on a similar vane profile.

The general arrangement of the Cerrobend vane and its pressure tap system are shown in Fig. 36.

The vanes used in the one-tenth scale model tunnel were all cut from bar lengths commercially extruded of aluminum using a special die made in accord with the profile of Fig. 32. This method of production proved the most efficient way of making a considerable quantity of vanes of an accurate profile in a nonrusting material of adequate structural strength. The ends of the vane bars were carefully cut to fit the contour of the elliptic miter block of cast aluminum which served as the corner piece for each of the four elbows of the tunnel. The miter blocks were carefully machined with trunnion holes to accommodate the trunnion rods anchored in the vane on their inner end and clamped to the miter block with nuts on their outer end. The general arrangement of the elbow, miter block, vane, and vane trunnion are shown in Fig. 37.

While most of the vanes in the model tunnel were not equipped for detailed measurement, the central vane in elbow I (Fig. 38) was fitted for taking comparative pressure readings at ten points on the surface. Copper tubing was laid in grooved slots milled in the vane and then led down the inside wall of the vertical, circular duct to the instrument access opening in the tunnel wall at station 6 (Fig. 38). The grooves were filled with aluminum solder and the surface was polished, then checked for dimensional accuracy. Small piezometer holes were drilled into the copper tube normal to the surface of the vane. These holes were staggered where there might be interference but were confined to a band an inch on either side of the center of the vane span. The manometer arrangement allowed pressure on the vane surface to be recorded relative to station 5, a position close enough to make the static pressure difference a negligible amount.

The instruments used in making velocity and energy traverses in the model tunnel consisted of the "long" and "cantilevered" Pitot cylinders described in the appendix. The method of mounting the "cantilevered" cylinder is shown in Fig. 37. The instruments used in the test bend traverses were of similar form but differed slightly in methods of support and reading. These instruments were connected so that pressure readings with water flowing in the duct were measured by a 100-in. U-tube using air as the indicating fluid, and a 50-in. U-tube using kerosene as the indicating fluid. An inclined manometer draft gage was used to measure the pressures for the flow of air and a very

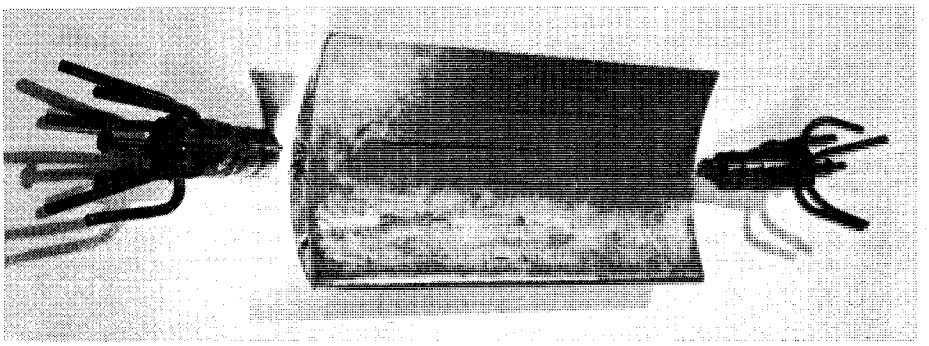

Fig. 36 - Duct Elbow Vane and Trunnions (Vane surface is polished smooth but is slightly discolored. Chord length = 2.93 in.)

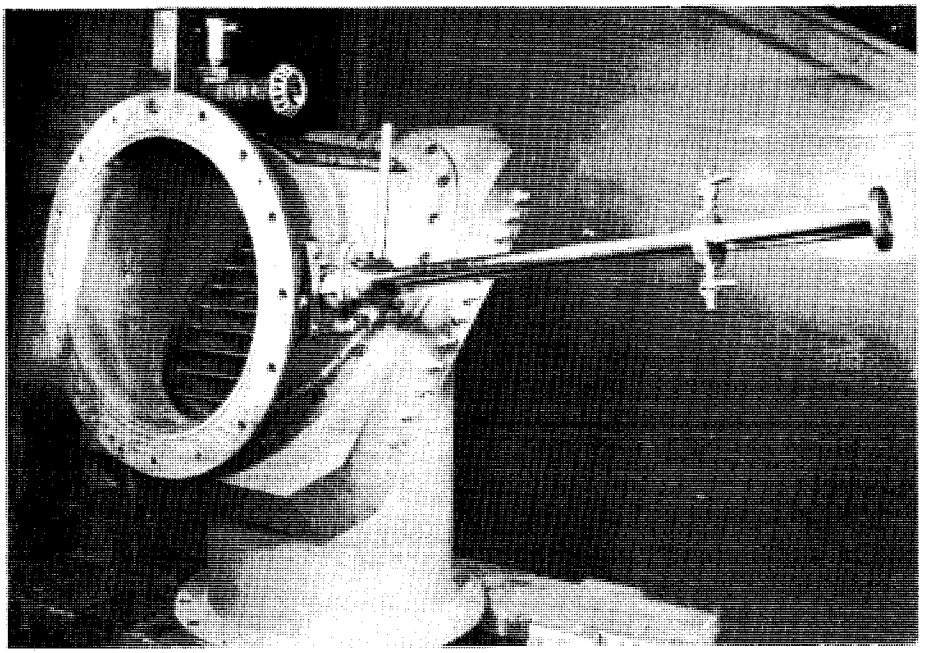

Fig. 37 - Upstream View of Elbow I (Showing Vanes and Vane Anchorage Arrangement Together with Pitot Cylinder and Its Main Mounting Arrangement at Station 5)

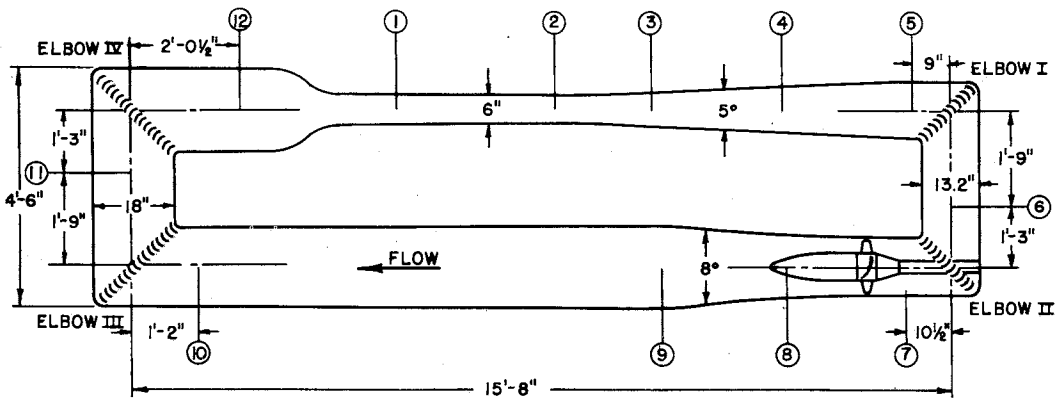

Fig. 38 - Designation of Vaned Turns and Velocity Traverse Stations

large manometer bank was used as a method of obtaining simultaneous photographic readings when using water.

Velocity traverses made in the model tunnel were taken at stations 5, 6, 7, 10, 11, and 12 (Fig. 38) and employed the manometers described in the appendix.

b. Visual and Photographic Studies

Preliminary studies of the flow mechanism and certain of the final conclusions were accomplished by visual and photographic studies in the transparent walled, square elbow. These observations employed four different techniques, each of which added to or confirmed the general fund of information. The four methods and their most significant findings follow:

(1) Photographs of the flow taken during a period when air bubbles were being introduced at mid-depth through the upstream distributor ring are typified by those shown in Fig. 39. The photographs indicate the existence of a more nearly axial flow immediately before and after the bend for a stagger of 101° than is true for the 90° and 96° settings. Since the density of the air bubbles differs materially from that of the water, areas of the flow involving curved streamlines or centrifugal forces cannot be interpreted too literally from the photographs. The flow streaks should, however, give quite reliable information on the approach-flow direction and the location of the front stagnation point.

(2) Analyses of the local directions of flow were obtained in many regions by cementing one end of short filaments of fine thread to the vane surface and by stretching a fine traversable wire across the duct and attaching short threads thereto. Visual studies under a variety of flow conditions served to clarify the directional pattern and strength of turbulence both in the core flow and near the boundaries and was most helpful in pointing out the manner in which the walls produced spiral flow near the ends of the vanes. The traverse at mid-depth at the 96° stagger showed an extremely turbulent region from a point directly behind the trailing edge of a vane to a point about 3/8 in. from the suction side. The same region at the 101° stagger was very smooth except directly behind the trailing edge, where only moderate disturbances were noted. The flow behind the portion of the gap closest to the pressured side of a vane was very smooth at the 96° stagger angle and exhibited a slight fluctuation at the 101° stagger.

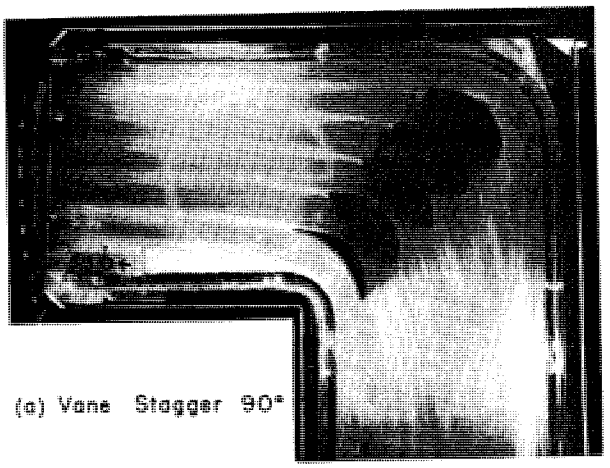

(a) Vane Stagger 90°

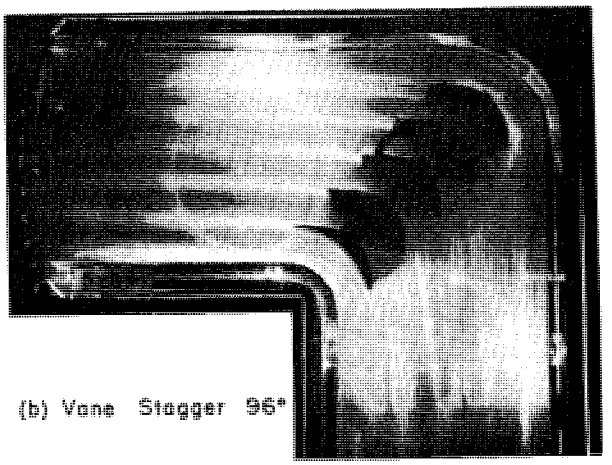

(b) Vane Stagger 96°

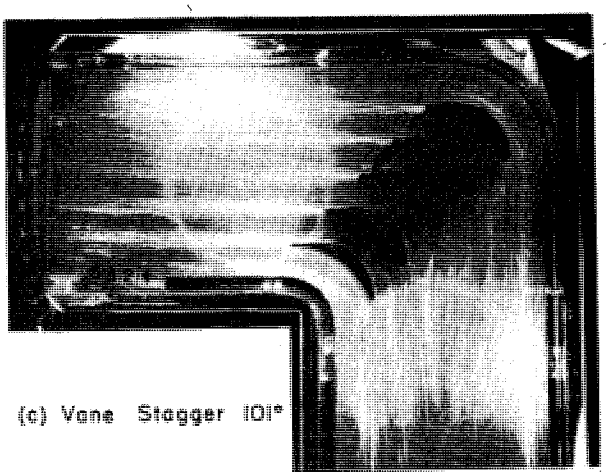

(c) Vane Stagger 101°

Average velocity of water ($\overline{V}$) = 7.9 fps.
Reynolds number (ℓ = duct depth) = 300,000
s/c = 0.48

Fig. 39 - Paths of Air Bubbles at Mid-Depth of Duct Elbow Cascade

(3) Information on local directions of flow on the vane boundaries was obtained by admitting colored water through the pressure measuring taps of the suction side while air flowed through the duct. Under the action of gravity the liquid ran vertically down the vane axis in all regions where the velocity was too low to stream it horizontally in the direction of flow. While the presence of vertical flow streaks cannot be presumed to be rigid evidence of separation, they are indicative of the low boundary velocities favorable to separation. It is of importance to note that while vertical streaks were evident about 3/4 in. ahead of the trailing edge for a stagger angle of 96°, they occurred only immediately adjacent to the trailing edge for the 101° stagger.

(4) General boundary-layer flow patterns were obtained by coating both the vanes and the boundary walls with a thin paste consisting of aluminum dust in SAE 30 machine oil. Photographs taken after a brief run with water served to

define the pattern, particularly near the vane ends. It is of interest to note that flow patterns defined in the boundaries usually show much stronger lateral directions than those observed in the core flow. This difference is seemingly conflicting but when it is rationalized that boundary particles are motivated largely by pressure gradients while core flow particles are motivated largely by their own inertia forces, the difference in pattern is quite compatible.

2. Quantitative Tests in the Duct Elbow

Since the vane shape and spacing had been selected, it was the purpose of the tests to determine the optimum stagger angle setting and the flow characteristics produced by this setting as confirmation of the findings of the visual and photographic studies. This determination was achieved by traversing the duct section at measuring stations D-D, K-K, and M-M (Fig. 34) with the Pitot cylinder and by boundary measurements of the pressure on the duct wall and on the vane surface.

Traverses with the Pitot cylinder determined the total head and local velocities; they were computed using static pressures interpolated from peripheral boundary pressure measurements. All of the measured pressures are with reference to the static pressure at an arbitrary section located near the upstream end of the approach tangent. Use of such a point as a pressure base eliminated local pressure errors which might have been caused by the presence of inserted instruments or small changes in the total head on the system. An integration of the local velocity and discharge elements was compared with the metered total discharge as a check on the accuracy. In addition to the total head values the Pitot cylinder also supplied information on the flow direction. The local flow direction was interpolated from the cylinder reading when it was positioned both horizontally and vertically.

While a large volume of data was gathered and analyzed for both air and water flows with the Reynolds number varying from 119,000 to 833,000 (based on ℓ = duct depth = 0.5 ft) only four representative conditions have been included in the velocity data of Figs. 40 to 43. These conditions were selected because they serve to show the influence of alternate vane angle settings over a wide range of the Reynolds number. In these figures the velocity value is reduced to a dimensionless comparative form by expressing it as the quotient $V/\overline{V}$ where V is the local velocity component and $\overline{V}$ is the average longitudinal velocity through the section. The longitudinal velocity component is entered

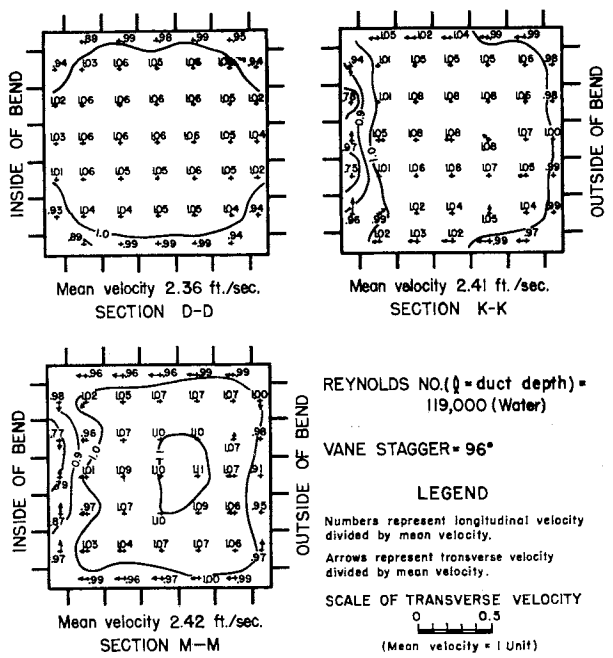

Fig. 40 - Duct Elbow Velocity Distribution (Series No. 10)

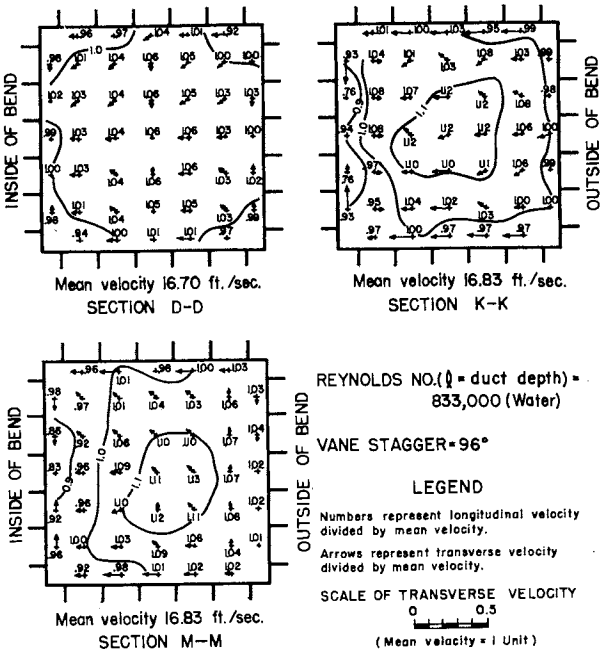

Fig. 41 - Duct Elbow Velocity Distribution (Series No. 15)

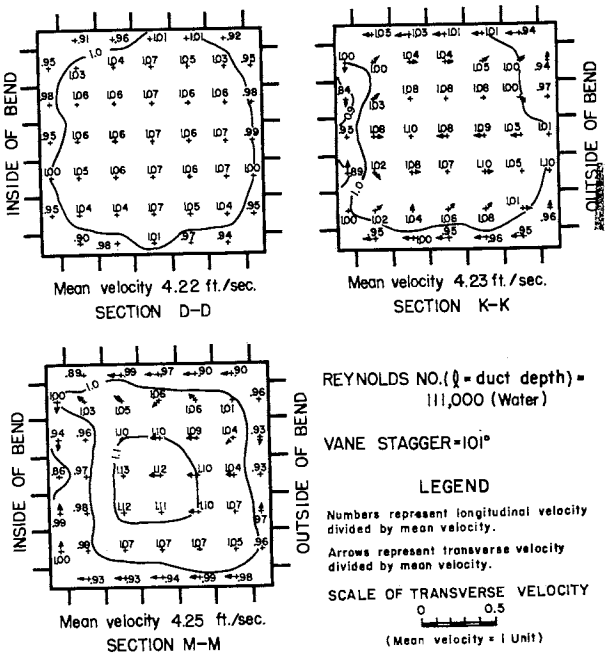

Fig. 42 - Duct Elbow Velocity Distribution (Series No. 16)

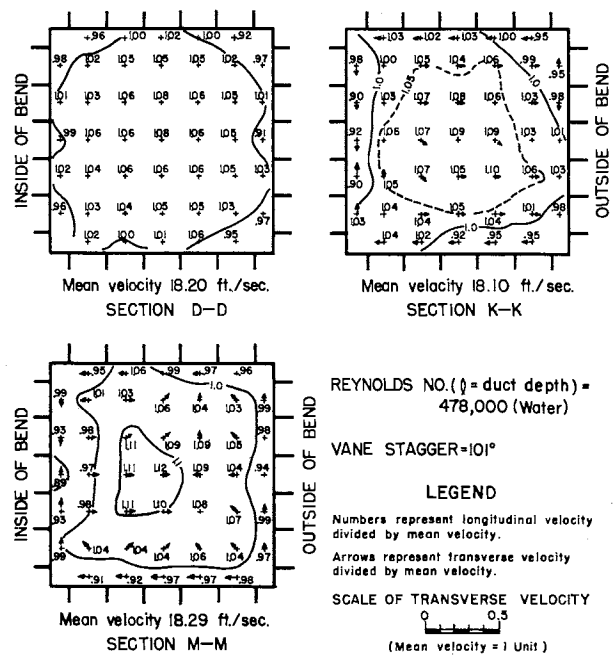

Fig. 43 - Duct Elbow Velocity Distribution (Series No. 18)

on the diagram at the point where the measurement was taken. The velocity components in the plane of measurement are plotted as vectors originating at the point of measurement and are scaled as shown. The diagrams are oriented such that the reader is looking downstream, with the inside of the bend on his left.

In addition to this velocity data, the relative pressure distribution around the bend was obtained at mid-depth of the side walls and dimensionless values of this are shown in Fig. 44. Pressures measured by taps on the vane surfaces are shown in a general comparative way in Figs. 45 to 47, while a more detailed distribution is shown in Fig. 48.

3. Quantitative Tests in the Model Tunnel Elbow

While the tests conducted in the duct elbow allowed flexibility and detailed flow study of the vanes, the environment was essentially a two-dimensional and somewhat idealized condition which did not wholly represent the prototype condition. Therefore, to assure a better understanding of prototype performance, it was deemed necessary to conduct model water tunnel vane studies in which the environment permitted the influence of other flow components. To this end velocity profiles and contours were determined at stations 5, 6, 7, 10, 11, and 12 (Fig. 38), utilizing the 3/8-in. diam "cantilevered" Pitot cylinder as described in the appendix. The profiles were taken on two diameters of the test plane, one of which lay in the plane of the tunnel loop while the other was at 90° thereto.

The most significant of these velocity studies were those measured at stations 5 and 6 and at stations 11 and 12. The former pair gives insight into the effect of the very bad entrance condition produced by the diffuser action, while the latter pair shows normalized approach conditions. The measured data for the former pair are shown in Figs. 49 and 50, while typical data for the latter pair are shown in Fig. 51. In examining Fig. 51, the reader is oriented facing upstream.

In addition to the foregoing velocity studies of the vane, pressure distribution studies were made on the surface of the middle vane of elbow I. Ten pressure measuring holes located around the vane periphery and disposed in a narrow band at the center of the vane were connected to a manometer which permitted pressure measurements to be made relative to the static pressure at station 5. Data from these pressure taps are plotted in Fig. 52 for three

vane stagger settings. In these plottings the local vane pressures are treated dimensionlessly by comparing them with the stagnation head of the local velocity. The pressure curves represent composites of data taken at three test section speed settings (18, 30, and 50 fps) since the scatter with speed was less than 5 per cent from the average.

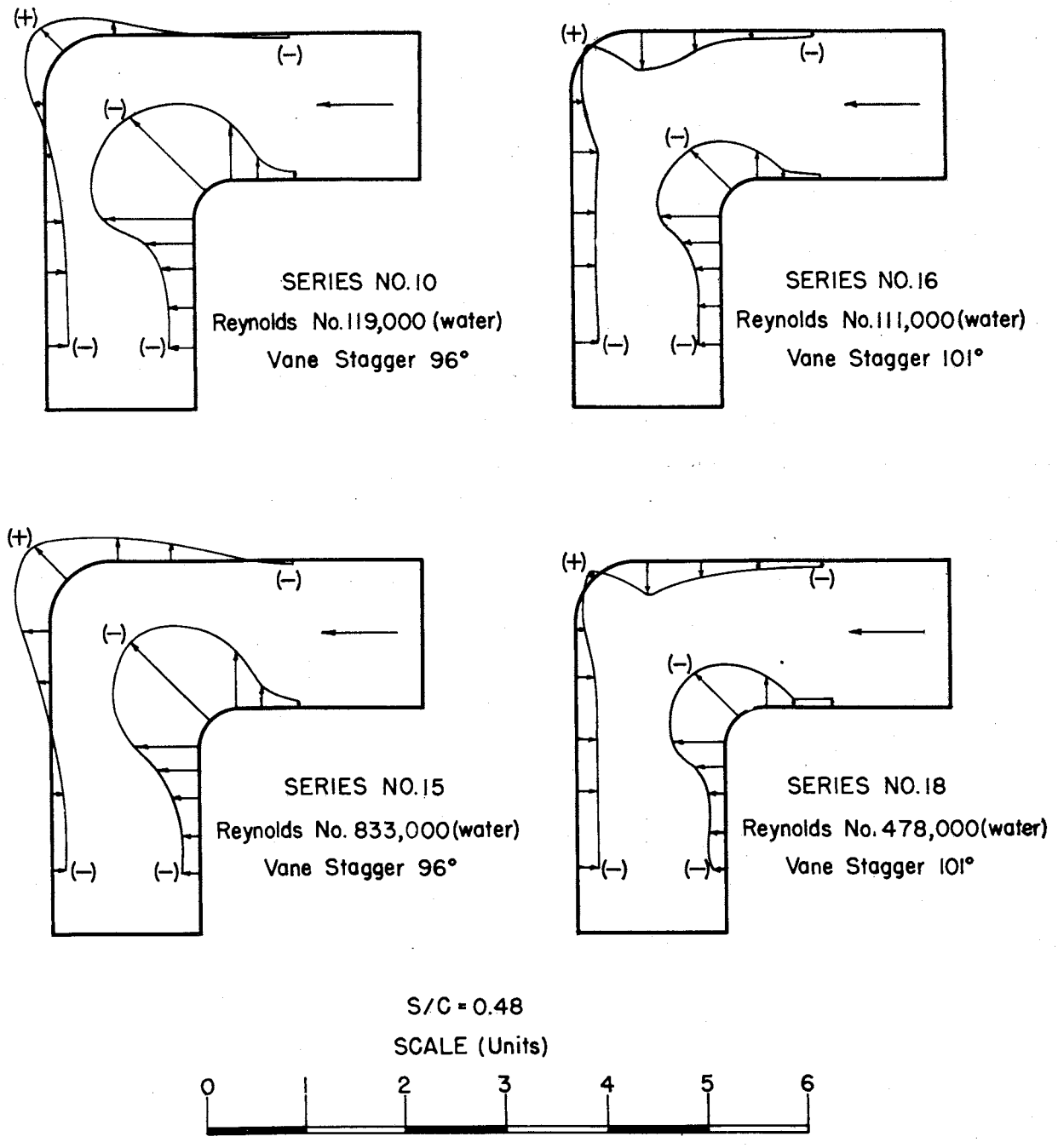

Fig. 44 - Wall Pressures at Mid-Depth of Duct Elbow
(Wall pressures in feet divided by mean velocity head in feet)

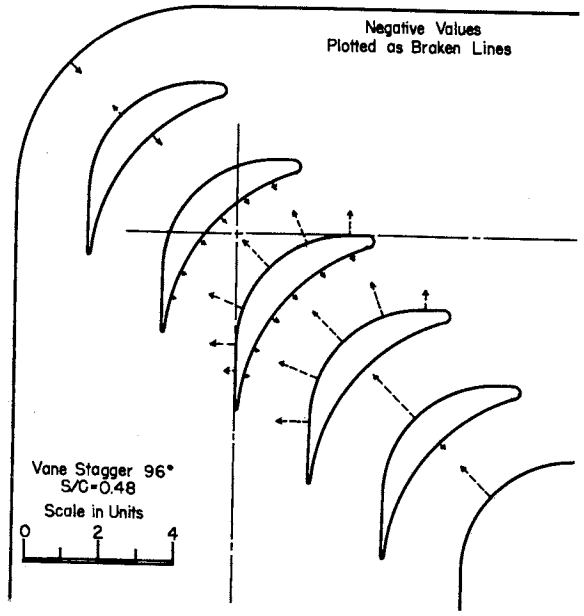

Fig. 45 - Pressures at Mid-Depth Across 96 Degree Cascade (Pressures in feet divided by mean velocity head in feet)

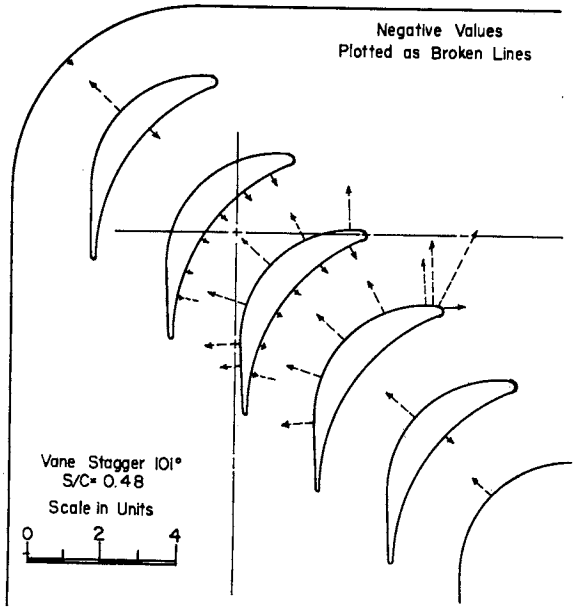

Fig. 46 - Pressures at Mid-Depth Across 101 Degree Cascade (Pressures in feet divided by mean velocity head in feet)

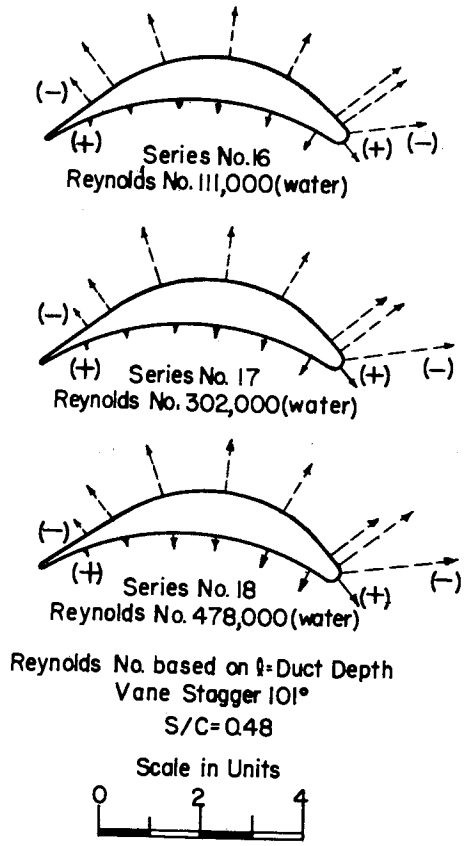

Fig. 47 – Pressure variation Around Vane as a Function of Reynolds Number (Pressure in feet divided by mean velocity head in feet.)

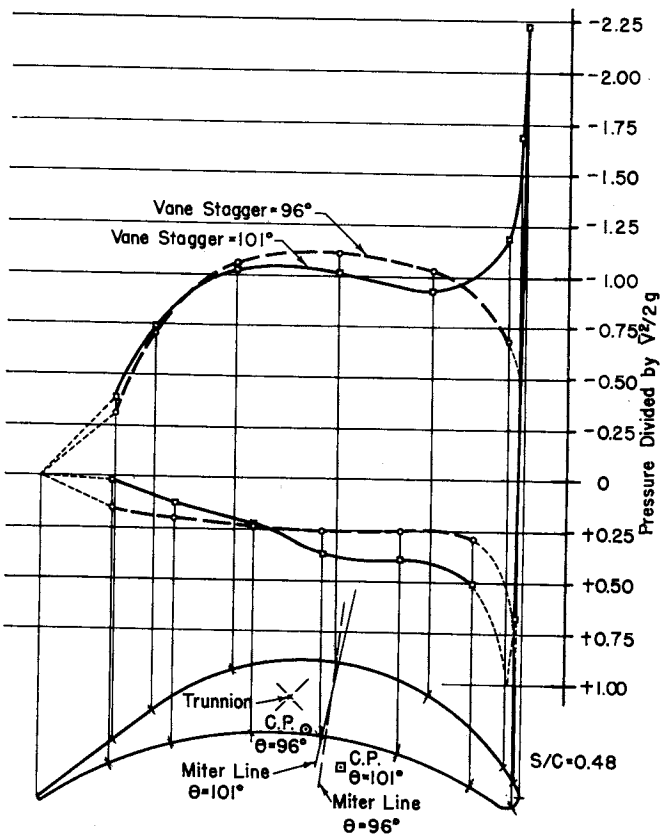

Fig. 48 - Duct Elbow Vane Pressure Distribution

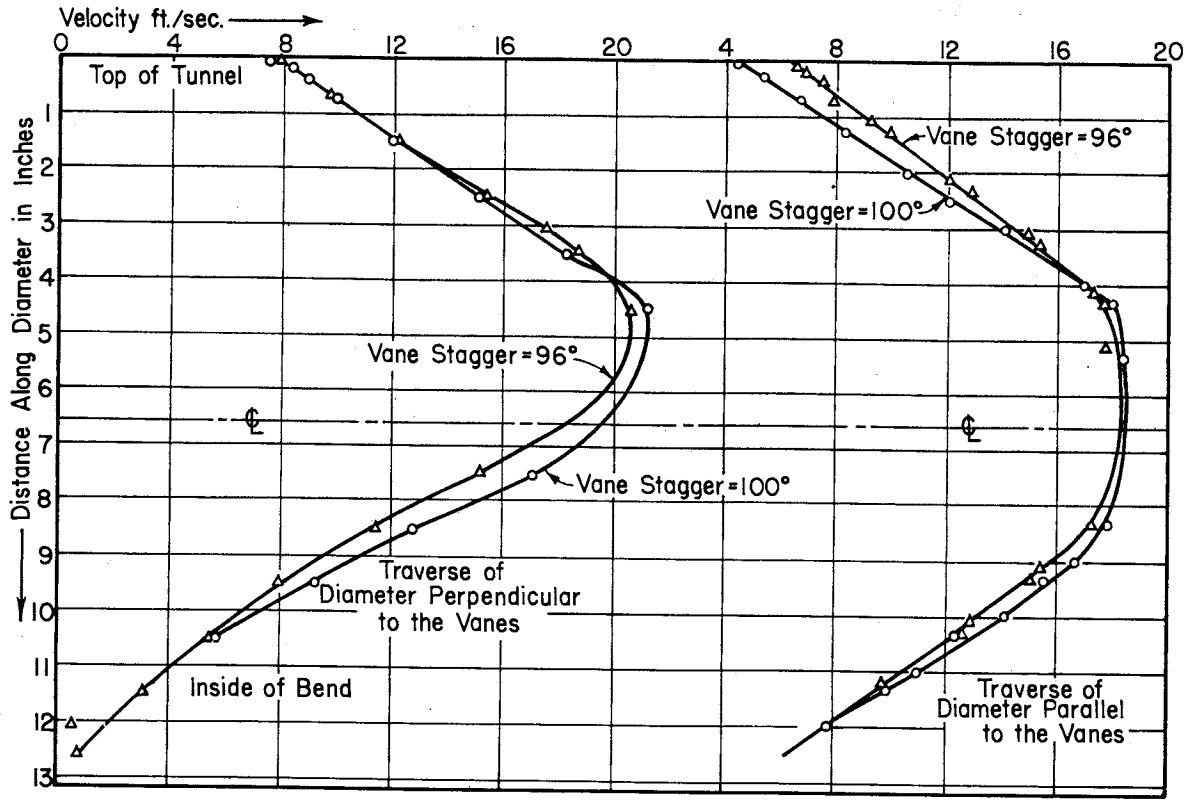

Fig. 49- Velocity Profiles at Station 5

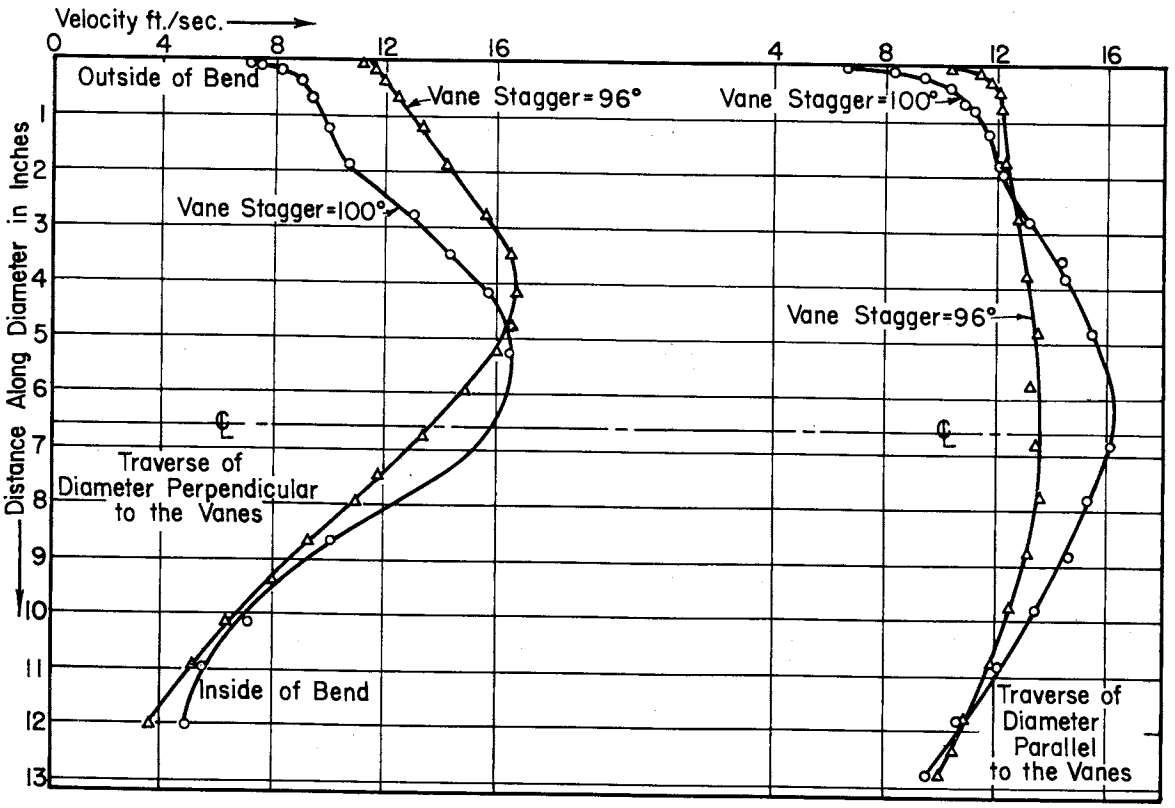

Fig. 50- Velocity Profiles at Station 6

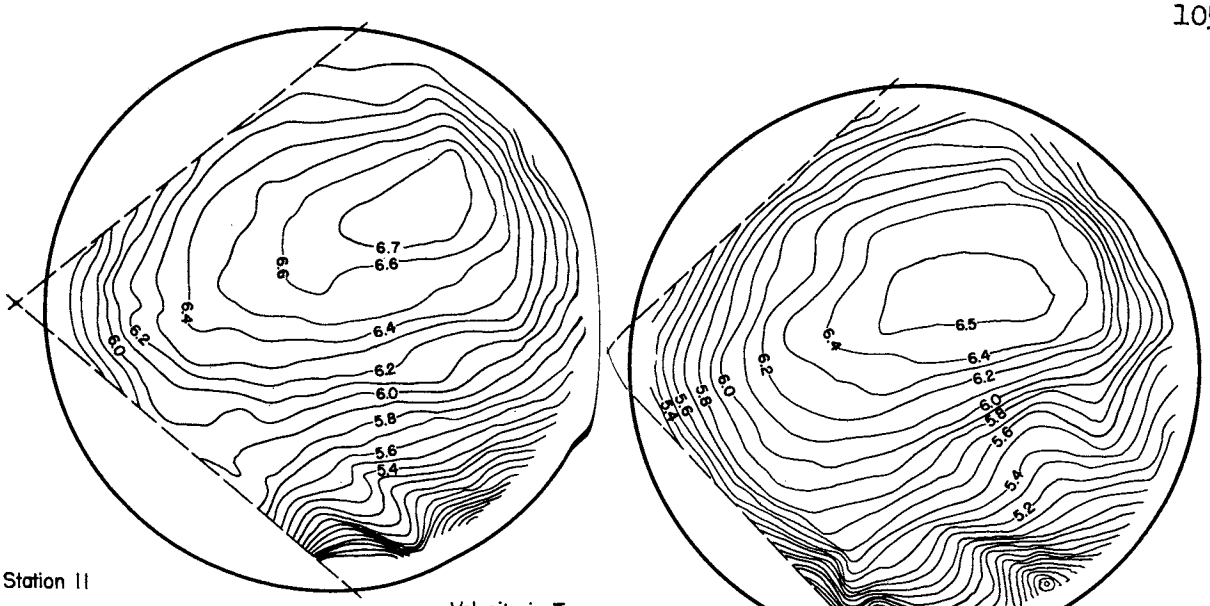

Station 11

Velocity in Test Section = 49.6 ft/sec.
Isovel Interval = 0.1 ft/sec.
Vane Stagger = 98°
S/c = 0.48

Station 12

Fig. 51 - Velocity Distributions at Stations 11 and 12

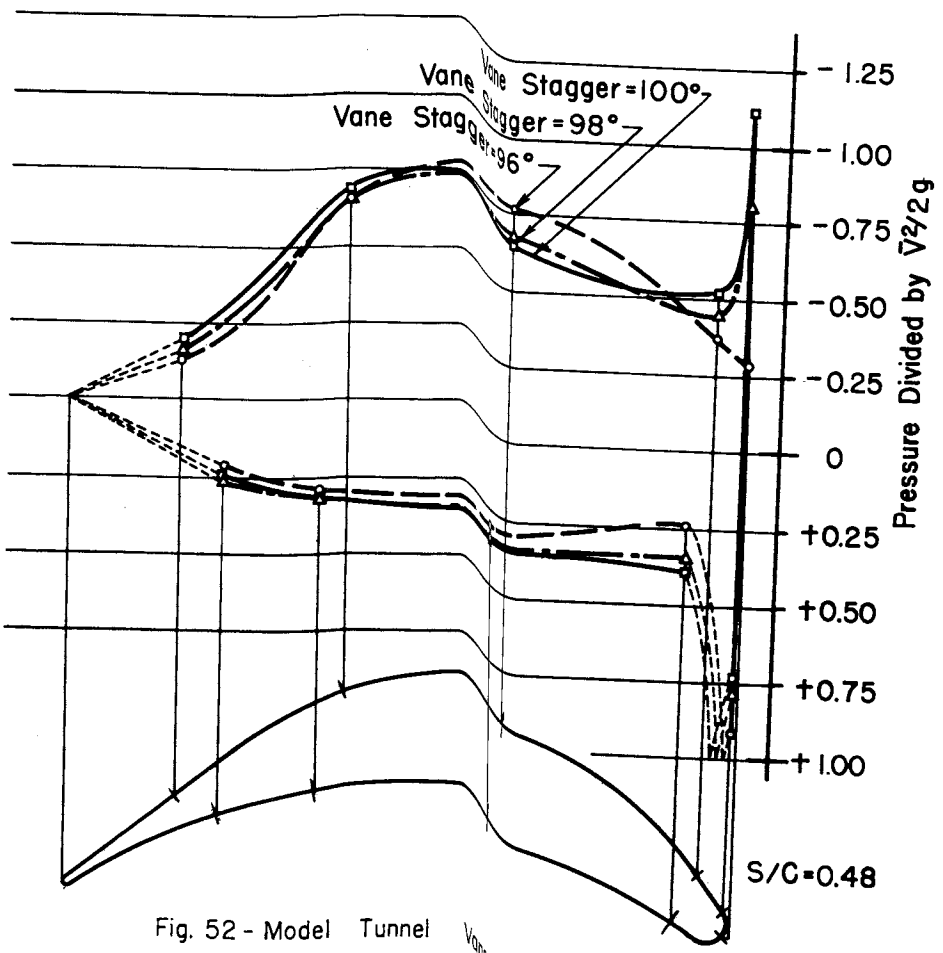

Fig. 52 - Model Tunnel Vane Pressure Distribution

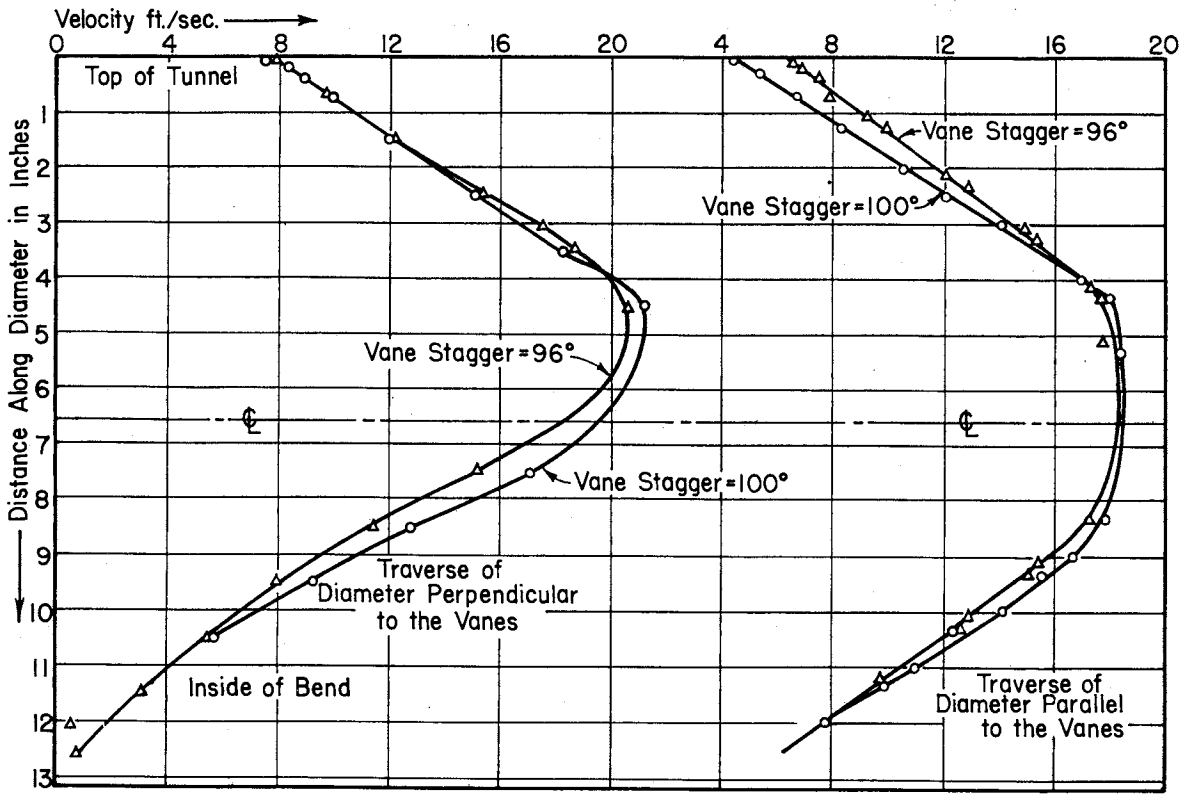

Fig. 49- Velocity Profiles at Station 5

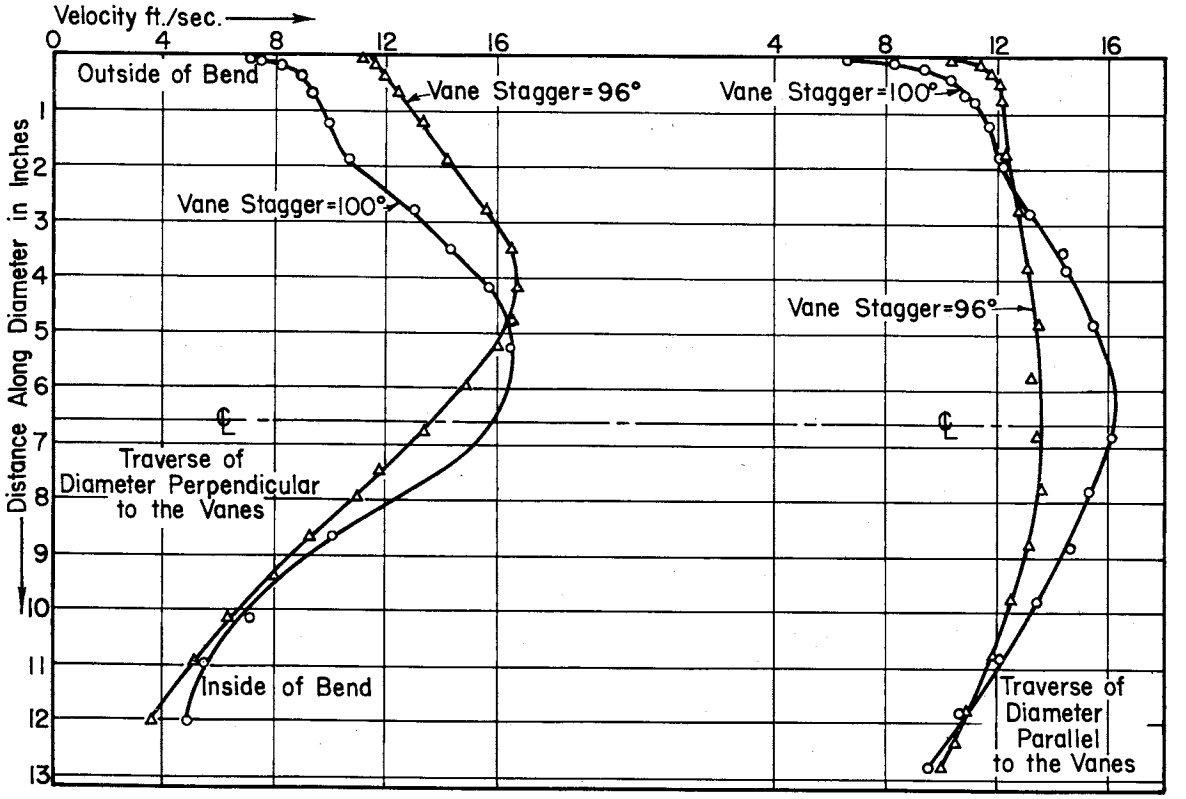

Fig. 50- Velocity Profiles at Station 6

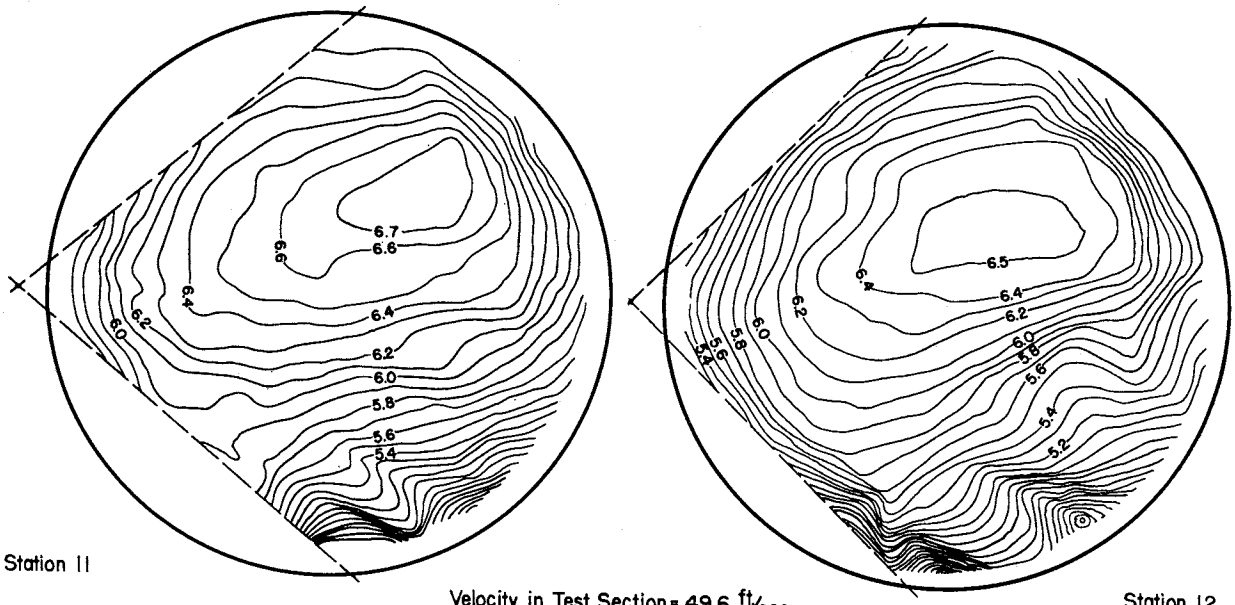

Station 11

Station 12

Velocity in Test Section = 49.6 ft/sec.
Isovel Interval = 0.1 ft/sec.
Vane Stagger = 96°
S/C = 0.48

Fig. 51 - Velocity Distributions at Stations 11 and 12

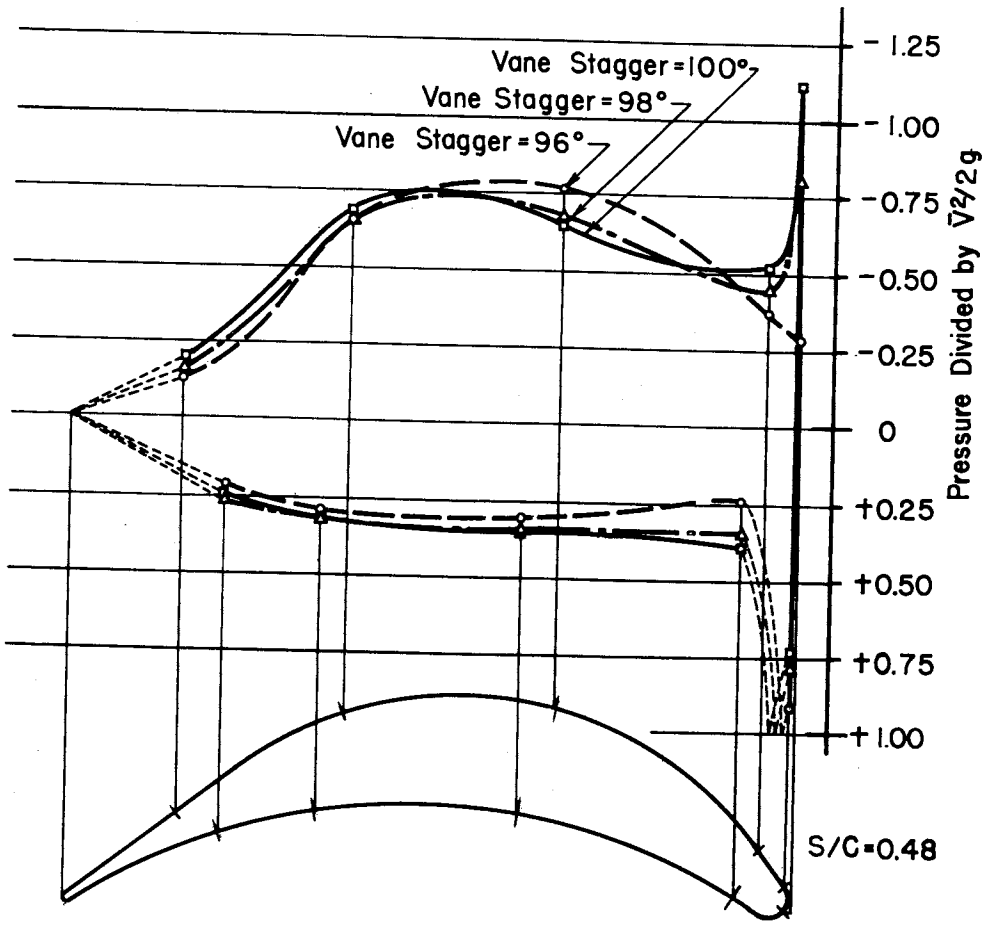

Fig. 52 - Model Tunnel Vane Pressure Distribution

4. Flow Distribution

An analysis of the physical geometry discussed on page 86 under the section on design studies, together with the measured values summarized in Figs. 39 to 43, 49, and 50, discloses the following characteristics:

(1) When arranged at a 90° stagger angle, the selected vane will materially underturn the bulk flow, according to Fig. 39. The condition is substantially improved by increasing the angle to 96° but evidences of some underturning are still apparent. An increase of angle to 101°, however, produced a flow in which the entering and discharging directions were substantially axial. This turning action, as shown in Fig. 39 for the duct elbow studies, is also confirmed by Figs. 49 and 50 of the model tunnel studies where the poorly distributed flow coming from the diffuser is shown to be turned effectively by the 100° elbow vanes but distinctly underturned by the 96° vanes.

(2) A more detailed probing of the velocity distribution, as evidenced in Figs. 40 to 43, shows that while all indicated settings had a quite uniform and symmetrical flow pattern in the entrance section D-D, the 96° blade settings at section K-K show a very considerable deficiency in velocity at the inside of the bend with a concentration of maximum velocities to the right or outside of center. The local velocity deficiency and lack of symmetry are evident not only at section K-K immediately adjacent to the bend but are also apparent 5 diam downstream at section M-M. On the other hand, a study of the comparable values for the 101° stagger angle shows only very slight evidence of the same effect.

(3) The velocity vectors near the wall, as shown in Figs. 40 to 43, indicate that a double spiral vortex is being generated in the boundary region by the pressure differentials evident in Fig. 44. The condition is apparent for the 96° and 101° stagger angles, but it is somewhat stronger in the case of the 96° angle.

(4) As evidenced by the core flow vector arrows, the velocity components which are other than axial are apparently random in nature and probably reflect small disturbances caused by the individual vanes.

(5) The change in velocity distribution between sections D-D and M-M evidenced in Figs. 42 and 43 is consistent with the progressive changes in distribution usually found near a pipe entrance, as the boundary-layer growth changes a uniformly distributed entering flow to a hyperbolic, stable, turbulent profile. That this change is a product of the duct boundary rather than the vane geometry

is borne out by the fact that very little change in profile is evident in passing through the vanes when the flow entering them has a well developed boundary-layer profile. This phenomenon is shown in Fig. 51, which shows velocities for the vaning of elbow IV in the model tunnel.

(6) A study of velocity patterns for a wide range of Reynolds numbers (data on all runs not shown) indicates that only those taken with very low Reynolds numbers, such as Figs. 40 and 42, differ from the general average represented by the high values shown in Figs. 41 and 43.

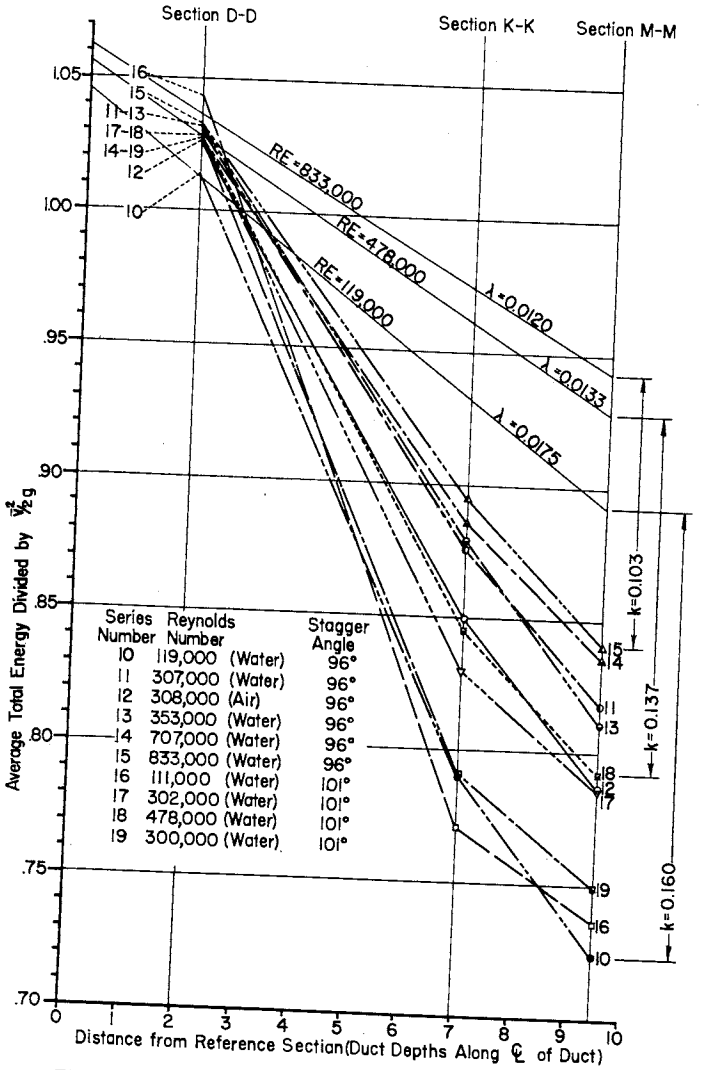

Fig. 53 - Duct Elbow Energy Progressions

5. Energy Loss

Since elbow energy loss is an important part of the total power requirement for a water tunnel, measurements to evaluate this loss were taken in both the duct elbow and the model water tunnel. These measurements consisted of the same basic total head and boundary pressure values used in the flow distribution studies, but they were interpreted to show the progressive changes in total energy as the flow proceeded along the duct. A summary graph of the energy data as recorded at duct sections D-D, K-K, and M-M is shown in Fig. 53. In this plotting, the abscissa scale is the dimensionless axial distance value while the ordinate is a dimensionless measure of the total energy as averaged for a particular cross section. It is to be noted that in addition to series 10, 15, 16, and 18, partially detailed in Figs. 40 to 43, data from six other series are included.

Evaluation of the loss occasioned by the elbow elements alone, as contrasted to an equivalent length of straight, smooth conduit, led to the

comparative plotting of the latter values at three representative levels of the Reynolds number. The straight, smooth pipe plottings are based on computation of the formula, $1/\sqrt{\lambda} = 2 \log R\sqrt{\lambda} - 0.8$*, where R is the Reynolds number and λ** is the dimensionless resistance coefficient. The validity of this formula had been established previously by measurements in a straight length of duct fabricated in the same manner as the duct elbow. The loss curve for the straight pipe was arbitrarily drawn through the D-D point of the corresponding Reynolds number curve for the duct elbow data of Fig. 53.

From the graphical data of Fig. 53, k, the coefficient of energy loss due to the bend, can be measured by taking the difference of ordinate values for the corresponding straight pipe and elbow curves at an abscissa distance where the two curves have become parallel. While the limited number of measuring sections shown in Fig. 53 do not fully establish that complete parallelism has been achieved, it is apparently very nearly true. On the basis of this assumption, the three representative values of k have been plotted as shown at the right of the figure. It is to be noted that the three values show an increase as the Reynolds number decreases.

The limited evidence of Fig. 53 does not show a marked difference in total energy loss when vane angles of 96° and 101° are compared but the slopes of the curves between sections D-D and M-M consistently show that the 101° vane series achieved most of the loss between D-D and K-K, whereas the 96° vanes show substantial loss still occurring between K-K and M-M. Such a loss distribution would seem consistent with the flow patterns of Fig. 39.

The data taken from the model tunnel elbows were recorded in a manner different from that summarized in Fig. 53 for the duct studies and are presented in the form shown in Table VIII. This table is based on use of the Bernoulli energy relation integrated across the tunnel section in the following manner:

$$\int_{A_1} \left(\frac{p}{w} + \frac{V^2}{2g}\right) V \, dA - \int_{A_2} \left(\frac{p}{w} + \frac{V^2}{2g}\right) V \, dA - \frac{E_t}{w} = 0$$

---

*Kármán-Prandtl resistance equation for turbulent flow in smooth pipes.

**$h_f = \lambda (\ell/d) (\bar{V}^2/2g)$

TABLE VIII

VANED ELBOW ENERGY LOSS DATA

Elbow	Test Section Velocity (fps)	18.00	30.00	49.62
I	Reynolds Number*	90,000	165,000	370,000
	$\bar{V}_5$ (fps)	3.72	6.20	10.25
	$\bar{V}_5^2/2g$ (in.)	2.58	7.16	19.58
	$\bar{V}_6$ (fps)	3.72	6.20	10.25
	$\bar{V}_6^2/2g$ (in.)	2.58	7.16	19.58
	α_5	1.812	1.812	1.812
	α_6	1.308	1.308	1.308
	$p_5 - p_6/w$ (in.)	+0.21	-0.41	+0.40
	k	0.554	0.416	0.493
II	Reynolds Number*	90,000	165,000	370,000
	$\bar{V}_6$ (fps)	3.72	6.20	10.25
	$\bar{V}_6^2/2g$ (in.)	2.58	7.16	19.58
	$\bar{V}_7$ (fps)	3.90	6.50	10.77
	$\bar{V}_7^2/2g$ (in.)	2.83	7.87	21.65
	α_6	1.308	1.308	1.308
	α_7	1.090	1.090	1.090
	$p_6 - p_7/w$ (in.)	1.17	3.57	8.8
	k	0.527	0.570	0.515
III and IV	Reynolds Number*	46,000	75,000	138,000
	$\bar{V}_{10}$ (fps)	2.0	3.33	5.51
	$\bar{V}_{10}^2/2g$ (in.)	0.75	2.065	5.66
	$\bar{V}_{12}$ (fps)	2.0	3.33	5.51
	$\bar{V}_{12}^2/2g$ (in.)	0.75	2.065	5.66
	α_{10}	1.050	1.050	1.050
	α_{12}	1.071	1.071	1.071
	$p_{10} - p_{12}/w$ (in.)	0.25	0.70	1.45
	2k	0.244	0.250	0.166
	k	0.122	0.125	0.083

*Reynolds number is based on chord length (2.95 in.)

where p = pressure,

V = axial velocity,

w = specific weight of fluid,

A_1 = area upstream of elbow,

A_2 = area downstream of elbow, and

E_t = total energy loss between sections 1 and 2.

Defining $\alpha = \int^{A} (V^3 dA/A\overline{V}^3)$, the energy equation reduces to

$$\frac{(p_1 - p_2)}{w} - \frac{\alpha_2 \overline{V}_2^2 - \alpha_1 \overline{V}_1^2}{2g} = h_t = k \frac{\overline{V}_1^2}{2g} + \lambda \frac{\ell}{d} \frac{V_1^2}{2g}$$

where h_t is the total head loss between sections 1 and 2, k is the bend loss coefficient, and λ is the friction factor (assumed to be 0.0170). Therefore,

$$k = \frac{\frac{p_1 - p_2}{w}}{\frac{\overline{V}_1^2}{2g}} + \alpha_1 - \alpha_2 \frac{\overline{V}_2^2}{\overline{V}_1^2} - \lambda \frac{\ell}{d}$$

In the tabulated computations the α-values are all based on traverses made when the test section velocity was 49.62 fps. This value was used because accurately measurable velocities could be achieved in all elbows, and tests established that the pattern was substantially the same for the lower velocities. The expressed values of the Reynolds number are based on the 2.95-in. vane chord as length parameter rather than the duct depth value as used in the other tests. The summary represents vane angle settings of 96°, since a greater amount of data was available for this condition than for the 100° or 101° angles. It is believed that the k-values obtained by the 96° angle setting may be applied to the 101° setting with only minor discrepancies. A comparison of the k-values on Table VIII for the four elbows used in the model tunnel indicates that elbows I and II have a much greater loss coefficient than elbows III and IV.

The reason for the high loss indicated in elbow I may be traced to the physical nature of the flow entering this elbow from the preceding diffuser. It may be recalled that the inherent nature of flow in a diffuser produces a discharge flow profile sharply peaked or indicative of a high kinetic energy content for the section (α = 1.812, as measured at station 5). Since a high α-value of this character is not the usual value for balanced conditions as found in stable, turbulent, duct flow (α-values in long pipes are about 1.1)

a rapid and inefficient conversion to pressure energy will follow such a velocity distribution in a duct. In other words, considerable energy loss is to be expected for normalizing an $\alpha = 1.812$ flow even if it is done in a straight pipe. Addition of a bend, plus large friction areas on the vane surfaces, serves to accelerate normalizing and to produce high energy loss in a very short length, as is evidenced by a measured $\alpha = 1.308$ at station 6. On the basis of this evidence it becomes apparent that the presence of the diffuser and not the presence of the elbow causes the high energy loss evident at the elbow.

The high losses for elbow II are of a different nature and are due to the presence of the large pump shaft fairing passing through the vaning so as to cause the following secondary losses: lessening of the aspect ratio of the cascade with accompanying increase in end spiral losses; increase of flow velocity around vanes due to reduction of flow area occasioned by shaft presence; and, form loss and skin-friction loss due to flow around the shaft fairing proper.

Despite a difference in vane angle setting, the indicated losses for elbows III and IV agree quite well with those obtained in the duct elbow.

6. Vane Pressure Distribution

The vane and wall pressure distributions shown in Figs. 44 to 48 and 52 serve to give considerable information on the structural loading and cavitation susceptibility of the selected vane geometry. The 96° stagger angle does not lead to equal loading of each blade, as evidenced by the comparative changes in negative pressure at corresponding points of different vanes in Fig. 45. On the other hand, relative similarity of loading for all vanes is evident in the 101° setting shown in Fig. 46. The approximate correctness of the 101° vane angle setting is verified by the fact that a total vane loading (determined by integrating the pressure distribution of Fig. 48) agreed closely with the theoretical momentum change forces required for the directional change of the flow mass. No comparable check was possible with the 96° data. The correctness of this setting is further verified by the fact that integration of the duct wall pressure at mid-depth indicated the walls carried approximately the same load as one vane, whereas the 96° integration shows the walls to be carrying much more than a single vane. Additional verification is also found in the observations discussed in paragraph (3) on page 98.

The integrated location of the centers of pressure, together with the trunnion and miter line positions, is shown in Fig. 48 for both the 96° and 101° angles.

Vane pressure distribution measurements made in elbow I of the model tunnel (Fig. 52) agree qualitatively with those made in the duct elbow, but do not allow an accurate quantitative comparison because of difficulties in determining the reference pressure.

In addition to the quantitative pressure measurements analyzed above, examination of the photographic and visual records of the duct elbow experiments yields two pressure evidences: (1) Separation of the flow from the 96° vane surface occurs locally at a point on the convex surface about 3/4 in. forward of the trailing edge. This was made evident by the admission of colored water streaks into the air flow, as previously described. The flow evidently returns to the surface a short distance downstream since it appears to have considerable strength and a downstream direction at the trailing edge. (2) Separation with the 101° stagger angle is confined to a very narrow region just forward of the trailing edge.

7. Scale Effects

Since the intention of the foregoing tests was to determine the adequacy of the proposed design for application to the prototype, it is necessary to examine the scale effects which may exist between the model and the prototype. For purposes of this analysis, it would appear that the flow may have two separate forms--the spiraling three-dimensional flow occurring near the ends of the vanes, and the two-dimensional flow occurring over the bulk of the central portion. A digest of the preceding tests indicates that for the 101° vane stagger the bulk of the flow is essentially two-dimensional and the end effects are of negligible magnitude; this is evidenced by the satisfactory correlation between the performance of the duct elbow and the model tunnel elbow. From this it follows that the spiral flow cannot contribute materially to scale errors if the 101° stagger is employed. Use of other stagger angles may change the energy emphasis and, accordingly, may show scale effects.

An analysis of physical forces which might cause variations with scale shows that neither compressibility nor gravitational effects are of consequence and only the viscous turbulent forces should contribute to scale variations of the two-dimensional bulk flow.

A review of the duct elbow data taken with water and air over a moderate temperature range and a considerable velocity range shows in a dimensionless Reynolds number interpretation that changes of flow pattern are appreciable for values below 150,000 (based on duct dimension) but are quite small above that value. The duct elbow data were utilized because, in comparison with the model tunnel, a better control and a greater accuracy were possible for this equipment.

Figure 47, which is partial evidence of the influence of Reynolds number on the pressure distribution, indicates the pattern is substantially the same for the two series above 150,000 but differs in the leading edge distribution for the series below 150,000. These data, combined with the visual and photographic studies, would indicate the stability of the flow pattern is primarily dependent on whether and where separation of flow or the laminar to turbulent boundary-layer transition takes place on the surface. Since all of the evidence indicates that a turbulent boundary layer is created almost immediately in the vicinity of the leading edge for a 101° vane angle with Reynolds number above 150,000, there is no reason to believe the much larger Reynolds number required for the prototype would cause a significant shift in this limiting position of the transition point. On the other hand, the evidence indicates the transition point for a 96° vane stagger may be well back from the leading edge for moderate flows but may shift toward the trailing edge for high Reynolds numbers with a consequent instability of all flow patterns.

On this basis it appears reasonable to assume the flow patterns as measured for the 101° model tests will apply to the prototype and a loss coefficient k between 0.09 and 0.12 is appropriate for the selected design when used in stable flow regions such as elbows III and IV.

It is appreciated that the Reynolds number measures only the viscous turbulent level and is not a full measure of the turbulence scale and intensity effects. However, the correlation between the duct elbow studies and the model tunnel studies discounts the probability of any significant secondary turbulence effects on the model-prototype relations.

8. Cavitation Analysis

In view of the low local dynamic pressures induced on the elbow vaning, it is apparent that location of an elbow in a region of low static

pressure and high velocity may drop the local pressure to the vapor pressure of water and thus produce cavitation. It is, therefore, desirable that the elbow vanes be examined for their cavitation susceptibility in the prototype. This is particularly true of elbow I, which operates with the highest velocity and lowest static pressure.

Experiments on the proposed vane design, as shown in Fig. 48, indicate that the lowest local pressure on the surface is 2.25 $V_o^2/2g$ below the pressure level of the approaching flow stream where V_o is the velocity of the approaching stream. It is then apparent that cavitation will occur on the vane when the approaching stream pressure drops to a value such that the corresponding local pressure is down to vapor pressure; that is, when

$$\frac{p_o}{w} - 2.25\,\frac{V_o^2}{2g} = \frac{p_{vp}}{w}$$

A rearrangement of this expression to the form

$$\frac{\frac{p_o}{w} - \frac{p_{vp}}{w}}{\frac{V_o^2}{2g}} = 2.25$$

makes it apparent that the value 2.25 is the same as σ_{cr}, the conventionally accepted critical cavitation parameter of the vane form. In other words, if evaluation of the ratio for any operating condition yields a σ greater than 2.25, cavitation will not be present, whereas, values less than 2.25 will be accompanied by cavitation. Since the vane cascade will cavitate if subjected to this pressure condition, when mounted in the tunnel its susceptibility to cavitation depends on the minimum stream value of p_o/w. This may be expected.

In view of the fact that the test section studies (Chapter II) establish the lowest practical boundary pressure at the top of the downstream end of the test section near station 2 (Fig. 38), operation of the tunnel to produce vapor pressure at that point will automatically determine the minimum useful p_o/w value of the stream at the centerline of elbow I.

It is assumed the vane at the centerline of the elbow will be most susceptible to cavitation since the high centerline velocity will probably cause cavitation here despite the lower static pressure prevailing on the top vanes of the cascade.

If pressure values in the plane of station 5 are assumed to represent p_o/w for the vanes, then the minimum prototype centerline p_o/w value and the local σ may be cleared by applying the Bernoulli energy relation to the centerline flow filament thus:

$$\frac{V_2^2}{2g} + \frac{p_{vp}}{w} + r_2 - h_\ell = \frac{V_o^2}{2g} + \frac{p_o}{w}$$

where $V_2 = \overline{V}_2$ and $V_o = 2\overline{V}_5$ (approximations from Fig. 28),

$p_o = p_5$,

$\overline{V}_2 = (r_5/r_2)^2 \overline{V}_5$,

r_5 = radius at station 5 = 5.5 ft,

r_2 = radius at test section = 2.5 ft, and

h_ℓ = diffuser energy loss = 0.067 $(\overline{V}_2^2/2g)$, as shown in Chapter IV.

It should be noted here that selection of a head loss factor of k = 0.067 from the data of Chapter IV assumes a bare tunnel without a test section model installation. This appears to be a less conservative selection than the value of k = 0.114 presumed to prevail in the presence of a test body. However, it is rather reasonable to assume that if a test body is capable of producing this loss, its wake will be sufficiently great to necessitate considerable reduction of the assumption of $V_o = 2\overline{V}_5$. Since these factors act to nullify each other, but in a manner not wholly defined by these tests, it appears reasonable to use the value of k = 0.067 together with $V_o = 2\overline{V}_5$, as determined by the tests. There is also some reason to question whether the bulk value of 0.067 is fully applicable to energy analysis along a centerline flow filament. For lack of further evidence, the 0.067 value will be presumed applicable.

If the equation given above is cleared to yield the local cavitation parameter, the following expression for the minimum cavitation index just upstream of elbow I will result:

$$\sigma_{min} = \frac{\dfrac{p_o - p_{vp}}{w}}{\dfrac{V_o^2}{2g}} = 4.46 + \frac{14.65}{\dfrac{\overline{V}_2^2}{2g}}$$

It is obvious that even extremely high values of $\overline{V}^2$ will give σ-values nearly twice the critical value σ_{cr} = 2.25 determined for the vane form. In this case there is no reason to believe cavitation will exist on the vanes of the tunnel.

9. Vibration and Stress Analysis

In view of the fact that most American water tunnels have experienced some difficulty with vibration noise in elbow vanes and in a few cases have experienced structural failure, it is important that the strength and vibratory characteristics of the vane design be critically examined. A check of the structural properties of the prototype vane was made by assuming the following:

(1) The center or longest vane of each elbow was examined as a beam with zero end restraint in the plane of the chord and full end restraint in the plane normal to the chord.

(2) The vane was assumed to have a cross section of solid steel or, alternatively, to be composed of solid nose and tail with 1/2-in. rolled steel surfaces.

(3) The principal forces acting are the lift-drag resultant and the dead weight. The lift-drag resultant was computed on impulse-momentum principles for the maximum velocities determined by tunnel velocity distribution studies. The point of application was based on integration of the measured pressure distribution diagrams.

(4) There are two principal tunnel generated pulses capable of exciting vibration in the vanes. These are the pulses from the pump blading and the separation vortices shed from the vane itself.

(5) The natural frequency of the vane can be assumed based on free beam action, with the weight of the beam increased to include the adjoining water between two adjacent vanes.

On the basis of these calculations, maximum tensile and compressive stresses in the vane would be about 3000 psi with end shear values about 50 psi; maximum center deflections would be about 0.06 in.; lowest frequency of natural vibration would be about 15 cps; highest frequency of pump blade pulse would be about 8 cps and would be damped to small strength before reaching the elbows; highest frequency of vane vortices would be 1.2 cps and such vortices should be of small size. This foresees no major stresses or vibrations and satisfactory operation should be expected of the proposed vane design.

D. Conclusions

On the basis of these experimental investigations, these conclusions are drawn concerning the vaned turns for the 60-in. tunnel:

(1) The selection of vaned turns and the particular design choices of vane shape and spacing-chord ratio (s/c = 0.48) were justified by the results of the experiments. The original selection of location of the vanes with respect to the miter line of the bend was changed slightly to conform more closely with the experimental results.

(2) The proper setting of the selected cascade to insure axial flow immediately before and after the turn is a stagger of 99° to 101°; that is, the angle between the chord of the vanes and the miter plane of the bend is 99° to 101° (the angle of attack is 54° to 56° with the approaching flow).

(3) With a normal turbulent velocity distribution in the approach flow, excess losses due to the vaned turns at the recommended setting of the cascade of vanes should be 10 per cent of the velocity head in the approach duct ± 2 per cent. This loss may appear to be much larger for abnormal entering velocity distributions such as those which may occur where the elbow follows a diffuser.

(4) When installed in the tunnel, the vanes will not be subject to cavitation.

(5) Either a solid steel or a hollow steel vane of nominal skin thickness will be free from excessive stresses or deflections under all expected conditions of operation and should not vibrate in resonance with either the tunnel impeller or vortices shed from the vanes.

(6) Data obtained with the experimental models should give a very close index of the performance to be expected in the vaned turns of the large tunnel because the Reynolds numbers used in the models were high enough to preclude the possibility of a loss in similarity at the higher Reynolds numbers of the prototype, and the onset of a turbulent boundary layer at a stable point near the leading edge of the model vanes at the stagger angle of 99° to 101° would be at a very similar position on the larger prototype vanes.

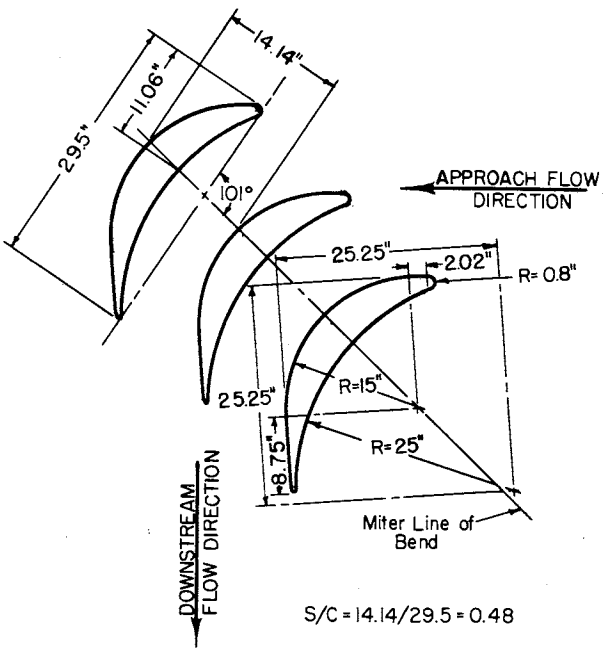

Fig. 54 - Recommended Prototype Vane Cascade Dimensions

(7) The dimensions shown in Fig. 54 are the dimensions of the prototype vanes in cascade. The miter line of the bend is shown to locate the position of the cascade in the bend. The stagger angle of 99° to 101° will insure that the vanes will be equally loaded and that the centers of pressure will fall in the miter plane.

References

[1] Madison, R. D., and Parker, J. R. "Pressure Losses in Rectangular Elbows." Transactions of the American Society of Mechanical Engineers, Vol. 58, pp. 167-76. April, 1936.

[2] Beij, K. H. "Pressure Losses for Fluid Flow in 90° Pipe Bends." Journal of Research of the National Bureau of Standards, RP 110, Vol. 21, pp. 1-18. July, 1938.

[3] Wirt, Loring. "New Data for the Design of Elbows in Duct Systems." General Electric Review, Vol. 30, No. 6, pp. 286-96. June, 1927.

[4] Davies, Powys, and Puranik, Shivram. "The Flow of Water through Rectangular Pipe Bends." Journal of the Institution of Civil Engineers, Vol. 2, No. 5035, pp. 83-134. 1935-36.

[5] Yarnall, D. L., and Nagler, F. A. "The Flow around Bends in Pipes." Transactions of the American Society of Civil Engineers, Vol. 100, No. 1914, pp. 1018-43. 1935.

[6] Patterson, G. N. Note on the Design of Corners in Duct Systems. Aeronautical Research Committee Reports and Memoranda No. 1773 (British), 1936.

[7] Anderson, Alvin G. Hydraulics of Conduit Bends. University of Minnesota St. Anthony Falls Hydraulic Laboratory Bulletin No. 1, 1948. 22 pp.

[8] Klein, G. J., Tupper, K. F., and Green, J. J. "The Design of Corners in Fluid Channels." Canadian Journal of Research, Vol. 3, pp. 272-85, 1930.

[9] Collar, A. R., Some Experiments with Cascades of Aerofoils. Aeronautical Research Committee Reports and Memoranda No. 1768 (British), 1936.

[10] Krober, G. Guide Vanes for Deflecting Fluid Currents with Small Loss of Energy. (Translated from the German in National Advisory Committee for Aeronautics Technical Memorandum No. 722.)

[11] Silberman, Edward. The Nature of Flow in an Elbow. University of Minnesota St. Anthony Falls Hydraulic Laboratory Project Report No. 5, 1947. 100 pp.

CHAPTER VI. PUMP STUDIES

A. General Considerations

The purpose of the recirculating pump in the prototype water tunnel is to supply energy to the water in such quantity and manner as to maintain the desired flow conditions in the tunnel test section. The primary design problem in the selection of a suitable pump is usually the determination of the necessary discharge quantity and the resistance head. In this particular study the discharge values have already been defined by the diameter and velocity range, as discussed in Chapter II (3 to 85 fps in a 60-in. diam test section), so it remains principally to determine the energy requirements imposed by the circuit resistance. However, before beginning a detailed discussion of the analysis and physical studies of the energy problem, it is perhaps appropriate to define certain of the secondary requirements which serve to harness the pump design. The important secondary requirements are considered to be:

(1) The velocity stream discharging from the pump shall be as precisely controllable and as free of pulsation and time variations as possible.

(2) The pump design shall contribute a minimum of turbulence or nonuniformity of velocity to the flow approaching the test section.

(3) Flow at the test section should be substantially free of rotation. Such rotation is suppressed rather than generated by most of the tunnel circuit components, with the exception of the pump. Certain types of pumps, most notably the axial flow type, inherently contribute rotation to their discharge flow; therefore, they usually include corrective devices to eliminate this. A water tunnel pump should specifically provide for substantial correction of such rotation at all rates of discharge.

(4) The efficiency of the energy conversion should be a maximum to permit best economy in the installation and operation of the pump drive.

(5) The pump shall be as free of cavitation as possible. This applies not only to the substantial cavitation attending noticeably poor energy performance but also to any minor local cavitation sufficient to produce background noise in the tunnel water. The latter limitation is essential if test bodies in the test section are to be studied with sonic cavitation instruments.

In any consideration of these requirements it is important to bear in mind that custom-built pumping machines are, in general, of such complexity in design and physical construction that they are built by specialized manufacturers who draw on their experience to produce a pump satisfying performance specifications. Since detailed design information is not generally available to the consumer-designer, he is confined to formulating somewhat ideal specifications which the state of the manufacturer's art may or may not permit achieving.

The constant dissipation of the pump input energy against flow resistances results in a cumulative increase in the temperature of the recirculated tunnel fluid. Since it is not considered advisable to permit an extreme temperature rise to occur in a large physical structure requiring precise axial or shaft alignments, it is highly desirable to obtain information relative to rate and maximum temperature values to be expected in an operating tunnel. While fluid temperature rise is not usually an inherent part of a pump design study, the intimate energy association makes it desirable to include temperature as a part of the studies of this chapter.

B. Design Studies

1. Discharge-Head Relations

The head against which the pump shall operate is variable with the discharge and is a function of the design efficiency of the various tunnel circuit components. In an attempt to evaluate the magnitude of this total head for original design purposes, a search was made of the literature relative to the energy losses represented in each of the flow components of the tunnel circuit. The major portion of this information was drawn from pipe friction theory and related studies conducted in prototype wind tunnels. This information was summarized for the proposed water tunnel in conformance with the methods of expressing and determining the power requirements of wind tunnels by individual components. To facilitate comparisons, all losses computed by this method are arbitrarily expressed as a portion of the kinetic energy that will exist in the test section jet at maximum velocity.

The test section jet energy, expressed in horsepower, is

$$(hp)_o = \frac{V_o^2}{2g} \frac{V_o A_o}{550} w$$

where w = unit weight of water, V_o = mean test section velocity in feet per second, and A_o = cross-sectional area of test section. The component energy losses may then be expressed thus:

$$(\text{Loss})_n = k \frac{V_o^2}{2g} \frac{V_n A_n}{550} w$$

where k is the local loss coefficient for the component and V_n and A_n are the corresponding mean velocity and cross-sectional area. In a closed circuit VA is a constant for all sections; therefore $V_o A_o = V_n A_n$ or

$$V_n = \frac{V_o A_o}{A_n} = V_o \left[\frac{d_o}{d_n}\right]^2$$

where d = diameter and

$$(\text{Loss})_n = k \left[\frac{d_o}{d_n}\right]^4 \frac{V_o^2}{2g} \frac{V_o A_o}{550} w$$

or

$$(\text{Loss})_n = k_o \frac{V_o^2}{2g} \frac{V_o A_o}{550} w$$

Thus $k_o = k\,(d_o/d_n)^4$ is the fractional part of the total jet energy equal in magnitude to the loss in the local component n.

On the basis of this method of summarizing the energy demands, an estimate table and curve were prepared for the proposed prototype and for the scale model tunnel. These curves were of the same general form as the curve of Fig. 55 and were the basis for selecting both the type of pump to be used in the prototype and the specific pump to be used in the model. As in the case of Fig. 55, the estimated data were summarized for two alternate tunnel operations, namely, the bare tunnel without a mounted test model and the tunnel with a large, high, drag model in place plus a honeycomb flow straightener in the contraction approach. For purposes of calculation, the test body was assumed to have a diameter one-sixth that of the test section and a conventional drag coefficient of 1.00. Since this method of estimating the energy losses for the several tunnel components was inexact, because of the mutual effects of the several components when assembled in various combinations, the estimated energy summary could not be considered too reliable. This, and the high cost of the pump installation, largely justified the model study.

While the determination and study of the k_o-values for various elements of the tunnel leads to an insight into the influence of component energy efficiencies, it should be noted that an index of total tunnel energy efficiency is available through determination of a quantity known as the "energy ratio." In wind and water tunnel design practice, this quantity is usually defined as the ratio of the jet horsepower to the input horsepower necessary to sustain the jet horsepower. The input horsepower is usually taken as the total energy supplied to the motor, presuming for comparative purposes that the motor and the pump efficiency are approximately the same for most installations. (It should be noted that Fig. 55 has been plotted with an input horsepower based on the assumption of a pump efficiency of 80 per cent.)

2. Type of Pump

Modern practice in pump design and selection is founded on a firm basis of actual experience with laboratory models and prototype installations; each manufacturer has extensive records of design modifications. Most of this is unpublished and unavailable, but in order that some measure of pump performance be available to systematize comparison between various pumps, a common denominator known as the "specific speed" has been evolved for use in this field. The specific speed of any pump may be calculated from the defining equation

$$N_s = \frac{\sqrt{gpm} \times rpm}{H^{3/4}} = \frac{21.2\sqrt{cfs} \times rpm}{H^{3/4}}$$

where N_s is the specific speed and H the head in feet for which the pump is designed, corresponding to its gallons per minute capacity. Specific speed of a pump is an index of its type. It is used when designing pumps to meet different conditions of head, capacity, and speed.

On the basis of published data and approximations of the specific speed from the estimated discharge-head data, the large discharges and small heads involved indicate the most suitable pump geometry for tunnel use will be found in the propeller or axial flow type. In current practice this type of pump has two principal forms, of which the more common is the fixed blade propeller and the less common is the variable blade type. In the variable blade type the geometry of the blade pitch angle may be mechanically varied.

For the wide range of discharge required of the pump in the proposed prototype tunnel, three possible applications come to mind, namely, fixed blade

with variable shaft speed, variable blade with constant shaft speed, and variable blade with variable shaft speed. Virtually all existing water tunnels employ the first of these, largely because of the economy of the common variable speed drive systems as compared to custom-built variable blade mechanisms. However, the narrowly peaked efficiency curve common to performance characteristics of the fixed blade pump means this type of pump cannot operate at high efficiency if the resistance head of the tunnel circuit is widely variable for different modes of operation. For this reason the variable blade pump, with its high efficiency over a broad range of heads, has distinct advantages. Unfortunately, the efficiency of the variable blade, fixed speed pump is partially nullified in tunnel use by the fact that the pump is prone to cavitate under conditions of low discharge and high shaft speed. This can be improved by providing variable speed with variable blade, but it increases the expense. It is the purpose of the model study to define the discharge-head characteristics of the basic tunnel to permit eventual judicious selection of the pump drive unit.

3. Pump Diameter

The 11-ft pump diameter tentatively selected for the prototype tunnel, as shown in Fig. 1, was based on a specific speed study of published information on the characteristics of propeller pumps and Kaplan turbines. This selection was confirmed by leading pump manufacturers as being a good approximation, pending more defined discharge-head conditions for the tunnel. The dimension was, therefore, fixed in this vicinity with the thought that eventualities dictating a slightly larger or smaller pump diameter could be met by a local expansion or contraction of the tunnel diameter. On this basis the dimensions of the model tunnel in the vicinity of elbows I and II of Fig. 38 were fixed at 13.2 in. even though the model was built, for reasons of expedience described in the appendix, with a 12-in. diam pump.

4. Pump Diffuser

The inherent tendency for the discharge from a propeller pump blade to possess a rotational component of motion requires that some provision be made to remove this component if satisfactory axial flow is to be expected in the tunnel test section. The flow straightening is usually accomplished by placing radial guide vanes in the path of the impeller discharge so that the rotational inflow is gradually converted to a nearly axial motion. This has the advantages of eliminating the undesirable rotation and recovering the

kinetic energy represented by the rotation, thus increasing the pump efficiency. The diffuser blading is also sometimes placed ahead of the pump impeller to influence prerotation. In some cases it may be used on both sides of the impeller. It should be noted that the most favorable corrective action of diffuser blading normally prevails only for a single discharge or pump speed condition. It will be less favorable if the device is required to run under variable conditions. Variable diffuser blading has been proposed to remedy this but is not yet a practical development.

In view of the intimate relation that exists between the impeller blading and the diffuser blading, the latter is normally considered the design responsibility of the pump builder and is, therefore, not considered a proper part of this analysis or model study.

5. Pump Location

The disposition of the recirculating tunnel conduit in a loop lying in a vertical plane, as shown in the frontispiece, is dictated by a design effort to place the pumping unit at a point a maximal vertical distance below the low pressure test section. By such disposition the cavitation susceptibility of the pump is inhibited by the presence of a maximum possible gravitational pressure head. This disposition is quite different from the usual horizontal loop employed in wind tunnels where cavitation is not a factor.

If a propeller pump is to be used the necessity of providing shaft entry from the motor dictates that the pump be placed inboard of one of the two lower elbows. Location of the pump just upstream of the lower elbow preceding the contraction would place a minimum distance between the eddy producing pump and the test section. This is an undesirable condition which can be remedied by placing the pump just downstream of the other elbow in the lower leg. Consideration was given to placing the pump in the vertical leg just upstream of the latter elbow, but this placement reduces the gravitational head on the impeller and complicates the motor mounting problem.

If the discharge from a propeller pump is to possess uniformity or steadiness in the pressure and velocity distributions, it is essential that the inflow be substantially uniform. This has been demonstrated in other propeller pump installations where pulsing electrical demand and water discharge resulted when the inflow contained local regions of high or low kinetic energy causing definite force pulses on the passing blading. The strength

of such pulses is reduced by increasing their number through an increase in the number of blades on the impeller; but, this is not a practical way to eliminate the pulse as about four blades appear to be the limit if a variable blade system is to be used.

To eliminate or minimize pulsing or other undesirable conditions in the tunnel pump, it is well to consider the nature of the inflow. The 11-ft diam vane elbow immediately preceding the pump has been designed to include eleven vanes dimensioned in accord with Fig. 54 and arranged as shown in Fig. 62 (page 141). The small dimension and the large number of spaces are believed incapable of producing any significant pulse when imposed on a four-bladed impeller even if a substantial shadow or wake region exists on the downstream side of each vane. Evidence in the literature indicated that even if a substantial wake exists immediately downstream of the vane, its strength is largely dissipated in a flow distance approximately four times the vane gap dimension, or in this case, 10 inches in the prototype. Because it would be difficult to fabricate a pump of the type shown in Fig. 62 with the vanes closer to the impeller than four vane gap units, there seems to be no reason to make any special effort to locate the impeller an appreciable distance from the elbow. The minimum space provided in a practical pump and elbow fabrication should suffice. To assure that velocity maldistributions are not created by other features of the geometry preceding the pump, it was considered advisable to make local velocity distribution studies in the model.

C. Experimental Studies

1. Head and Energy

Because the total energy summary necessary to a proper pump design is merely the summation of the energy requirements of the tunnel components, the data will be found in previous chapters of this paper. A tabular summary of this information is shown in Table IX, based on the use of the previously determined k_o-values plus the losses of straight cylindrical components computed from values of f for a steel surface obtained from a standard curve of pipe friction. For convenience in comparing all values are expressed as k_o or multiples of the test section velocity head. As discussed in this chapter under the section on Design Studies, the summary is prepared in alternates, namely, the minimum resistance or bare tunnel circuit, and the maximum resistance circuit presumed to contain a honeycomb straightener and a large, high resistance test model.

TABLE IX

ENERGY LOSS FACTORS FOR PROTOTYPE TUNNEL CIRCUIT

Loss expressed as multiples (k_o) of the test section velocity head

Test Section Velocity	k_o			
	$\overline{V}_1$ = 18.00 fps	$\overline{V}_1$ = 30.00 fps	$\overline{V}_1$ = 50.00 fps	$\overline{V}_1$ = 84.5 fps
Element of Circuit				
Test Section	0.0563	0.0524	0.0487	0.0454
5° Diffuser without Test Installation	0.0673	0.0673	0.0673	0.0673
5° Diffuser with Test Installation	0.1141	0.1141	0.1141	0.1141
11-ft Conduit	0.0022	0.0022	0.0021	0.0020
Elbows I and II	0.0435	0.0435	0.0435	0.0435
8° Diffuser	0.0051	0.0051	0.0051	0.0051
15-ft Conduit	0.0014	0.0014	0.0013	0.0013
Elbows III and IV	0.0012	0.0012	0.0012	0.0012
Honeycomb Straightener	0.0062	0.0062	0.0062	0.0062
Contraction	0.0300	0.0300	0.0300	0.0300
Test Installation	0.0278	0.0278	0.0278	0.0278
With Test Installation, Σk_o =	0.2878	0.2839	0.2800	0.2766
Without Test Installation, Σk_o =	0.2070	0.2031	0.1992	0.1958

Note: The use of values carried to the fourth significant figure is a calculating and reference expedient and is not indicative of the order of accuracy of the experimental work which, in general, can only justify the third significant figure.

To facilitate comparison and study, the energy data of Table IX have been plotted with varying velocities in Fig. 55 and supplemented in Table X and Fig. 56 by a tabular and graphical summary of the conventional energy gradient. In computing the energy gradient, the total energy at a section was computed from the local head loss data in Table IX, and the pressure was arbitrarily assumed to be absolute zero at the beginning of the diffuser transition (section II of Fig. 56). For convenience of interpretation, the total energy and the kinetic energy at a section were divided by the velocity head of the

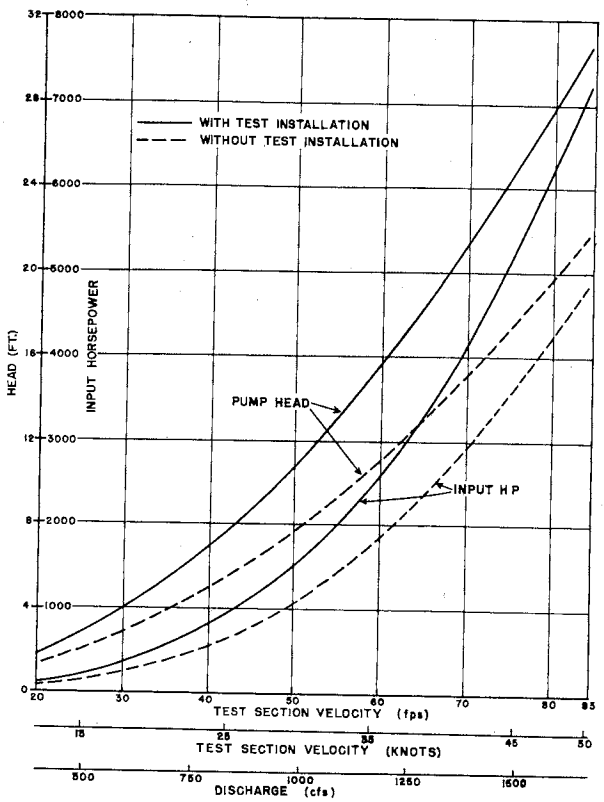

Fig. 55 - Discharge - Head Relations for the Prototype Pump. (Computed values based on model findings.)

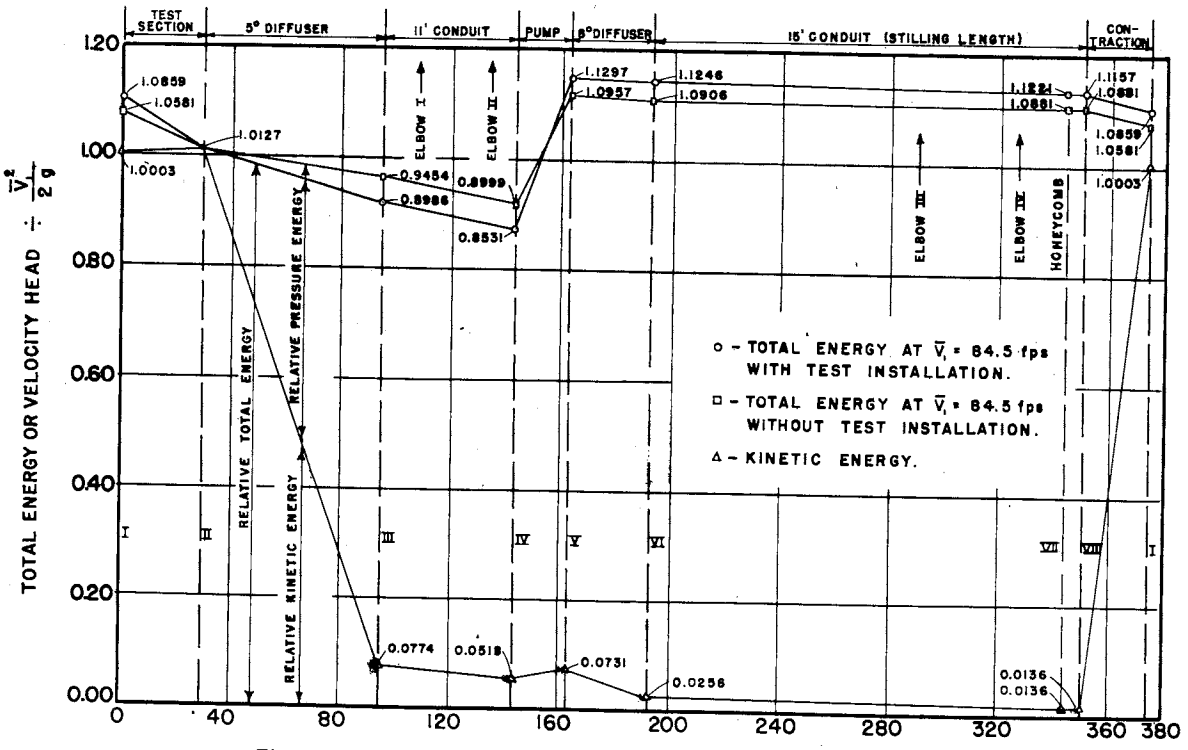

Fig. 56 - Energy Gradients for Prototype Tunnel

TABLE X

PROTOTYPE ENERGY GRADIENT VALUES

(for $\overline{V}_1$ = 84.5 fps)

Section (See Fig. 56)	$\frac{\alpha \frac{\overline{V}^2}{2g}}{\frac{\overline{V}_1^2}{2g}}$	Total Head ($\overline{V}_1^2/2g$)	
		With Test Installation and Honeycomb	Without Test Installation or Honeycomb
I	1.0003	1.0859	1.0581
II	1.0127	1.0127	1.0127
III	0.0774	0.8986	0.9454
IV	0.0518	0.8531 } o	0.8999 } #
V	0.0731	1.1297 }	1.0957 }
VI	0.0256	1.1246	1.0906
VII	0.0136	1.1221	1.0881
VIII	0.0136	1.1159	1.0881
I	1.0003	1.0859	1.0581

o - Total head factor represented by pumping = 0.2766.

\# - Total head factor represented by pumping = 0.1958.

Note: (a) Numerical values refer to the upstream end of the section.
(b) The use of values carried to a large number of significant figures is a calculating and reference expedient and is not indicative of the order of accuracy of the experimental work which, in general, can only justify the third significant figure.

test jet to reduce the value to a dimensionless number. The α-values used in the kinetic energy evaluation were assumed to be the same in both model and prototype except in the test section region. In addition to the graphic summary of Fig. 56, the energy values of Table IX may be interpreted in the form of the conventional energy ratio by evaluating the reciprocal of Σk_o. On this basis the energy ratio for the prototype tunnel will vary from 5.1 to 4.8 when operating with no test installation, and from 3.6 to 3.5 when operating with a test installation.

2. Velocity Distribution

For the reasons given on pages 125 and 126 under the paragraphs on pump location, velocity distribution traverses were taken at stations 7 and 8 (see Fig. 38) and are shown in Figs. 57 and 58. It is to be noted that the inflow velocity shown in Fig. 57 has an undesirable concentration of velocity

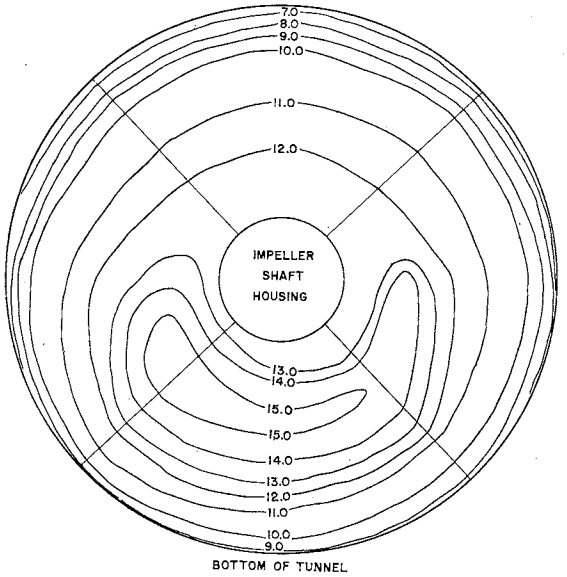

Fig. 57 – Velocity Distribution at Station 7

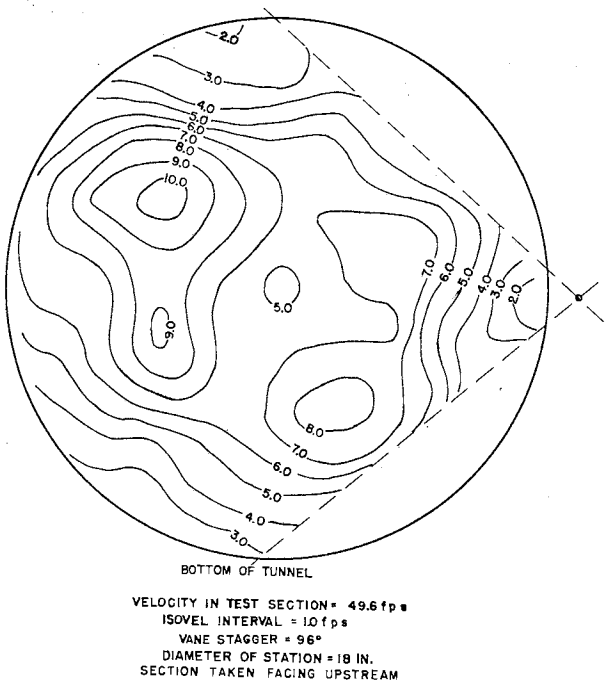

Fig. 58 – Velocity Distribution at Station 8

at the bottom of the tunnel section. This evidence is consistent with the maldistribution which originates in the main diffuser, as shown in Fig. 28, and which is enhanced by the excessive turning action of the 96° elbow vane setting shown in Fig. 50. A later resetting of the vanes of elbow I to 100° materially improved the velocity distribution shown in Fig. 50. It is presumed, although not tested, that setting the vanes of both elbows I and II to 100° would eliminate the bulk of the pump inflow maldistribution shown in Fig. 57.

A comparison of Figs. 57 and 58 indicates that the pump, at least in the model, was a powerful factor in regrouping the velocities and that a satisfactory discharge distribution in the prototype will be considerably dependent on the design quality of the pump. Considerable protection against pump deficiencies is, however, contained in the long stilling reach existing between the pump and the test section. This corrective ability is evidenced in a comparison of Figs. 51 and 58.

The combined guide vane and shaft streamlining elements shown in the pump elbow of Fig. 62 (page 139) were intended to minimize the flow disturbances inherent to this portion of the tunnel. A limited ability to make good instrument probes in this region (Pitot studies were restricted to the four

radial lines of Fig. 57) leaves some question as to the detailed validity of Fig. 57 and does not conclusively establish the worth of the vane and fairing design. However, the design seems reasonable and the available measurements are not seriously unfavorable.

3. Cavitation Susceptibility

The objective of this portion of the experimental studies was to evaluate the likelihood of vapor or cavitating pressures being achieved in the high velocity, low pressure regions of the pump unit. Since this susceptibility to cavitate is defined in pump practice by a numerical quantity known as the cavitation index, the evaluation of this quantity for the proposed tunnel will serve to indicate the probability of cavitation. The cavitation index used in pump work is conventionally defined as

$$\sigma = \frac{\frac{p_s - p_{vp}}{w}}{H}$$

where p_s = absolute static pressure at the centerline of the pump intake (pounds per square foot),

p_{vp} = vapor pressure (pounds per square foot),

w = specific weight of fluid (pounds per cubic foot), and

H = head added by pump (feet).

It is to be noted that the form of this index is not quite the same as that previously employed in the test section and guide vane cavitation studies since it emphasizes the pump head rather than the flow velocity.

In applying the above index it is apparent that the least tolerable value will occur when incipient cavitation exists at the crown of the tunnel diffuser transition. Using this point as a minimal pressure source, the pressure at the pump intake may be computed by an application of the Bernoulli equation as follows:

$$\alpha_D \frac{\overline{V}_D^2}{2g} + \frac{p_D}{w} + Z_D - h_\ell = \alpha_s \frac{\overline{V}_s^2}{2g} + \frac{p_s}{w} + Z_s$$

where $\alpha = \Sigma \Delta A V^3 / A \overline{V}^3$,

A = area of flow (square feet),

p = absolute pressure (pounds per square foot),

$\overline{V}$ = mean velocity of flow (feet per second),

Z = height above datum (feet),

h_ℓ = head loss between points D and s,

D - refers to the top of the downstream end of the test section, as represented by tap D of Fig. 2, and

s - refers to the pump intake as represented by station 7 of Fig. 38.

In the foregoing equation p_D, the least tolerable mean pressure energy measure for the cross section, may be evaluated using the cavitation data associated with Eq. (5) of Chapter II.

If the sum of the last two terms of Eq. (5), which were proved to have mean values of 0.013 and 0.058, respectively, is cleared

$$\frac{p_D}{w} = (0.013 + 0.058)\frac{\overline{V}_D^2}{2g} + \frac{p_{vp}}{w}$$

Other pertinent measured values from the previous tests are:

α_D = 1.0127 (from page 25),

α_s = 1.10 (computed from data of Fig. 57),

$A_s = \pi/4\ (\overline{11}^2 - \overline{2.5}^2)$ sq ft (corrected for pump shaft),

$A_D = \pi/4\ (\overline{5}^2)$ sq ft,

$h_\ell = (0.1141 + 0.0020 + 0.0435)\ \overline{V}_D^2/2g$ (from Table IX with test installation),

$= 0.16\ \overline{V}_D^2/2g$,

$Z_D - Z_s$ = 32.5 ft (from Fig. 1), and

$H = \Sigma k\ (\overline{V}_D^2/2g)$ (evaluated from Table IX).

This yields

$$\frac{p_s}{w} = \left[\alpha_D - \alpha_s\left(\frac{A_D}{A_s}\right)^2\right]\frac{\overline{V}_D^2}{2g} + (0.013 + 0.058)\frac{\overline{V}_D^2}{2g} + \frac{p_{vp}}{w} + Z_D - Z_s - 0.16\frac{\overline{V}_D^2}{2g}$$

$$= 0.874\frac{\overline{V}_D^2}{2g} + 27 + \frac{p_{vp}}{w}$$

If this value of p_s is applied to the pump, the minimum cavitation index at the pump centerline before cavitation occurs elsewhere in the tunnel (diffuser transition) is:

$$\sigma_{min} = \frac{\frac{p_s - p_{vp}}{w}}{H} = \frac{0.874 \frac{\overline{V}_D^2}{2g} + 32.5}{\Sigma k \frac{\overline{V}_D^2}{2g}}$$

A plotting of this equation for various test section velocities is shown in Fig. 59. This indicates that the lowest value of σ will be approximately 4.2 at the maximum tunnel speed of 85 fps.

Evidence in the literature indicates that a σ-value of 4.2 should be quite safe since values of 1.5 to 2.0 are apparently readily obtainable on the basis of past designs. In fact there is a sufficient margin of safety to justify some reduction of the vertical dimension between the horizontal legs of the tunnel represented by the value of 32.5 ft occurring in the final expression for σ_{min}.

4. Temperature Factors

The continued addition of pumping energy to a finite quantity of water in a water tunnel will progressively raise the temperature of the water. The rate of temperature rise will be a function of the rate of heat addition (pump input energy), the mass concerned, and the rate of heat loss via the boundaries. While the first two quantities may be calculated for the proposed prototype design with a fair degree of accuracy, the latter item is a variable depending on a number of unpredictable environment factors. For this reason, it is not desirable to attempt to predict the prototype temperature until all the environment factors are determined. However, as a guide to such an evaluation, the model tunnel was operated at top speed for an extended period. The resulting experimental observations are shown by the plotted points in Fig. 60. The tunnel is placed in a large room heated with unit heaters involving mild air circulation; its surface is a medium gray, high gloss paint over galvanized hot rolled steel; the equivalent heat capacity of the tunnel structure and contained water is 2970 lb of water; and the external tunnel area is 142.5 sq ft. On the basis of these observations and conditions, an attempt was made to approximate the probable rate of temperature rise for the prototype. These approximations for three different prototype speeds are also shown in Fig. 60.

In addition to the rate of rise curves, Fig. 60 contains a curve approximating the rate of cooling of the prototype. While this curve is not offered as an accurate index, it does serve to show certain relative values

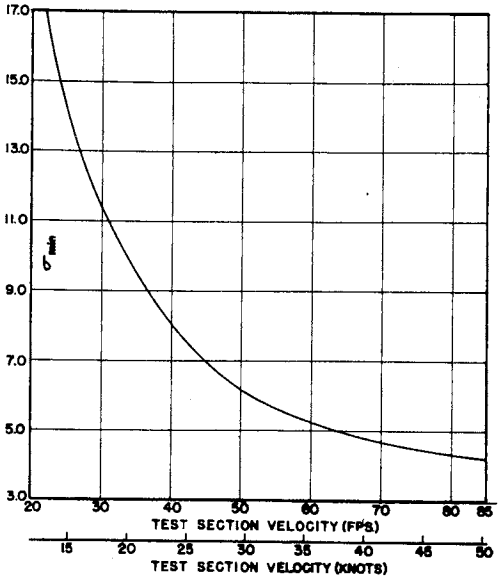

Fig. 59- Minimum Cavitation Index To Be Achieved at Centerline of Prototype Pump

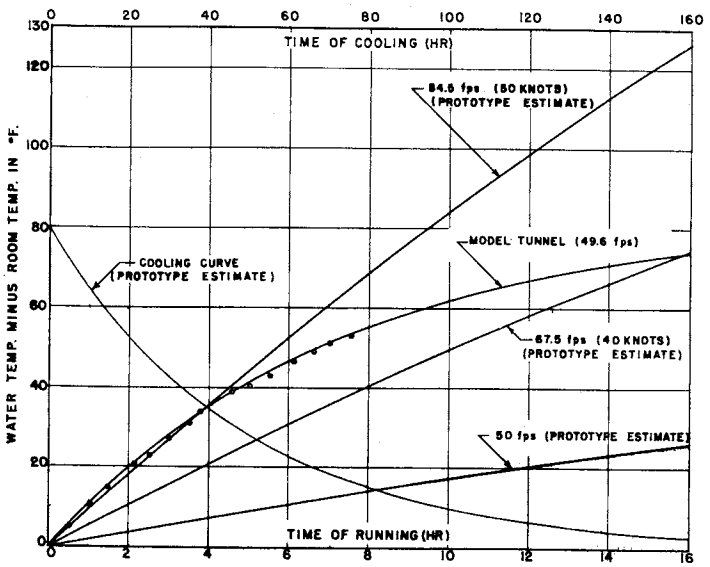

Fig. 60 - Temperature Rise and Cooling Relations

useful as a guide to certain phases of tunnel operations and to indicate the necessity or desirability of adding auxiliary heat extracting equipment to the tunnel accessories. It is improbable that normal, short run speed tests in the tunnel will necessitate artificial cooling. However, the possibility of conducting extended high speed endurance tests does exist.

D. Conclusions

On the basis of this general design study and summarization of experimental investigations, the following general and specific conclusions are drawn with regard to the 60-in. prototype tunnel pump design procedures.

(1) At a test section velocity of 50 knots (84.5 fps) and an assumed pump efficiency of 80 per cent, the maximum head required of the pump will be 30.7 ft, the maximum required discharge will be 1660 cfs, and the maximum required power input will be 7220 hp.

(2) It is deemed improbable the pump will produce discharge pulsations if the approach conduit geometry is arranged as tested, except for an elbow vane angle adjustment to a stagger of 100°, and provided normal good practice is observed in the pump design.

(3) The pump design should attempt to correct or unify maldistribution of velocity and to provide a discharge as free as possible of rotary components. The proposed pump location serves to provide considerable damping of pump disturbances.

(4) The location of the pump in the tunnel circuit and the pressure recovery affected by the circuit design appear to be adequate to inhibit all major cavitation and probably most minor cavitation in a pump designed in accord with best modern practice.

(5) An axial flow pump with either variable speed or variable blade is assumed necessary to proper operation of the prototype tunnel.

(6) The rate of heating and cooling of the tunnel water may necessitate artificial cooling under test conditions calling for extended operations at high speed.

References

[1] Collar, A. R. Cascade Theory and the Design of Fan Straighteners. Aeronautical Research Committee Reports and Memoranda No. 1885 (British), 1940.

[2] Silberman, Edward. The Pitot Cylinder. University of Minnesota St. Anthony Falls Hydraulic Laboratory Circular No. 1, 1947. 18 pp.

APPENDICES

APPENDIX I. TEST APPARATUS

The tunnel was reduced to elements of such size that all parts could be worked on available tools; reduction also permitted flexibility in altering the form as might be required by subsequent tests. The conduit members were largely fabricated in the Laboratory shop by using plane or rolled steel sheets in welded assemblies subsequently galvanized for corrosion resistance. A limited number of other conduit members were made of machined aluminum castings, aluminum being used where refinement of surface finish or complexities of form dictated. The separate tunnel components were assembled with bolt-up flanges and sealing gaskets. Care was taken that all joints and interior surfaces were as smooth as practically attainable. In the case of the wholly machined components used in the high velocity sections, this surface finish was deemed hydraulically smooth. Viewing ports of formed Lucite were fitted into the conduit wall at numerous strategic points. A sectional elevation of the model tunnel assembly is shown in Fig. 61 and the frontispiece.

The ideal pump for a model installation of this kind would have been a unit for which the head-discharge output relation matched that of the tunnel circuit resistance. However, since this relation was one of the principal unknowns of the test program and could vary considerably with methods of tunnel operation, a compromise selection was evidently necessary. Compromise was also necessary because the Laboratory was not in a position to fabricate a pump impeller even if the design conditions could have been crystallized. Accordingly, best use was made of the commercial offerings. These were distinctly limited because of postwar procurement difficulties at that time. The final selection was a three-bladed, axial flow, bronze impeller with an outside diameter of 11.96 inches. While this impeller did not have a diameter

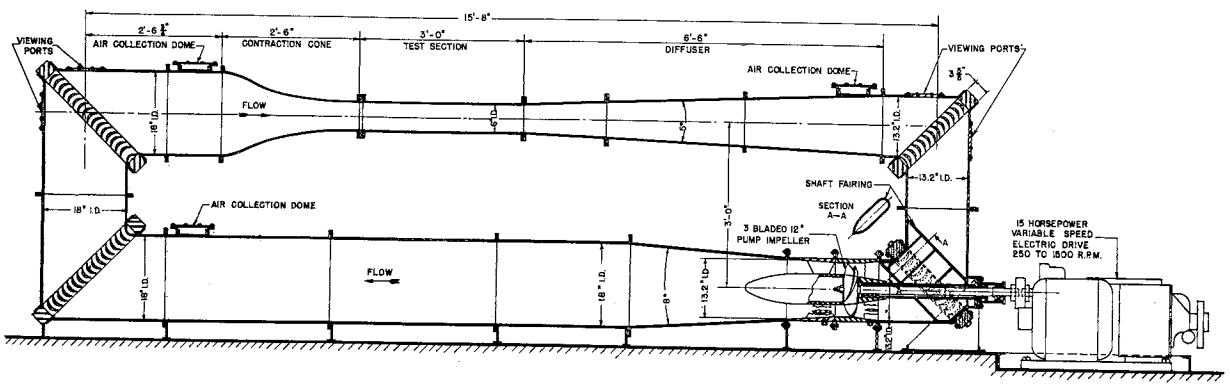

Fig. 61 - Sectional Elevation of 6-in. Model Water Tunnel

consistent with the model scale ratio, it was deemed the best compromise on the basis of anticipated performance requirements. Therefore, local flow conditions at the pump were not expected to agree with prototype similitude and the pump test program was considered primarily a matter of determining correct specifications for the pump construction.

Since the Laboratory was faced with the problem of fabricating the remainder of the pump unit without detailed design data and without facilities for economical fabrication of the conventional warped suction and discharge vaning, the design was reduced to the simplest possible geometry. As can be seen from Fig. 62, the principal features of the model pump geometry include:

(1) A housed drive shaft.

(2) A vaned approach elbow in which a streamlined splitter has been provided to minimize the disturbance in flow created by the presence of the drive shaft.

(3) Four streamlined radial struts supporting the inboard shaft bearing. These struts are axial vanes and make no attempt to apply selected rotary vector components to the flow.

(4) A hub fairing piece formed to diffuse the flow as gradually as possible consistent with practical length limitations.

(5) Seven straight diffuser vanes with dimensions based on Collar's findings (reference [1] of Chapter VI). In his design studies, Collar concluded that radial vanes with axial alignment provide adequate straightening of the rotary impeller discharge if the vane is an airfoil section operating at less than the stall angle and if it is of varying chord length so that the ratio of peripheral vane spacing to chord is unity. While a spacing ratio of 0.5 would have given better results, little flow quality is sacrificed and the structure is simplified if a ratio of 1.0 is used.

(6) A conventional packing gland placed at the point where the drive shaft pierced the pressure swell. Sealing against air leakage under subatmospheric tunnel operations was accomplished by a shaft lantern ring and an external pressure tap to the city water supply.

The pump drive system consisted of a 15-hp electric motor integrally connected to a variable speed, V-belt transmission. Speed changes were accomplished by a mechanism which varied the diameters of the V-belt pulleys to permit an output shaft speed continuously variable between 250 and 1500 rpm.

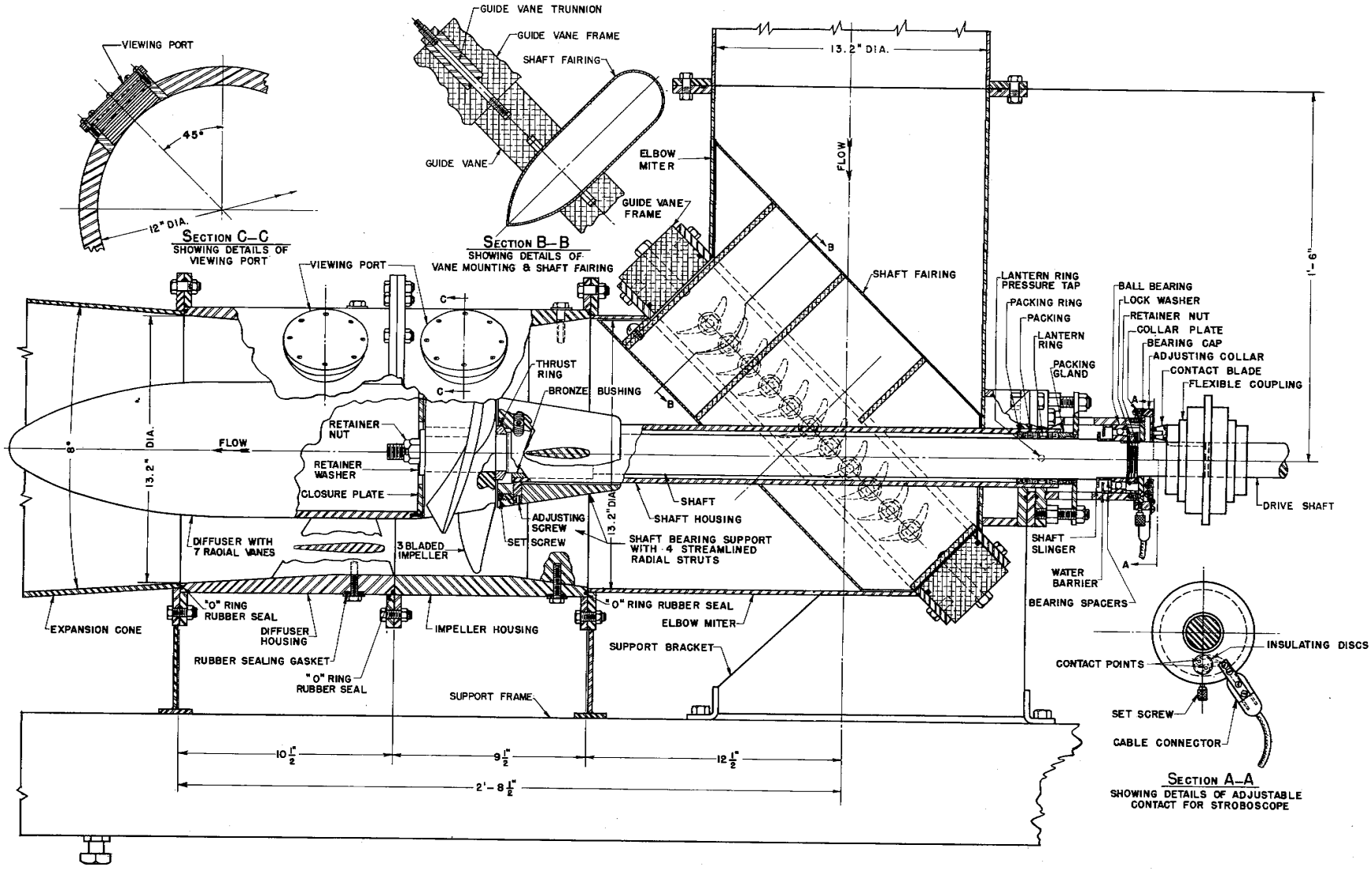

Fig. 62 – Model Pump Assembly

The speed change mechanism was driven by a small auxiliary electric motor, controlled in turn by push buttons mounted on the main control panel.

A remote reading electric tachometer was connected to the output shaft and mounted with the indicating head at the main control panel. This arrangement served as a ready means of establishing approximate test section speeds. While a larger speed and power range, together with elimination of the slight vibratory characteristics inherent to a V-belt drive, would have been desirable, procurement of this unit was considered an expedient and economical solution to the problem.

Since the ambient pressure value existing in the test section of a water tunnel is one of the most important variables in any tunnel cavitation study, it is essential that convenient means of varying it and accurate means of measuring it be provided. A review of the methods used in other tunnels indicated that, in general, control was effected by connecting the tunnel to a regulated vacuum or pressure source while measurement was frequently accomplished with a modified mercury manometer. A notable exception was the Massachusetts Institute of Technology tunnel employing a tilting pipe leading from the test section to the atmosphere. The elevation of the free liquid surface in the atmospheric end of the pipe relative to the elevation of the test section established the test section pressure. Since the elevation of the free surface could be varied by tilting the pipe, a wide range of test section pressures could be achieved.

In view of the large vertical space available in the St. Anthony Falls Hydraulic Laboratory and the inherent accuracy and simplicity of a water manometer, it was decided to employ a modified and extended version of the Massachusetts Institute of Technology pressure system. The pressure control portion of this system replaced the tilting pipe of the MIT system with a flexible rubber hose ending in a free surface overflow pan, with the pan being raised and lowered vertically on an electric hoist. Separate water supply and waste hoses served to keep the free liquid surface at an established position in the overflow pan.

Measurement of the elevation of the free surface height relative to the tunnel centerline was accomplished by affixing a surveyor's measuring tape to the overflow cup with the zero set at the water surface. An index mark opposite the tape and at the elevation of the test section centerline permitted

direct readings of the test section pressure in feet of water. Elevation of the free surface could be varied from +16 to -31 ft of water and some additional tunnel pressure variation could be accomplished by varying the point at which the pressure hose is attached to the tunnel boundary. The latter technique is possible since the tunnel possesses regions (most notably the contraction) with steep axial pressure gradient as a result of the dynamics of the recirculating flow. Because the measuring tape was graduated to 0.01 ft, all pressure settings greater than 1.00 ft could be easily and accurately measured with an error of less than 1 per cent.

All moving body flow studies are fundamentally dependent on accurate knowledge of the relative velocity; therefore, it was essential that the model tunnel be fitted with a meter capable of accurate indication of the test section flow velocity. While some tunnels have employed fixed Pitot tubes and current meters to indicate velocity, it has been more common to employ differential pressures measured along the tunnel boundary and, particularly, the large differentials occurring along the contraction cone boundary.

A review of the problems led to the selection of the method of differential pressure measurement for the model tunnel studies and resulted in the installation of three pressure manifolds located at the upstream end, midpoint, and downstream end of the contraction. Each of the manifolds consisted of four pressure taps, with two on a horizontal diameter and two on a vertical diameter of the cross section. Each tap consisted of a 1/32-in. diam hole carefully deburred at its inner end and expanded to a 1/8-in. pipe connection at its outer end.

To avoid locating the upstream pressure tap in a region of flow separation, it was placed as far upstream as the casting structure permitted, or 1-1/2 in. from the end of the model casting. Subsequent boundary streamline experiments in the model (Chapter III, Contraction Studies) indicated a slight separation might exist in this region; this would make it advisable to move even farther upstream for any similar prototype meter. The middle manifold was located 17 in. downstream of the beginning of the contraction and was employed whenever the head between the upstream and downstream manifolds exceeded the limits of convenient reading on the attached manometers. The downstream manifold was located 1-1/2 in. upstream of the downstream end of the contraction at a point where the minimum or test section diameter had been

reached. This manifold, in addition to serving as a prime tap for velocity determinations, also served as the usual external pressure application and control point. The three manifolds are shown in Fig. 20.

Pressure forces from the manifold system were originally intended to be indicated by a water manometer reading directly to the nearest 0.01 ft; however, mechanical difficulties with this system led to its replacement with conventional 50-in. glass U-tubes and adjustment of gage fluid specific gravity to match the pressure magnitude. As indicated previously the velocity was controlled by adjusting the pump speed with electric push button controls. The measured relation between the manometer reading and the flow discharge was determined by an experimental calibration separately described in Appendix III.

APPENDIX II. TEST INSTRUMENTS

Since the primary purpose of the experimental model studies was the determination of the progressive velocity and pressure energy changes along the flow axis, the basic instrumentation consists of velocity meters capable of traversing a cross section of the flow and pressure meters for determination of the pressure gradient.

While a variety of instruments have been developed for probing internal velocities in closed pressurized conduits, the problem of traversing a maximum area with an instrument which is readily insertable, retractable, velocity sensitive, direction sensitive, and of low flow disturbance led to adoption of the Pitot cylinder. The Pitot cylinder is a little-known instrument, essentially an impact device similar to the Pitot tube. A search of the literature to ascertain fully the properties of this instrument disclosed a lack of facts and stimulated a special investigation at the St. Anthony Falls Hydraulic Laboratory summarized in reference [2] of Chapter VI. From this investigation two types of cylinders were developed, notably the "cantilevered" cylinder supported from a single insertion point in the duct wall and the "long" type which completely spans the duct and has physical support at two insertion points in the duct wall. The "cantilevered" type has the advantage, when equipped with a suitable ball joint, of permitting the cylinder to be swung or extended to allow the tip to probe the cross-sectional area from a single insertion point. However, the cantilevered nature of the support for the cylinder tip vibrates when fully extended and subjected to moderate flow velocities. The vibration was capable of structurally destroying the tube and produced false pressure readings at the impact holes. In view of this limitation, the "cantilevered" cylinder was replaced by the doubly supported "long" cylinder where higher velocities were to be studied, despite the fact that the "long" cylinder was restricted to probing on a single line across the flow stream.

With each of the two forms of cylinder, two small pressure tap holes were drilled normal to the cylinder wall 80° apart in a plane perpendicular to the cylinder axis. The central angle of 80° was chosen because the pressure distribution curve for flow around a cylinder is very steep at central angles of 40° from the stagnation point. This steepness gave high directional sensitivity (measurement showed a change of 5 to 10 per cent of the velocity head per degree when used to determine flow direction). The two taps separately

conveyed pressure through the cylinder interior and thence to external pressure reading manometers. If either of the two taps were oriented to face the principal flow direction, the corresponding pressure reading would represent the total or stagnation head and in conjunction with a static pressure tap in the duct boundary wall would serve to give the local velocity head. The direction of this local velocity could then be ascertained by orienting the cylinder so that the pressures at the two cylinder holes were the same. The physical position of the Pitot pressure tap in the tunnel cross section was determined by external readings of scales "A", "B", and "C" shown in Fig. 63. A coefficient of unity was used with these tubes because the tests described in reference [2] of Chapter VI indicated such a practice introduced an error of less than 1/2 per cent in obtaining the average energy over a cross section.

The tunnel boundary was arranged with insertion points located by the station numbers of Fig. 38. At stations 3, 4, 5, 6, 8, 9, 10, 11, and 12, one ball type swinging mounting and three nonswinging mountings were spaced at 90° around the periphery to permit insertion of a 3/8-in. diam "cantilevered" cylinder. The construction and mounting of this instrument are shown in Figs. 37 and 63. At station 7 four nonswinging mountings were provided. The nonswinging mountings were also suitable as static pressure taps when the cylinder was removed. In the high velocity regions of stations 1 and 2, the 3/8-in. "cantilevered" cylinder was supplanted by a 1/4-in. "long" cylinder and nonswinging mounts located on a diameter.

Pressure measurements on the tunnel boundary wall and the Pitot taps were generally made using 50-in. glass U-tube manometers. Four metering fluids--carbon tetrachloride, ethylene bromide, bromoform, and mercury--were used selectively to give the maximum readable deflection in any particular pressure study. Where the readings were less than 6 in., and thus of excessive error due to the coarse reading scales on the U-tubes, a micromanometer was used. The micromanometer was an inverted U-tube with an air loop. Reading was accomplished with two micrometer depth gages modified to act as hook gages measuring to the nearest 0.001 inch. Water levels and air pressure in the micromanometer were controlled by a hand pump and bleed-off valve.

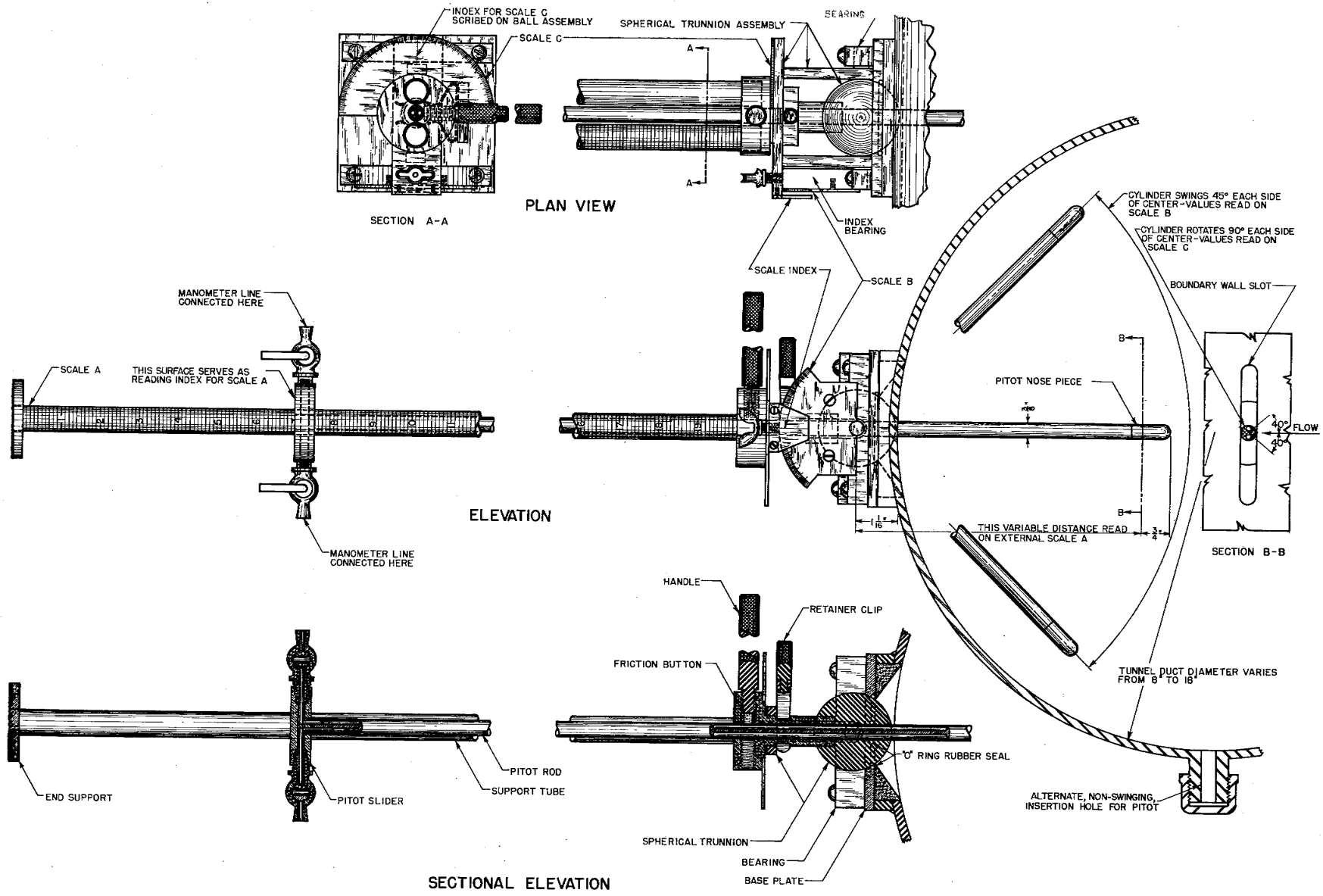

Fig. 63 - Cantilevered Pitot Cylinder and Mounting

APPENDIX III. TEST PROCEDURE

The physical measurements made in the model studies consisted of calibrating the contraction nozzle for use as a general velocity meter, taking velocity traverses at selected test stations on the tunnel circuit, taking boundary pressure gradients around the tunnel circuit, and determining critical cavitation conditions. Since the last three of these were previously described, only the velocity meter calibration will be described here.

Because all instruments for measuring liquid velocities are subject to some correction for inherent errors of indication, it was desirable that the basic velocity measuring device be calibrated to minimize such errors. Therefore, in accord with accepted hydraulic practice, the velocity was determined by measuring the total discharge of the flow stream with a primary weight system. The calibration of the contraction cone differential pressure drop as an index of velocity necessitated breaching the tunnel loop and diverting the flow at a point where the diversion would have least influence on the meter performance. It was decided, therefore, to remove a portion of the tunnel loop in the vicinity of elbow I (Fig. 38) and to substitute an external water supply connection just above elbow II and a discharge connection to the downstream end of the main diffuser. The supply connection was in turn tied into the main water supply system of the Laboratory, while the discharge connection was conveyed to the main weighing tanks of the Laboratory for precise discharge determinations.

A large number of discharge determinations were made with the mean test section velocity varying from 9 to 47 fps. The weighed discharge measurements, together with the contraction pressure differentials, pump shaft revolutions per minutes, and measured velocity distribution traverses at stations 1 and 12, served to give the basic velocity data necessary to subsequent tunnel testing.